National Library
of Canada

Bibliothèque nationale
du Canada

Canadian Theses Service

Services des thèses canadiennes

Ottawa, Canada
K1A 0N4

CANADIAN THESES

THÈSES CANADIENNES

NOTICE

The quality of this microfiche is heavily dependent upon the quality of the original thesis submitted for microfilming. Every effort has been made to ensure the highest quality of reproduction possible.

If pages are missing, contact the university which granted the degree.

Some pages may have indistinct print especially if the original pages were typed with a poor typewriter ribbon or if the university sent us an inferior photocopy.

Previously copyrighted materials (journal articles, published tests, etc.) are not filmed.

Reproduction in full or in part of this film is governed by the Canadian Copyright Act, R.S.C. 1970, c. C-30.

AVIS

La qualité de cette microfiche dépend grandement de la qualité de la thèse soumise au microfilmage. Nous avons tout fait pour assurer une qualité supérieure de reproduction.

S'il manque des pages, veuillez communiquer avec l'université qui a conféré le grade.

La qualité d'impression de certaines pages peut laisser à désirer, surtout si les pages originales ont été dactylographiées à l'aide d'un ruban usé ou si l'université nous a fait parvenir une photocopie de qualité inférieure.

Les documents qui font déjà l'objet d'un droit d'auteur (articles de revue, examens publiés, etc.) ne sont pas microfilmés.

La reproduction, même partielle, de ce microfilm est soumise à la Loi canadienne sur le droit d'auteur, SRC 1970, c. C-30.

THIS DISSERTATION
HAS BEEN MICROFILMED
EXACTLY AS RECEIVED

LA THÈSE A ÉTÉ
MICROFILMÉE TELLE QUE
NOUS L'AVONS REÇUE

NL-339 (r.86/06)

Canada

THE UNIVERSITY OF ALBERTA

FINITE ELEMENT VIBRATION ANALYSIS OF A MODEL TURBINE ROTOR

by

WILLIAM I. ROBERTSON

A THESIS

SUBMITTED TO THE FACULTY OF GRADUATE STUDIES AND RESEARCH
IN PARTIAL FULFILMENT OF THE REQUIREMENTS FOR THE DEGREE
OF MASTER OF SCIENCE
IN
MECHANICAL ENGINEERING

DEPARTMENT OF MECHANICAL ENGINEERING

EDMONTON, ALBERTA

SPRING 1986

Permission has been granted to the National Library of Canada to microfilm this thesis and to lend or sell copies of the film.

The author (copyright owner) has reserved other publication rights, and neither the thesis nor extensive extracts from it may be printed or otherwise reproduced without his/her written permission.

L'autorisation a été accordée à la Bibliothèque nationale du Canada de microfilmer cette thèse et de prêter ou de vendre des exemplaires du film.

L'auteur (titulaire du droit d'auteur) se réserve les autres droits de publication; ni la thèse ni de longs extraits de celle-ci ne doivent être imprimés ou autrement reproduits sans son autorisation écrite.

ISBN 0-315-30296-8

THE UNIVERSITY OF ALBERTA

RELEASE FORM

NAME OF AUTHOR WILLIAM I. ROBERTSON

TITLE OF THESIS FINITE ELEMENT VIBRATION ANALYSIS OF A MODEL TURBINE ROTOR

DEGREE FOR WHICH THESIS WAS PRESENTED MASTER OF SCIENCE

YEAR THIS DEGREE GRANTED SPRING 1986

Permission is hereby granted to THE UNIVERSITY OF ALBERTA LIBRARY to reproduce single copies of this thesis and to lend or sell such copies for private, scholarly or scientific research purposes only.

The author reserves other publication rights, and neither the thesis nor extensive extracts from it may be printed or otherwise reproduced without the author's written permission.

(SIGNED) W. I. Robertson

PERMANENT ADDRESS:

5208 - 91 AVE
EDMONTON, ALTA
CANADA T6B 0R2

DATED FEB. 12 1986

THE UNIVERSITY OF ALBERTA

FACULTY OF GRADUATE STUDIES AND RESEARCH

The undersigned certify that they have read, and recommend to the Faculty of Graduate Studies and Research, for acceptance, a thesis entitled FINITE ELEMENT VIBRATION ANALYSIS OF A MODEL TURBINE ROTOR submitted by WILLIAM I. ROBERTSON in partial fulfilment of the requirements for the degree of MASTER OF SCIENCE IN MECHANICAL ENGINEERING.

Supervisor

Kennedy

Date FEB. 12, 1986

Dedication

To my parents

Colin and Beryl Robertson

ABSTRACT

A Finite Element Analysis of a 286 MW steam turbine was conducted in order to determine the design parameters for the construction for a dynamically scaled model.

This model turbine was then tested for its various vibration characteristics. This vibration data was the basis for a numerical (Finite Element) balancing program.

The numerical program provided good correlation for the mode shapes, natural frequencies, and forced response. More refinement is required before the program can produce satisfactory results for balancing purposes on multi-span systems.

ACKNOWLEDGEMENTS

For a project as large and complicated as this many people must be recognized. Without the guidance and support of my supervisor, family, and fiancée this thesis would never have been completed.

I would first like to express my utmost gratitude to Dr. A. Craggs for his technical expertise and especially his patience. Dr. F. Ellyin and Dr. P. Kim also supplied valuable advice and technical knowledge towards the completion of this project.

Special thanks also goes to Dr. Craggs and Dr. Ellyin for financial support which was supplied through a PRAI grant from NSERC.

Several technicians provided the means by which the model turbine rotor was constructed. Among these are A. Muir, D. Fuhr, and T. Nord.

I am extremely grateful to my mother for spending hours typing and retyping this thesis.

TABLE OF CONTENTS

Page

1. INTRODUCTION 1

 1.1 Balancing Methods : Current Vs Proposed . . 1
 1.2 Scope of Thesis 5

2. DESIGN OF THE IN-HOUSE RIG 8

 2.1 Finite Element Model of a 286 MW Turbine Rotor 8
  2.1.1 Rotor and Blades 9
  2.1.2 Bearings 14
  2.1.3 Results 16

 2.2 In-House Rig 21
  2.2.1 Scaling Parameters 25
  2.2.2 Natural Frequencies 25
  2.2.3 Sommerfeld Numbers 27
  2.2.4 Stiffness Ratios 29
  2.2.5 Mode Shapes 30
  2.2.6 Modelling Procedure 30

3. NON-ROTATING ANALYSIS 35

 3.1 Beam Theory 35
 3.2 Natural Frequencies and Mode Shapes 42

4. ROTATING ANALYSIS 51

 4.1 Gyroscopic Effects 51
 4.2 Effect of Bearings 56
 4.3 General Dynamic Model 57
 4.4 Natural Frequencies and Mode Shapes 64

5. RESPONSE DUE TO A ROTATING LOAD 82

 5.1 Linearity Tests 84
 5.2 Forced Response 84
  5.2.1 Orbits 89
  5.2.2 Polar Plots 95
 5.3 Comparison of Experimental Results With Theoretical 100
 5.4 Prediction of Load 103

6. CONCLUSIONS 110

 6.1 Dynamic Model 110
 6.2 Numerical Model 111
 6.3 Balancing 112

TABLE OF CONTENTS

Page

REFERENCES 113

LIST OF TABLES

Page

2.1 Bearing Film Stiffness 18

2.2 Eigenvalues 20

2.3 Scaling Parameters 26

3.1 Natural Frequencies 43

4.1 Bearing Coefficients 61

4.2 Natural Frequencies 74

5.1 Load Distributions for Forced Response . . 89

LIST OF FIGURES

Page

1.1 Rotor Bearings System with Foundation 4

1.2 Rotor Bearings System 5

2.1 Equivalent Diameter for Element 11

2.2 Finite Element Models for a 286 MW Steam Turbine 12

2.3 Grounding the Rotor 14

2.4 Relative Movement of Flanged Sections 15

2.5 Rotor Stages on Simple Supports 16

2.6 286 MW Turbine Modes 19

2.7 Critical Speed Map 21

2.8 In-House Rig 23

2.9 Low Vs High Tuning a Machine 24

2.10 Mode Shapes of Rig Compared to 286 MW Turbine 31

2.11 Scaling Parameters Flow Chart 33

2.12 Effect of Independent Variables 34

3.1 Timoshenko Beam Element 36

3.2 Definition of Nodal Rotation 36

3.3 Disc Dimensions and Inertia 39

3.4 Single Degree of Freedom System 40

3.5 In-House Rotor on Rigid Foundations 42

3.6 Frequency Vs Amplitude Plot for In-House Rotor 44

3.7 Finite Element Model for In-House Rig 46

3.8 Definition of ½ Power Points 48

3.9 Mode Shapes for Non-Rotating Test 49

LIST OF FIGURES

Page

4.1 Gyroscopic Terms for a Disc 52

4.2 Effect of Bearing Coefficient on the Orbit of a Rigid Rotor 58

4.3 Bearing Stiffness Terms 59

4.4 Static Vs Rotating Loads 60

4.5 Polar Response for a Single Degree of Freedom System 66

4.6 Vector Addition of Two Normal Modes 68

4.7 Rate of Change of Phase Angle Vs Speed . . 69

4.8 Polar Response for Natural Frequencies . . 75

4.9 Polar Plots for Mode Shapes 77

4.10 Mode 1 78

4.11 Mode 2 79

4.12 Mode 3 80

5.1 Linearity Test #1 85

5.2 Linearity Test #2 86

5.3 Load Vs Displacement for Linearity Tests #1 & 2 87

5.4 Linearity Test #3 87

5.5 Linearity Test #4 88

5.6 Definition of Coordinate System 89

5.7 Response Coordinate System 90

5.8 Direct Vs Synchronous Signal 91

5.9a Orbit For 2900 RPM 93

LIST OF FIGURES

Page

5.9c Orbit For 3100 RPM 94

5.10 Load Distribution 1 97

5.11 Load Distribution 2 99

5.12 Load Distribution 3 99

5.13 Scatter In Bearing Coefficients 101

5.14 Effect of Proportional Damping Factor . . 102

5.15 Prediction of Load 108

NOMENCLATURE

[A] - Influence Coefficient Matrix

A - Cross Sectional Area

[C] - Damping Matrix

c - Bearing Radial Clearance

C_{HH}, C_{HV}, C_{VH}, C_{VV} - Bearing Damping Terms

[D] - Dynamic Stiffness Matrix

D - Element/Disc Diameter

E - Modulus of Elasticity

{F} - Forcing Function Vector

F_1, F_2 - Element Forces

F_v, F_n - Forces in Vertical/Horizontal Direction

f - Bearing Constant

G - Shear Modulus

g - Damping Ratio/Gravitational Constant

H - Whirl Ratio

I, I_p - 2nd Moment of Area/Polar Moment of Area

$\bar{i}$ $\bar{j}$ - Unit Vectors

J - Rotatory Inertia per Unit Length

[K] - Stiffness Matrix

$[K]_r$, $[M]_r$, $[C]_v$ - Stiffness/Mass/Damping/Matrices After Guyan Reduction

K_{HH}, K_{VH}, K_{HV}, K_{VV} - Bearing Stiffness Terms

K_{FILM} - Bearing Film Stiffness

K_{SPAN} - Shaft Span Stiffness

k - Shape Factor

l - Element Length

[M] - Mass Matrix

M_1, M_2 - Element Moments

m - Mass Per Unit Length

N - Rotor Speed in RPS

P - Bearing Unit Load

r - Shaft/Disc Radius

t - Time

Sn - Sommerfeld Number

$\{U\}$ - Displacement Vector

U_H, U_V - Displacement in Horizontal/Vertical Direction

V - Shear Force

W - Bearing Load

W_1, W_2 - Element Loads

$\{X\}$ - Radial Displacement Vector

$\{\dot{X}\}$ - Radial Velocity Vector

$\{\ddot{X}\}$ - Radial Acceleration Vector

$\bar{Z}(t)$ - Position of Shaft on Orbit as a Function of Time

β, $\dot{\beta}$, $\ddot{\beta}$ - Angular Displacement/Velocity/Acceleration of Shaft With Respect to x-y Plane

γ, $\dot{\gamma}$, $\ddot{\gamma}$ - Angular Displacement/Velocity/Acceleration of Shaft With Respect to X-Z Plane

η - Oil Viscosity

λ - Eigenvalue

θ_1 θ_2 - Element Bending Slope

ρ - Density

$\{\phi\}$- Eigenvector

ϕ_V/ϕ_H - Vertical/Horizontal Time Based Phase Angles

ψ - Shear Slope

ω - Rotor Angular Velocity

ω_1 ω_2 - Natural Frequencies at ½ Power Points

ω_d - Damped Natural Frequency

ω_n - Natural Frequency

1. INTRODUCTION

1.1 Balancing Methods : Current Vs Proposed

Balancing any rotating machinery is both a complicated and time consuming procedure. With the onset of large, high speed machines the need for a practical balancing method has become apparent. Most large rotating machines are classified as flexible systems in which the shape of the centroidal axis changes with speed. This system requires a more sophisticated vibration analysis than that of a rigid body motion such as a car wheel. The shape of a rigid rotor's centroidal axis does not change with speed, and therefore balancing can be done with a very simple vectorial analysis.

To date, most flexible balancing has been conducted using two major techniques described in detail by Kim(7). These are:

1. Influence Coefficients
2. Modal Balancing

The influence coefficient method requires extensive vibration measurements which render the machine inoperative for long periods of time. The test runs are conducted in order to generate a complex influence coefficient matrix. This matrix is inverted and then multiplied by the initial response vector which yields the balance vector (1.1).

$$[A]^{-1}\{u\} = -\{F\} \tag{1.1}$$

[A] = Influence Coefficient Matrix
{U} = Initial Response Vector
-{F} = Balance Vector

Several disadvantages are inherent in this method:

1. Errors are introduced in the inversion of the measured matrix A which are further increased by multiplying this by the initial response vector.
2. Several test runs at the highest balance speed may be required.
3. Has low sensitivity at higher modes.

The modal balancing method also requires several runs. Each mode is balanced in turn, beginning with the fundamental. At each stage the unbalance due to that mode is determined experimentally and balanced with suitable correction masses.

Before any balancing can be done the mode shapes of the rotor-bearing system must be known and this requires a fairly extensive experimental or numerical analysis. The major disadvantage in this method is that only one mode can be balanced at a time. In addition, to balance subsequent modes the masses must be placed in such a way as to leave all the lower modes undisturbed. This requires a great deal of operator insight.

The method presented in this Thesis deals with the numerical generation of the dynamic stiffness matrix [A] using finite elements. Three major advantages are consequently obtained:

1. The errors, in first measuring the [A] matrix, and then inverting it, are eliminated.
2. Operator insight will not be as large a factor in the success of the balance.
3. Shutdown time for the machine is substantially reduced since only the initial response vector is measured.

These advantages present the reason for studying the method which will be termed "Dynamic Matrix Balancing Technique". Equation 1.1, as in the influence coefficient method, is the basic balancing equation.

In order to study the feasibility of such a technique a testing facility is required. The obvious choice is a machine which is already in operation. This was considered inappropriate for two reasons:

1. A new method could be disastrous to a machine by placing the balance weights in the wrong place. This would not necessarily imply that the method does not work since there are several factors influencing the size and location of the balance weights:
    - i) retained degrees of freedom
    - ii) measurement devices
    - iii) accuracy of stiffness, damping, and mass matrices from finite elements.
2. On a machine in operation vibration data can only be readily obtained at the bearings. For an initial study, measurements at mid-span will also be required.

For these reasons an in-house rig was designed and constructed and will be described in detail in Chapter 2.

Any rotating system consists basically of the rotor, the bearings, and finally the foundation.

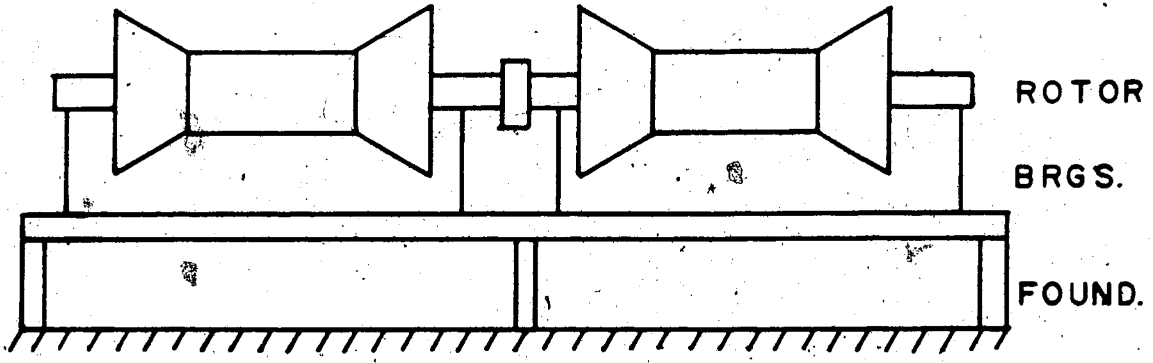

Fig. 1.1 Rotor Bearing System with Foundation

Most vibrational problems begin with a rotational imbalance in the rotor. This force is transmitted through the bearings into the foundation. A full mathematical model to generate the [A] matrix would require a system similar to the one shown in Fig. 1.1. For this analysis, the foundation is excluded. The purpose of this Thesis is to study the rotor-bearing response due to an imbalance in the rotor. This can be accomplished by taking relative measurements between the rotor and foundation. This is done by mounting the vibration probes on the foundation. The system is subsequently reduced to that of Fig. 1.2.

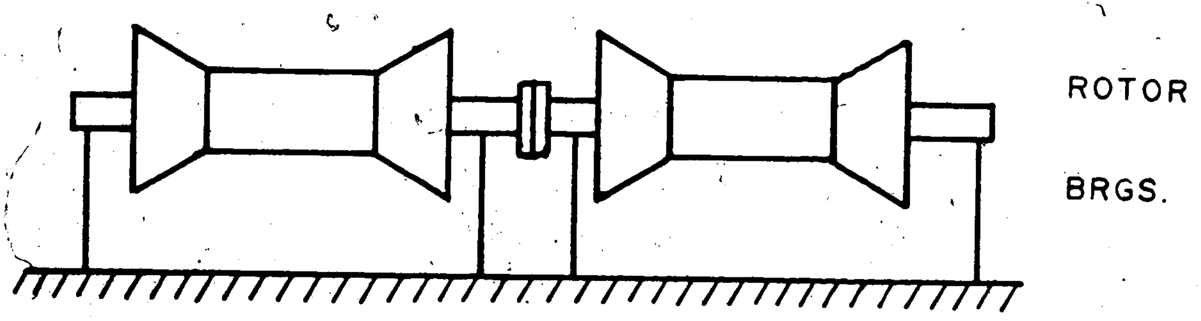

Fig. 1.2 Rotor Bearing System

1.2 Scope of Thesis

The overall purpose of this thesis involved first analysing the vibrational characteristics of a large steam turbine. Using a finite element technique the mode shapes and natural frequencies were generated. From this information a testing facility called the "in-house rig" was designed and constructed. The same finite element analysis was used for the in-house rig.

The second goal was to use a finite element analysis to examine the vibrational characteristics of the rig with the ultimate purpose of developing a numerical balancing program. Many such attempts have been made in the past but with limited success for complex rotating systems.

The procedure attempts to include most of the parameters which affect the rotating system. These include: bearing stiffness, bearing damping, proportional damping, gyroscopic terms, disc inertia (etc.). Gash(15) presents a good overview of the complexity of the numerical approach to rotor dynamics.

The rotating shaft (rig and turbine) rides on journal bearings which yield a non-symmetric numerical system. A two plane analysis was therefore, necessary. This two plane system is described in much detail by Adams and Padovin(16). Many of the problems with a symmetric, non positive definite systems are described and this thesis presents one method of dealing with them.

The numerical technique which will be presented produced reasonable results for eigenvalues, and response due to a rotating load but as far as a balancing program the method is not adequate. This subject is a complex one which requires a great deal more study than this thesis can possibly hope to present.

2. DESIGN OF THE IN-HOUSE RIG

Abstract

A finite element analysis of a 286 MW steam turbine will be presented. The turbine is unit #4 located at the Trans-Alta Power Station on Lake Wabamun. A similar analysis is conducted to aid in the design of a physical model which simulates the vibrational characteristics of the large turbine. This model will be called the "in-house rig" and its detailed design parameters will also be outlined. Vibration characteristics of both the rig and turbine will then be compared numerically.

2.1 Finite Element Model of a 286 MW Turbine Rotor

The turbine in question has a history of vibrational problems originating within the low pressure stages. Displacement probes are located on each of the turboset's nine bearings. These probes measure the displacement in two planes which can be used ~~to determine~~ the phase angle and orbit plots. The vibration problems and the available measurement system make this an ideal turbine for an in depth simulation study.

The turboset consists of five rotor sections: high pressure (HP), intermediate pressure (IP), low pressure #1 (LP1), low pressure #2 (LP2), and the generator (GEN) rotor. The five sections are joined together with flange couplings. The entire rotor rides on nine oil fed journal bearings. A thrust bearing is located between the high and intermediate pressure stages. For this part of the project, the shaft and bearings were modelled in order to find the natural frequencies and mode shapes which were the basis for the design of the in-house rig.

Drawings of the turbine were provided by Trans-Alta. Pertinent drawings included rotor details, bearings, blading arrangement and foundation. From these drawings simplified, two dimensional finite element models were developed. For the purpose of creating a dynamic model of the turbine, only the vertical plane was considered, i.e., in the direction of the load on the bearings. Of course, for balancing purposes both the vertical and horizontal planes must be analyzed simultaneously.

2.1.1 Rotor and Blades

To analyze the rotor and blade arrangement, three finite element models were considered consisting of 8, 29, and 111 elements. The models are shown in Fig. 2.2. The smaller element models (8 & 29) were used in the dynamic analysis to reduce the degrees of freedom of the system. The 111 element model was used in the static analysis to determine the bearing loads and the weight distribution of the shaft. The derivation of these models will be discussed in the following paragraphs.

The first step was to model the rotor. The basic Timoshenko beam element (Fig. 3.1) was used in the finite element program, and therefore the model had to be divided into elements of constant diameter. These elements were then used to find the mass and stiffness matrices for the system.

The detailed drawings of the rotor reveal a large number of tapered sections and steps in the shaft, and it would have been almost impossible to account for all of them, even with the 111 element model. An equivalent diameter that incorporates several steps in the rotor is a compromise between the stiffness and mass of the element. The mass of the element is proportional to the square of the diameter, while the stiffness is proportional to the diameter to the fourth power. Both the stiffness and mass matrix are of equal importance, so an average equivalent diameter was used to determine the 111 element model dimensions, i.e.

$$D_{eq} = \left[\frac{1}{2} \left[[\sum_i D_i{}^4 (\frac{Li}{L})]^{\frac{1}{4}} + [{}_i D_i{}^2 (\frac{Li}{L})]^{\frac{1}{2}} \right] \qquad (2.1)$$

Di = segment of element diameter

Li = segment of element length

L = element length

The elements were chosen to minimize the magnitude of the steps in the shaft.

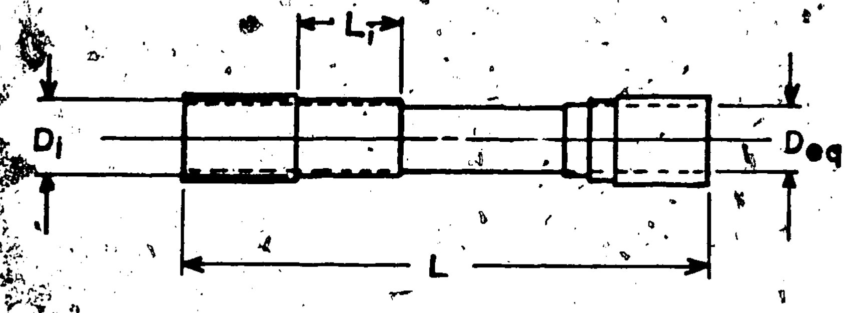

Fig. 2.1 Equivalent Diameter for Element

The next stage in modelling the rotor, was to reduce the size of the system for a dynamic analysis. The 111 element system has 224 degrees of freedom which is very large for an eigen-system analysis and therefore a 29 element model was used (Fig. 2.2). The use of equation 2.1 is only valid where the steps in the shaft are not too excessive. From Fig. 2.2 it is seen that the diameter of the blade rings is twice that of the shaft. In the 29 element model these blade ring regions were incorporated into one element. The diameter of these elements were taken to be that of the average rotor diameter between the blade rings. To account for the subsequent reduction in mass, large discs were placed on either side of the blade ring elements. For the low pressure stages the reduction

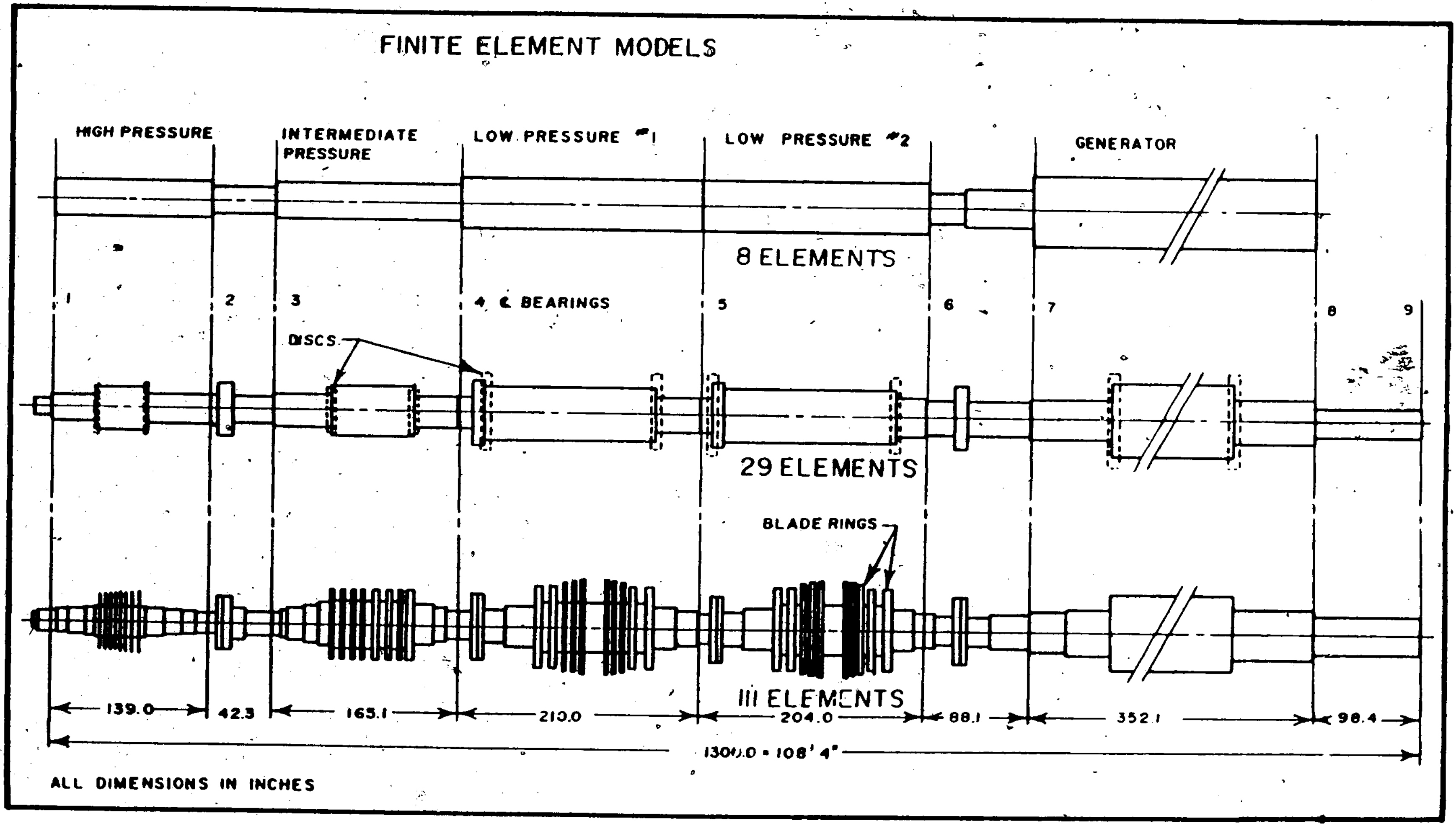
FINITE ELEMENT MODELS
HIGH PRESSURE
INTERMEDIATE PRESSURE
LOW PRESSURE #1
LOW PRESSURE #2
GENERATOR
8 ELEMENTS
1
2
3
4 ℄ BEARINGS
5
6
7
8
9
DISCS
29 ELEMENTS
BLADE RINGS
111 ELEMENTS
139.0
42.3
165.1
210.0
204.0
88.1
352.1
98.4
1300.0 = 108' 4"
ALL DIMENSIONS IN INCHES

Fig. 2.2 Finite Element Models for a 286 MW Steam Turbine

in weight was 25%. The reduction in stiffness was calculated to be only 1% and was therefore considered negligible. The mass of the rotor was determined by the 111 element model. Each of the power stages was analyzed separately and the size of the discs was determined simply by subtracting the weight of the 29 element model from the 111 element model.

The addition of the discs into the system did not add any additional stiffness since they were only added to the mass matrix as point masses. The rotatory inertia is also added at the same point in the mass matrix (see Chapter 3).

The blades on the shaft also needed to be taken into account. The elements which contained the blade rings were increased in diameter by approximately 10%. This was a rough approximation since the blade rings are not solid but hollow to allow the passage of steam. The mass added to the element was about 10% and the increase in stiffness was negligible. Each blade ring is different, but in order to reduce the complexity of the system a 10% increase in diameter was used for each.

2.1.2 Bearings

For the purpose of computer modelling, the shaft's support system must be added into the stiffness matrix.

In this way the shaft is "grounded" which means that it is physically attached to the ground and not free in space. This was done by adding an equivalent bearing film stiffness to the appropriate node in the stiffness matrix.

The turbine and generator ride on oil-fed journal bearings. The bearings are mounted on spherical seats which allows rotation of the bearing and for this reason the bearings have no rotational stiffness. The grounding is therefore only in the direction of load. The bearings also have stiffness perpendicular to the load but again, only vibration in one plane was considered.

Adding equivalent film stiffness in this manner yields a shaft mounted on springs, i.e.

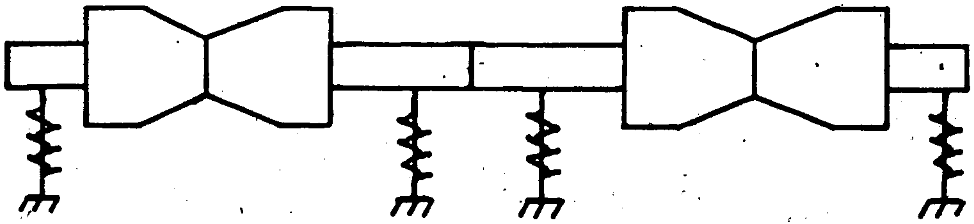

Fig. 2.3 Grounding the Rotor

The "springs" supporting the rotor are only the film stiffness of the bearings. As discussed in Chapter 1 the stiffness of the foundation is not included in the analysis. For oil journal bearings the stiffness is non-linear.

The film stiffness of the bearings is defined as

$$K_{FILM} = \left(\frac{W}{C}\right) f \tag{2.2}$$

K_{FILM} = Film Stiffness

W = Load

f = Constant

C = Radial Clearance

where the constant "F" was found from Kim and Lowe$^{(10)}$. The constant F is plotted against the bearing characteristic or Sommerfeld number (see Fig. 4.3).

The load on the bearing needed to be found accurately to find the film stiffness. The film stiffness has a large effect on the dynamics of the system since they determine the flexibility of the system (Fig. 2.7). Most bearings, for large turbines, are mounted on a catenary. This is done to aid in coupling the shaft sections together. The catenary ensures that the static (non-rotating) bending moment and shear force at the couplings are small. If this was not the case then when the sections are uncoupled there would be relative motion between the flanges, i.e.

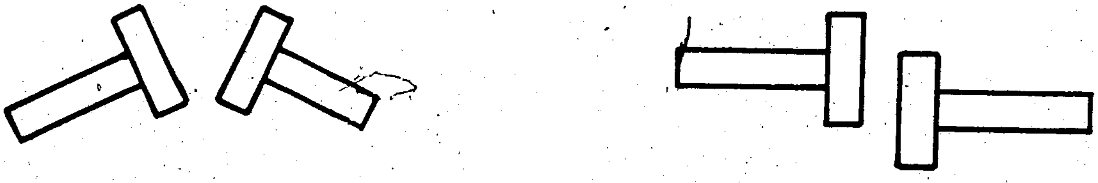

Fig. 2.4 Relative Movement of Flanged Sections

To find the loads on the bearings then became a matter of analyzing each of the stages between the flanges separately, i.e.

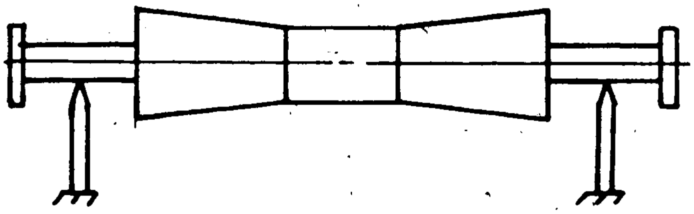

Fig. 2.5 Rotor Stages on Simple Supports

The 111 element model was used and the sections were taken as simply supported beams with the load being the weight of the shaft.

The radial clearance, length, and diameter of the bearings was determined from the drawings. The oil viscosity was found from steady state temperature data from the plant. Table 2.1 summarizes the bearing data.

2.1.3 Results

In order to find the film stiffness the Sommerfeld number is also required. The speed chosen for this was halfway between the first and sixth critical, i.e., an average value in the speed range of interest.

Once the system stiffness and mass matrices were defined the natural frequencies and mode shapes were generated. The equations of motion are:

$$[M]\underline{\ddot{x}} + [K]\underline{x} = 0$$

[M] Mass Matrix

[K] Stiffness Matrix (2.3)

which can be rewritten:

$$[D]\underline{\Phi} = \lambda^2\underline{\Phi}$$

$$[D] = [M]^{-1}[K]$$

λ^2 = eigenvalues

$\underline{\Phi}$ = eigenvector (2.4)

It should be noted here that for the purposes of designing the in-house rig the damping in the system was not considered. The eigenvalues and eigenvectors correspond to the natural frequencies and mode shapes respectively. The turbine operates above the sixth critical speed which makes starting up the unit a difficult process.

Table 2.2 shows the eigenvalues generated by the program both with and without the generator rotor. It can be seen by comparison that the first and sixth natural frequencies are the generator's effect on the system. It is interesting to note that the addition

Table 2.1 Bearing Film Stiffness

BEARING	L/D	RAD CL (IN)	LOAD (LB)	CHAR. NO.	STIFF. (LB/INx10^{-6})
1	0.56	0.007	5,400	0.84	1.40
2	0.59	0.00875	5,800	0.85	1.61
3	0.59	0.00875	12,000	0.88	1.55
4	0.75	0.01175	31,700	0.41	5.50
5	0.82	0.013	41,300	0.35	5.90
6	0.59	0.013	25,100	0.58	4.60
7	0.62	0.01125	49,700	0.37	12.0
8	0.62	0.01125	48,900	0.38	1.16
9	0.67	0.007	-	-	1.00

of the generator adds natural frequencies to the system without affecting most of the natural frequencies of the turbine by itself. Fig. 2.6 shows the corresponding mode shapes.

Fig. 2.7 shows a "critical speed map" for the turbine. The position of the present system is shown. From the graph it can be seen that the turbine exhibits a combination of rigid body and flexural motion. For rigid body motion the support stiffness is much less than the shaft stiffness. The natural frequencies for this situation are fairly low. Flexural motion

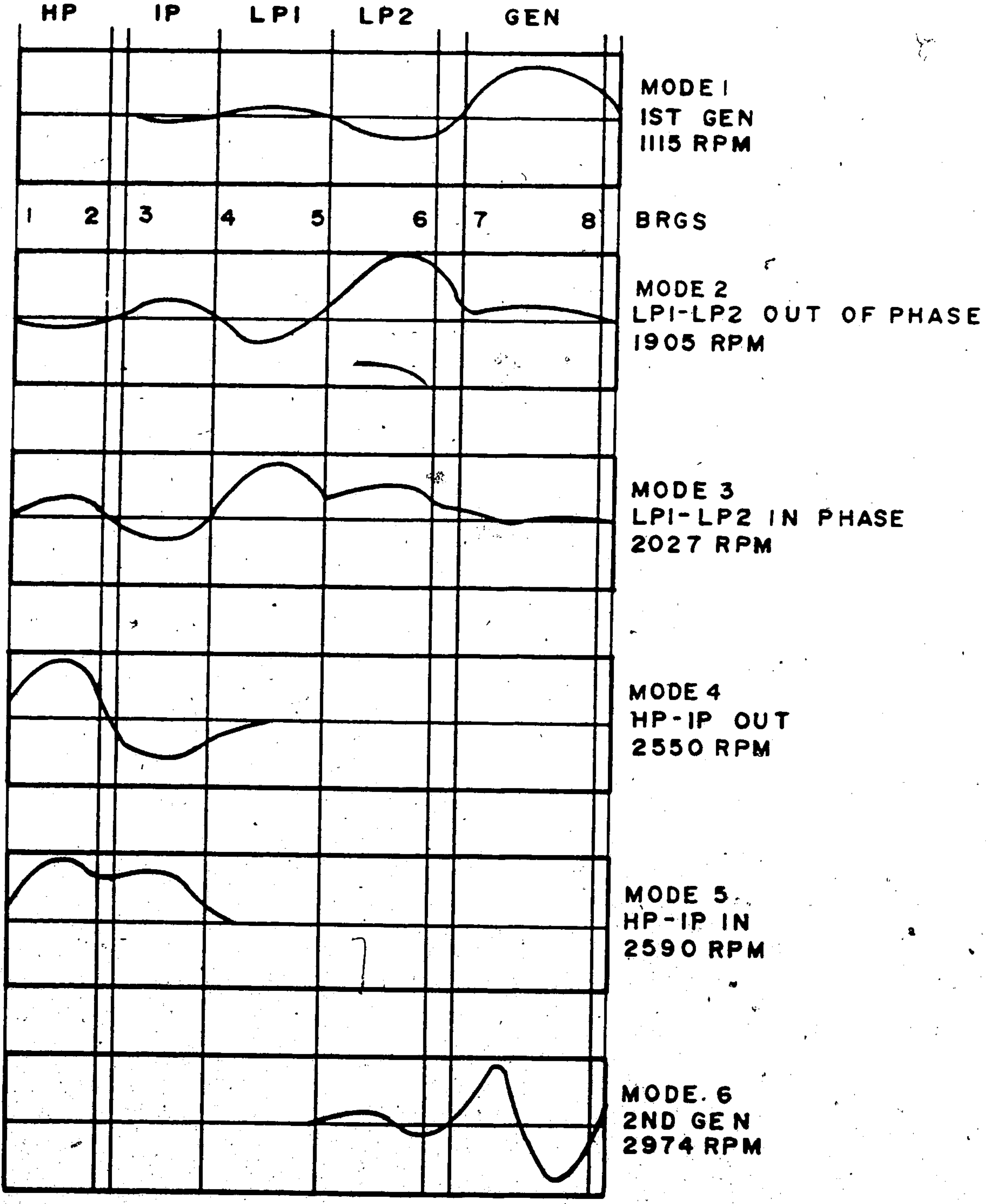
HP
IP
LP1
LP2
GEN
MODE 1
1ST GEN
1115 RPM
1 2 3 4 5 6 7 8
BRGS
MODE 2
LP1-LP2 OUT OF PHASE
1905 RPM
MODE 3
LP1-LP2 IN PHASE
2027 RPM
MODE 4
HP-IP OUT
2550 RPM
MODE 5
HP-IP IN
2590 RPM
MODE 6
2ND GEN
2974 RPM

Fig. 2.6 286 MW Turbine Modes

Table 2.2 Eigenvalues

MODEL 1	MODEL 2	DATA FROM TRANS-ALTA*
1860 RPM	1115	1000 (GEN)
2024	1905	1800 (LP-1-LP2)
2549	2027	
2590	2550	2800-3200
-	2590	2800-3200
-	2974	3200-3300

MODEL 1: 24 Elements - Turbine only

MODEL 2: 29 Elements - Turbine and Generator

*Data taken from measurement system installed on Unit #4 at Wabamun Power Station.

greatly affects the dynamics of the system as can be seen by the large differences in frequencies for different support stiffness.

In order to design a dynamic in-house model the relative stiffness of the shaft and bearings had to be kept constant for both the real turbine and the in-house model.

The natural frequencies and mode shapes described in this chapter were the basis for the design of the in-house model. Dimensionless ratios were formulated from the data and the in-house rig was designed to match these ratios in order to have a rig that behaved the same way from a dynamical point of view.

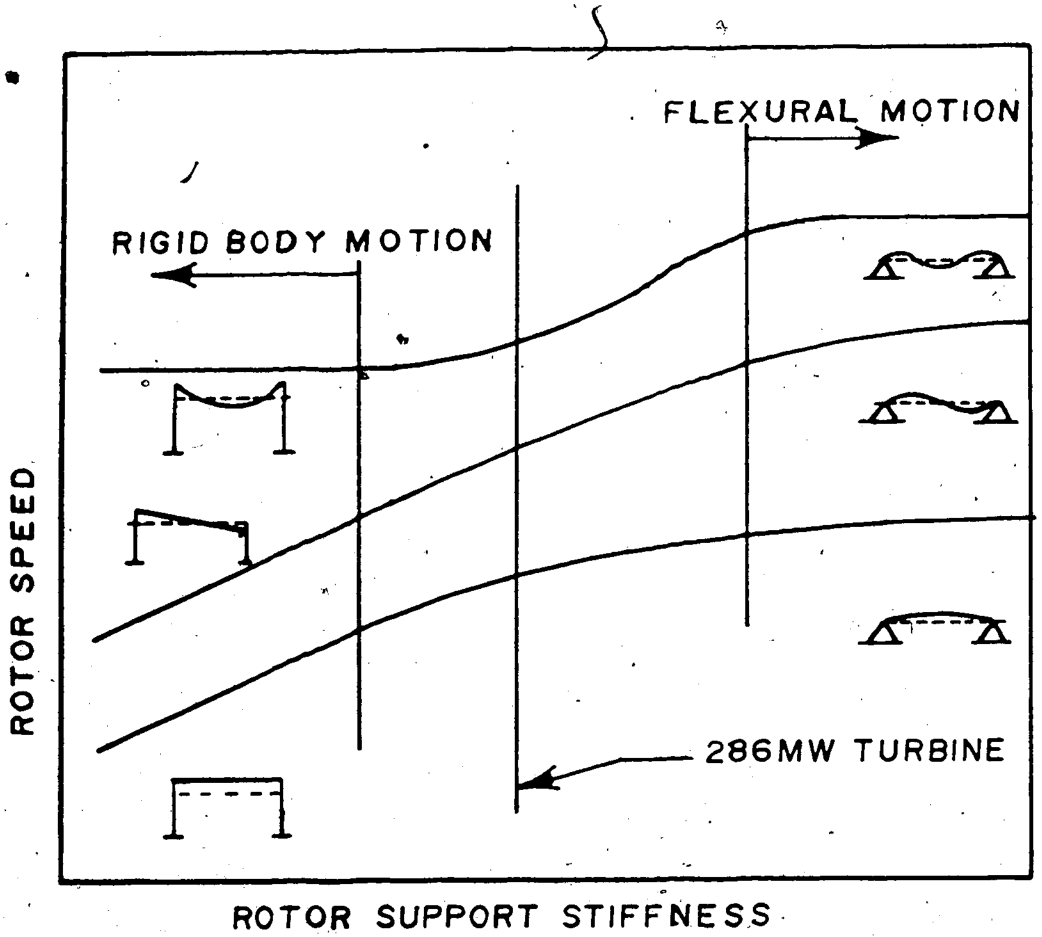
FLEXURAL MOTION
RIGID BODY MOTION
ROTOR SPEED
286MW TURBINE
ROTOR SUPPORT STIFFNESS

Fig. 2.7 Critical Speed Map

2.2 In-House Rig

The in-house rig is a dynamically scaled replica of the 286 MW steam turbine rather than a static one. A static replica would physically resemble the real turbine and the real turbine's overall dimensions and mass distribution would simply be scaled down to produce a miniature replica. If the rig were then rotated the natural frequencies would be completely different. The vibration characteristics would then have to be modified in order to be compared with the real turbine. A dynamic model, on the other hand, may not resemble the real turbine but when it is rotated there is some correlation between the mode shapes, natural frequencies, and response to an imbalance.

The in-house rig is basically a shaft and disc system (Fig. 2.8). The shaft represents the rotor while the discs simulate the blades. The shaft rides on four oil fed journal bearings. The rig consists of three "power" stages: high pressure, low pressure #1, and low pressure #2. The high pressure section represents the real turbine's high and intermediate pressure spans combined. To keep the rig as simple as possible the generator of the real turbine is not physically represented but its effect on the system is taken into account.

As shown in Fig. 2.8 the rig is driven by a variable speed D.C. motor. The coupling between the driving shaft and rig is a rubber type which damps-out vibration noise from the motor. The coupling also allows for misalignment which occurs when the shaft is whirling.

The four bearings are mounted to a steel frame which

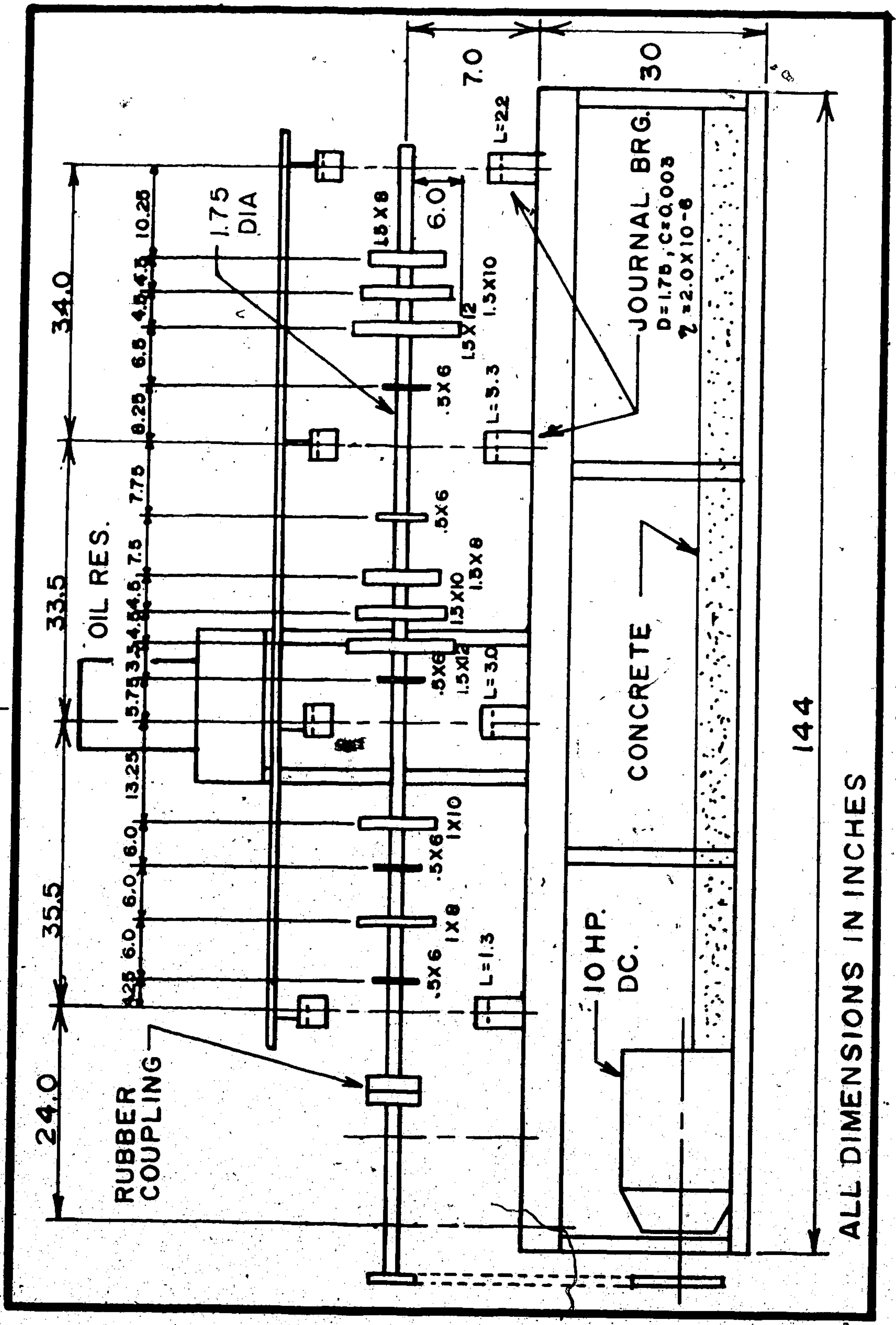
7.0
30
L=22
6.0
1.75 DIA
1.5 X 8
1.5X10
1.5 X 12
.5X6
L=3.3
JOURNAL BRG.
D=1.75, C=0.003
η =2.0X10-6
34.0
10.25
4.5
4.5
6.5
8.25
7.75
7.5
4.5
4.5
3.5
5.75
13.25
6.0
6.0
6.0
4.25
33.5
OIL RES.
.5X6
1.5X8
1.5X10
1.5X12
L=3.0
CONCRETE
144
1X10
.5X6
1X8
.5X6
L=1.3
35.5
10 HP.
DC.
24.0
RUBBER COUPLING
ALL DIMENSIONS IN INCHES

Fig. 2.8 In-House Rig

acts as the foundation for the rotor. This "pillar" type of support is not unlike the foundations for large steam turbines where the condensers are located between the pillars. Most large turbines are "low tuned". This means that the fundamental structural natural frequency is below the running speed of the machine. This produces less transmitted force to the ground (see Fig. 2.9). The in-house rig is also low tuned which will simulate the real case more accurately.

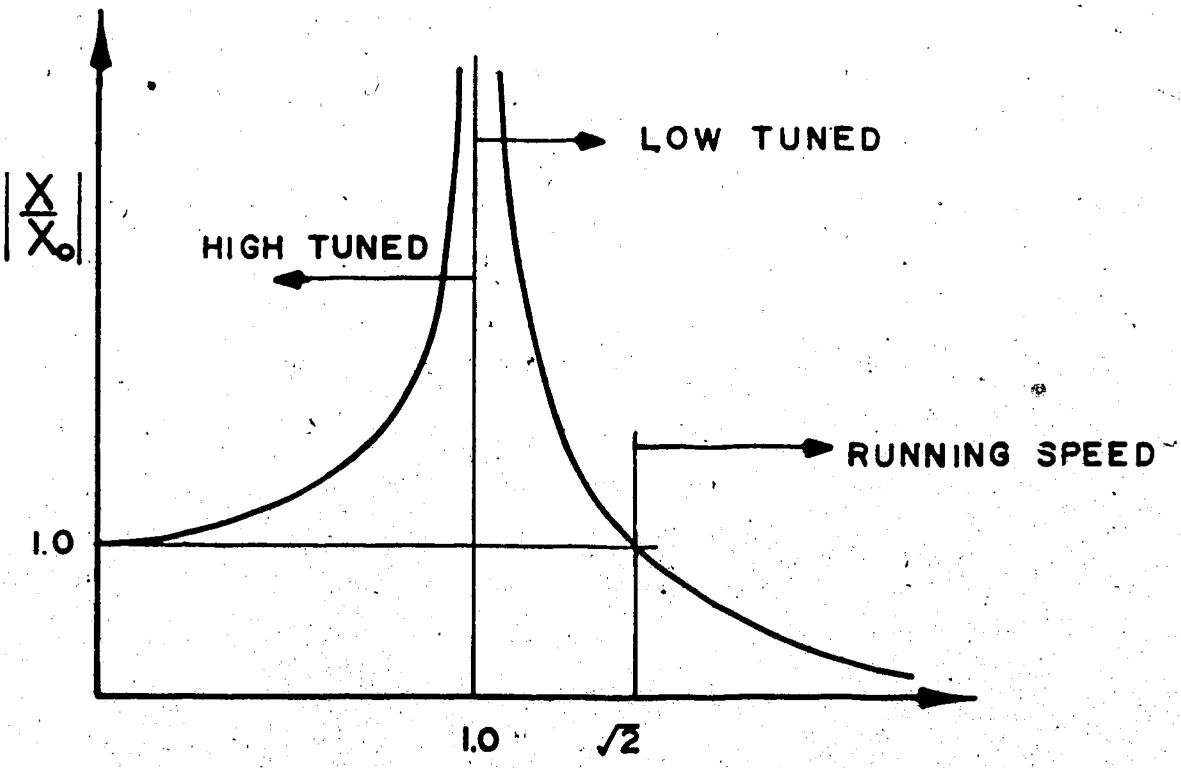

Fig. 2.9 Low Vs High Tuning a Machine

The effect of the low tuning on the vibrational characteristics is not included in the analysis.

2.2.1 Scaling Parameters

Four non-dimensional scaling factors were the basis for the design:

1. The ratio of the first three natural frequencies (i.e. ω_1/ω_2, ω_1/ω_3) of the rig are consistent with those of the real turbine.
2. The bearing Sommerfeld numbers are the same to within a reasonable accuracy.
3. The stiffness ratio is defined as the bearing film stiffness divided by the equivalent shaft span stiffness. The span stiffness is a simply supported beam loaded at its center. This ratio has been calculated to be the same for the real turbine and the in-house rotors.
4. The first three mode shapes of the rig have the same shape as those of the real turbine.

Table 2.3 summarizes the above scaling factors which will now be described in more detail.

2.2.2 Natural Frequencies

The operating speed of the real turbine is 3600 RPM, which is above the sixth critical speed (Fig. 2.6). If the generator is uncoupled from the turbine then 3600 RPM is above the fourth critical speed. If the H.P. and I.P.

stages were both incorporated into one span then it would be reasonable to say that the turbine operates above the third critical speed. The three critical speeds of the real turbine that are to be matched (as ratios) by the rig are: (LP1/LP2), (LP1/(HP-IP)AVE).

The second ratio LP1/(HP-IP)AVE is found by averaging (HP-IP) in phase and (HP-IP) out of phase (see Fig. 2.6). This is reasonable for two reasons. (1) the major vibration problems occur in the low pressure end of turbine, and (2) to have four spans in the rig would make it too complicated.

Table 2.3 Scaling Parameters

Natural Freq. Ratios

	286 MW Turb.	In-House Rig
ω_1/ω_2	.90	.91
ω_1/ω_3	.78	.73

Sommerfeld Numbers

BRG	286 MW Turb.	In-House Rig
1	.79	.75
2	.43	.49
3	.39	.47
4	.48	.57

Stiffness Ratios

	286 MW Turb.	In-House Rig
BRG 1/SPAN 1	1.00	.97

Table 2.3 Scaling Parameters (Cont.)

Stiffness Ratios

	286 MW Turb.	In-House Rig
BRG 2/SPAN 1	2.12	1.88
BRG 2/SPAN 2	1.65	1.65
BRG 3/SPAN 2	1.98	1.70
BRG 3/SPAN 3	1.81	1.70
BRG 4/SPAN 3	0.9	1.30

2.2.3 Sommerfeld Numbers

The rig has four bearings while the real turbine has nine. The bearings eliminated in the construction of the rig are the three supporting the generator (7, 8 and 9) and the two between the HP and IP stages (2 and 3). The bearings retained are shown in Fig. 2.10. The Sommerfeld number (Sn) defined by Shigley(9) is

$$Sn = \left(\frac{r}{c}\right)^2 \eta\, N/P$$

r = journal radius (IN)
c = radial clearance (IN)
η = absolute viscosity (REYNS)
N = speed (RPS)
P = unit load (LB/SQ.IN.) (2.5)

The speed region that is of interest, as in the case of the real turbine, is between the first and third critical speeds. To compare the Sommerfeld numbers the speed used for the real turbine is 2500 RPM and the speed fcr the rig was determined by an iterative procedure.

Unlike the real turbine, the rig's shaft center line is not built on a catenary. To calculate the loads on the bearing is, therefore, a more complicated procedure. The loads on the bearings are speed dependent. Since each span is not simply supported and the bearing film stiffness does not change linearly with speed the loads on each bearing will change slightly with speed. This is not the case for the real turbine because most of the spans are simply supported.

The determination of the bearing loads for the rig was an iterative procedure since to find the film stiffness the load and Sommerfeld numbers are required, and conversely, the load on the bearings is determined by the stiffnesses. The natural frequency ratios were already determined by the real turbine analysis. An approximate speed for comparison was therefore determined. Once this speed was determined, the loads were found as follows:

1. Assume a stiffness for all the bearings
2. Calculate, using a finite element analysis, the bearing loads for the statically indeterminate problem.

e.g.

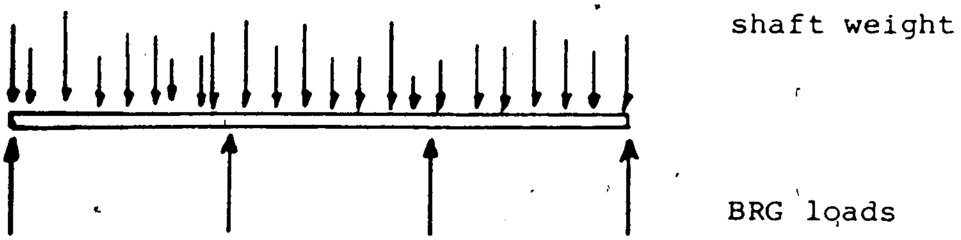

3. Calculate the Sommerfeld numbers from these loads.

4. Use the NRC charts[(10)] to find the stiffness of the oil film.

5. Compare this stiffness with the assumed stiffness.

2.2.4 Stiffness Ratios

The stiffness ratio is defined as the shaft span stiffness (K_{SPAN}) divided by the bearing film stiffness (I_F):

i.e.

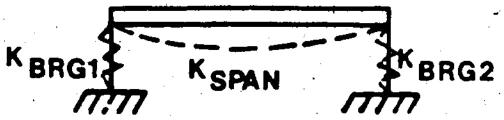

Each span had, therefore, two ratios

$$K\ \text{span}/_{K_{BRG1}}\ , \qquad K\ \text{span}/_{K_{BRG2}}$$

The method used to determine the bearing film stiffnesses has already been described.

The spans, both for the real turbine and the rig, per node: the vertical displacement (W) and the nodal were taken to be simply supported beams. To determine the equivalent stiffness of each span a load was placed at the center and the corresponding deflection was calculated. The shaft, for this calculation, was assumed to have no mass. The span stiffness was then calculated by dividing the load by the deflection at the center span.

2.2.5 Mode Shapes

The real turbine, as stated before, has six modes below 3600 RPM, while the rig has only three. The real turbine modes that were chosen for comparison are 1, 2, 4 (see Fig. 2.8). Mode #4 was chosen since the HP and IP are in-phase and with the rig this also had to be the case. Fig. 2.10 compares the mode shapes.

2.2.6 Modelling Procedure

It should be noted here that these scaling parameters are merely a method of design. To completely describe the vibrational characteristics of any rotor is a two plane problem. Thus far both the real turbine and the rig have been described as one plane systems. The single plane comparison is considered sufficient for design purposes.

Obviously all four parameters are interrelated and, therefore, the procedure used was

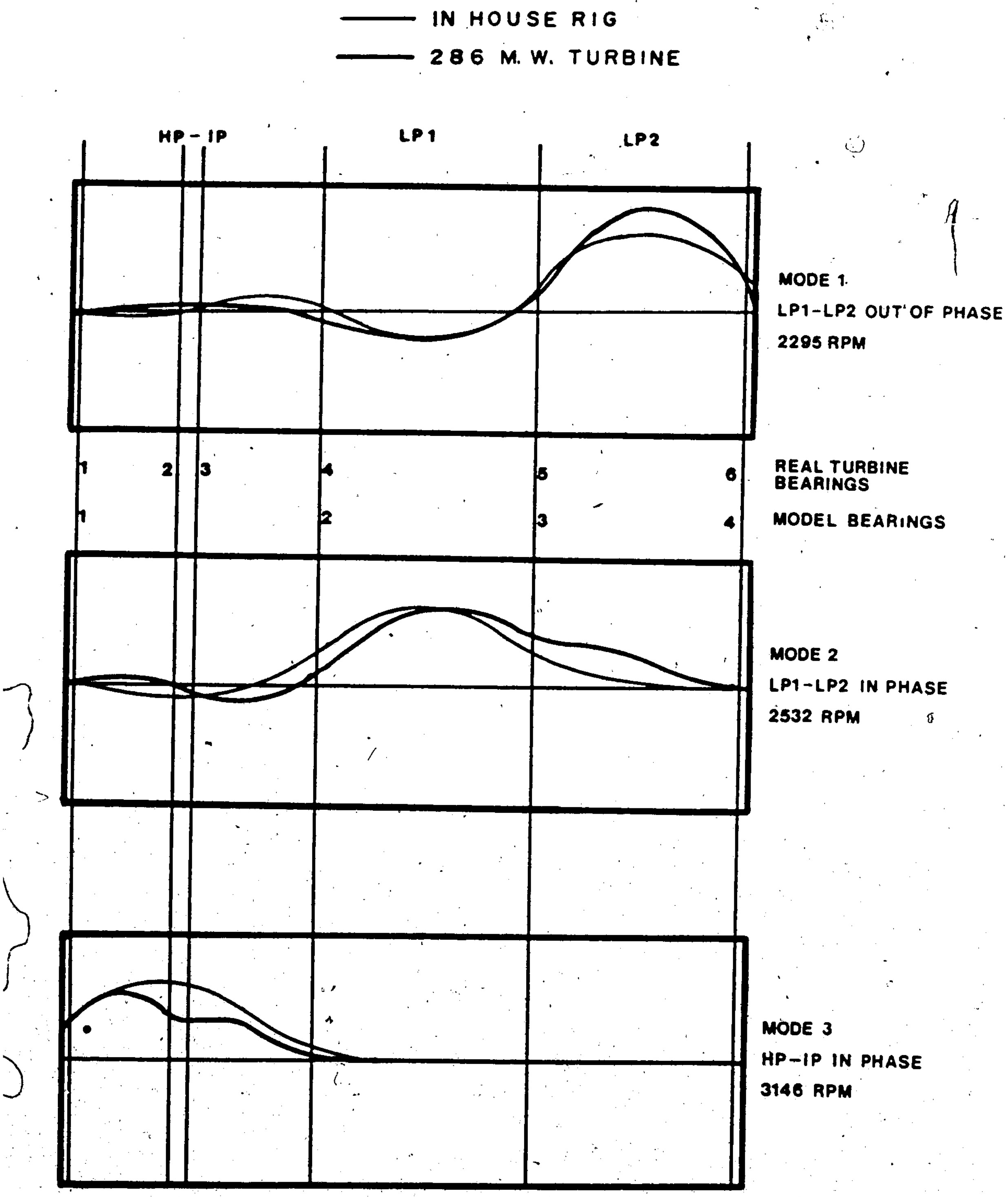

Fig. 2.10 Mode Shapes of Rig Compared to 286 MW Turbine

an iterative one. Fig. 2.11 shows a flow chart for the convergence.

There are several independent variables: shaft length, shaft diameter, disc size, disc position, bearing stiffness, etc. Changing any one of these has some effect on the overall dynamic system. Fig. 2.12 shows all of the independent variables and their subsequent effect on the scaling parameters. The flow chart gives the reader an idea of the complexity and interrelationship of the scaling parameters.

A three span system was chosen in order to match the three mode shapes 1, 2, 4 of the real turbine. From Fig. 2.11 the mode shapes and natural frequencies were the first parameters to be matched with the real turbine. The mode shapes and natural frequencies were changed by varying the span lengths and size/position of the discs.

Once the mode shapes and natural frequencies showed good comparison with the real turbine the stiffness ratios and Sommerfeld numbers were analyzed. The stiffness ratio was changed by varying the span lengths and film stiffnesses, while the Sommerfeld numbers varied by L/D ratio, radial clearance, and oil viscosity.

This procedure was repeated until all four scaling factors were within ± 10%.

Parameter

(Dependent Variable)

Changes made

(Independent Variable)

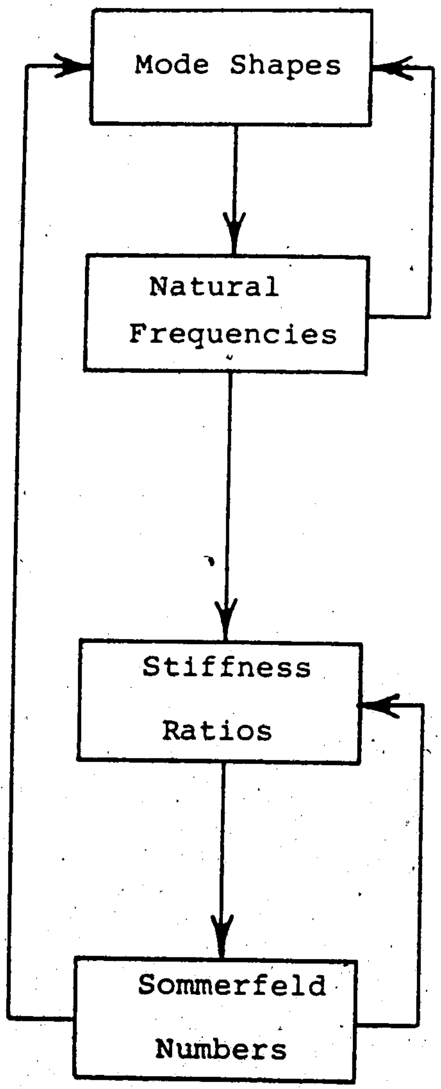
Mode Shapes
Natural Frequencies
Stiffness Ratios
Sommerfeld Numbers

1. Disc size and position
2. Span length
3. Bearing film stiffness

1. Span length
2. Bearing film stiffness

1. L/D ratio
2. Radial clearance
3. Oil viscosity

Fig. 2.11 Scaling Parameters Flow Chart

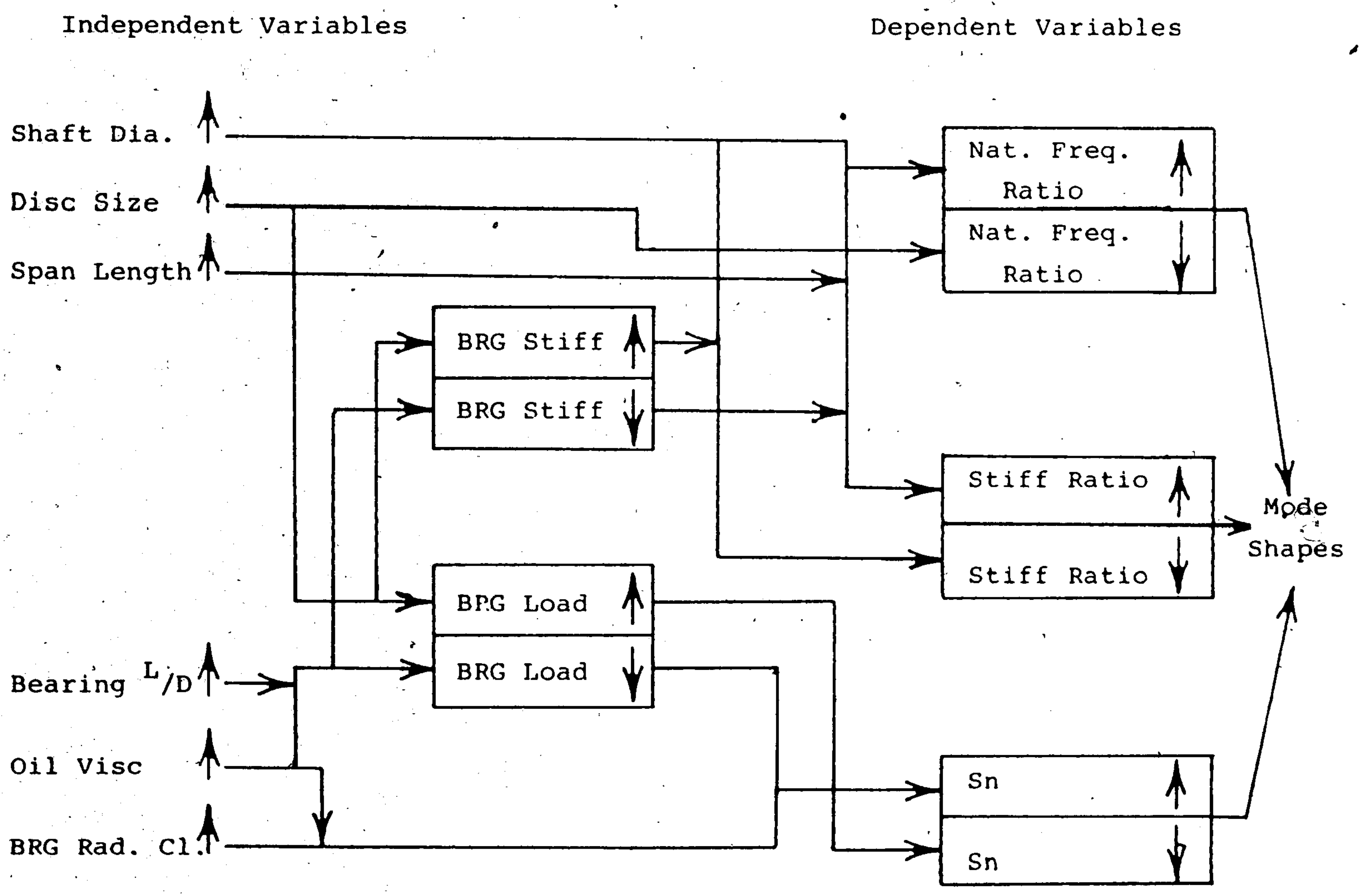
Independent Variables
Dependent Variables
Shaft Dia.
Disc Size
Span Length
Bearing L/D
Oil Visc
BRG Rad. Cl.
BRG Stiff
BRG Stiff
BRG Load
BRG Load
Nat. Freq. Ratio
Nat. Freq. Ratio
Stiff Ratio
Stiff Ratio
Sn
Sn
Mode Shapes

Fig. 2.12 Effect of Independent Variables

3. NON-ROTATING ANALYSIS

Abstract

This chapter will discuss the non-rotating vibrational characteristics for the in-house model. Numerical results are compared with experimental in order to test the accuracy of the symmetric stiffness and mass matrices. Also, a measure of the system's structural damping is discussed.

3.1 Beam Theory

All of the numerical work presented in this thesis utilizes the Timoshenko beam element given by Thomas(1). The two-dimensional analysis of the real turbine and the design of the rig were based on this element. For a single plane or two dimensional analysis the system is assumed to be symmetric for any plane passing through the shaft axis. For non-rotational testing the system is symmetric, and a single plane numerical analysis was adequate. For rotating systems with oil film bearings and gyroscopic effects, however, the system is not symmetric and a three dimensional or two plane analysis is required.

The Timoshenko element has two degrees of freedom rotation (θ). (See Fig. 3.1).

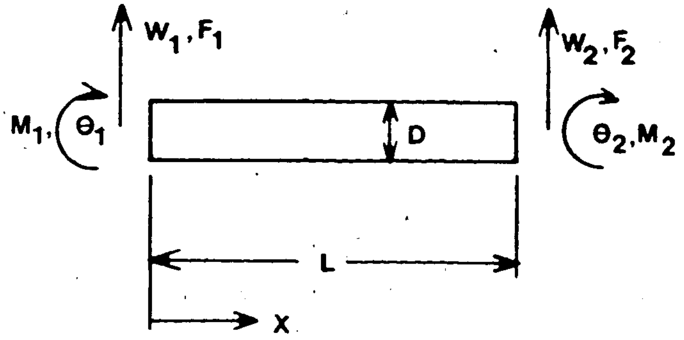
W_1, F_1
W_2, F_2
M_1, θ_1
θ_2, M_2
D
L
X

Fig. 3.1 Timoshenko Beam Element

The sign convention adopted is positive displacement upwards and positive rotation counter clockwise. The nodal rotation θ is the slope due to the bending moment M. The slope $\partial W/_{\partial X}$ is due to the moment M and the shear force F. These parameters are related by

$$\theta = \partial W/_{\partial X} + \psi \qquad (3.1)$$

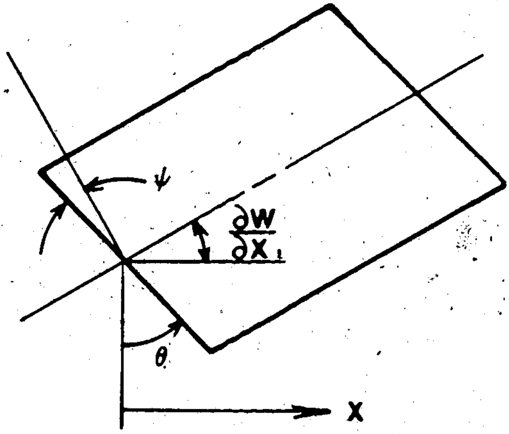
ψ
$\frac{\partial W}{\partial X}$
θ
X

Fig. 3.2 Definition of Nodal Rotation (θ)

For long and slender elements the simple euler beam given by Archer(13) is sufficient to describe the dynamics of the system. In this element the deflection $\omega(x,t)$ is assumed to be due only to the bending moment. This means that the shear deformation and the rotatary inertia are neglected in the analysis. For the present analysis however, the elements are not long and slender and the Timoshenko element is used.

The equation of motion for an Euler-beam is

$$EI\frac{\partial^4 W}{\partial X^4} + m\frac{\partial^2 W}{\partial t^2} = 0 \qquad (3.2)$$

where:

m - mass/unit length

E - modules of elasticity

I - 2nd moment of area

Two additional terms are added due to the shear and rotatary inertia:

$$M\frac{\partial^2 W}{\partial t^2} = \frac{-\partial V}{\partial X}; \quad J\frac{\partial^2 \theta}{\partial t^2} = \frac{\partial M}{\partial X} - V; \quad \theta = \frac{\partial W}{\partial X} + \frac{V}{KAG} \qquad (3.3)$$

which yields the equation for the Timoshenko element:

$$EI\frac{\partial^4 W}{\partial X^4} + M\frac{\partial^2 W}{\partial t^2} - \left(J + \frac{EIM}{kAG}\right)\frac{\partial^4 W}{\partial t^2 \partial X^2} + \frac{JM}{kAG}\frac{\partial^4 W}{\partial t^4} = 0 \qquad (3.4)$$

where:

k - shape factor (based on geometry of X-sec)

A = cross sectional area

G - shear modulus

J - rotatary inertia/unit length

In matrix form the stiffness and mass terms are as follows:

$$K = \frac{EI}{\ell^3(1+\phi)} \begin{bmatrix} 12 & & & \\ 6\ell & \ell^2(4+\theta) & & \text{sym} \\ -6\ell & & 12 & \\ 6\ell & \ell^2(2-\theta) & -6\ell & \ell^2(4+\theta) \end{bmatrix}$$

where: $\phi = \dfrac{12EI}{GKA\ell^2}$

$$M = \frac{\ell A \ell}{(1+\phi)^2} \begin{bmatrix} M_1 & & & \\ M_2 & M_5 & \text{sym} & \\ M_2 & -M_4 & M_1 & \\ M_4 & M_6 & -M_2 & M_5 \end{bmatrix} \tag{3.5}$$

$$+ \frac{\ell A \ell}{(1+\phi)^2}\left(\frac{r}{\ell}\right)^2 \begin{bmatrix} M_7 & & & \\ M_8 & M_9 & \text{sym} & \\ -M_7 & -M_8 & M_7 & \\ M_8 & M_{10} & -M_8 & M_9 \end{bmatrix}$$

where:

$M_1 = (13/25 + 7\phi/10 + \phi^2/3)$

$M_2 = (11/210 + 11\phi/120 + \phi^2/24)\ell$

$$
\begin{aligned}
M_3 &= ({}^{9}/70 + {}^{3\phi}/10 + {}^{\phi^2}/24) \\
M_4 &= -({}^{13}/420 + {}^{3\phi}/40 + {}^{\phi^2}/24)\ell \\
M_5 &= ({}^{1}/105 + {}^{\phi}/60 + {}^{\phi^2}/120)\ell^2 \\
M_6 &= -({}^{1}/140 + {}^{\phi}/60 + {}^{\phi^2}/120)\ell^2 \\
M_7 &= {}^{6}/5 \\
M_8 &= ({}^{1}/10 - {}^{\phi}/2) \\
M_9 &= ({}^{2}/15 + {}^{\phi}/6 + {}^{\phi^2}/3)\ell^2 \\
M_{10} &= ({}^{-1}/30 - {}^{\phi}/6 + {}^{\phi^2}/6)\ell^2
\end{aligned}
\tag{3.6}
$$

The inertia of the discs is added at a node in the mass matrix. The location of the discs determined the length of the elements since the mass of the disc had to be added between two elements, i.e., at a node in the system. The mass of the disc is $M = \rho \ell \pi r^2$ and the rotatary inertia $I = \frac{1}{2}Mr^2$.

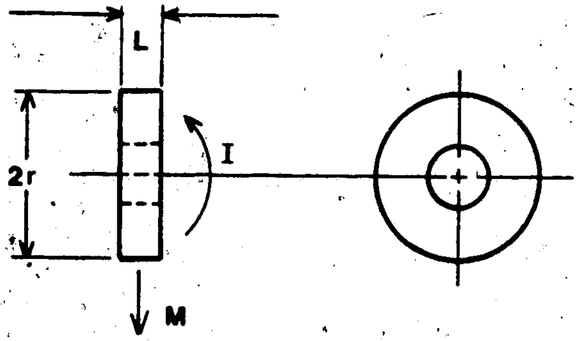

Fig. 3.3 Disc Dimensions and Inertia

The discs have a hole at their centre and the mass and inertia of each was adjusted accordingly.

The single degree of freedom system shown in Fig. 3.4

has equation of motion $K X + C \dot{X} + M \ddot{X} = Fe^{i\omega t}$ (3.7)

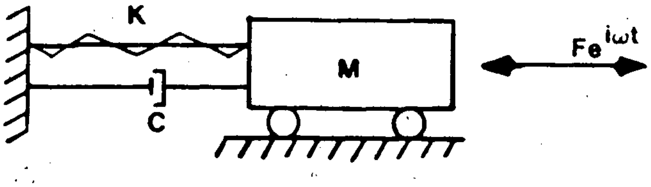

Fig. 3.4 Single Degree of Freedom System

Assuming a harmonic forcing function, the solution is of the form:

$$X(t) = Xe^{i\omega t} \tag{3.8}$$

and therefore, the general solution is:

$$\{[K-M\omega^2] + iC\omega\}X = F \tag{3.9}$$

This solution is the basis for the non-rotating analysis. To expand the solution to a system of more than one degree of freedom a normal mode approach is used. The damping term C in equation 3.7 is termed "viscous" damping and the force it exerts on the mass is proportional to the velocity. For the problem of a beam vibrating in reverse bending this term is non-existent. The type of damping present is referred to as "structural" damping. From Thompson(6) the energy dissipated per cycle is independent of the frequency over a wide frequency range, and proportional to the square of the vibration amplitude.

The structural damping factor, from Kennedy and Pancu$^{(2)}$ can be introduced into equation 3.7 as a complex stiffness, i.e.,

$$M\ddot{X} + K(1+ig)X = Fe^{i\omega t} \qquad (3.10)$$

From this the steady state amplitude becomes

$$X = \frac{F}{(K-M\omega^2) + igK} \qquad (3.11)$$

The damping factor g will be referred to as the proportional damping coefficient.

For a multi-degree of freedom system this proportional damping coefficient may have different values corresponding to different modes. An average value will be determined from the experimental data and this will be used in the numerical calculations for the rotating system (Chap. 4). For the rotating tests, both structural and bearing damping are present and therefore the determination of the structural coefficient, from non-rotating tests was a necessity.

The damping natural frequency for a single degree of freedom system with structural damping is

$$\omega_d = \omega_n(1-(g/2)^2)^{\frac{1}{2}} \qquad (3.12)$$

and therefore, for small (>0.1) values of g the natural frequencies and mode shapes of the multi-degree of freedom system shown in Fig. 3.7 can be determined numerically from an eigen value analysis (equation 2.3) utilizing the stiffness and mass matrices (equation 3.5 and 3.6).

3.2 Natural Frequencies and Mode Shapes

The numerical values for the natural frequencies and mode shapes have been verified through the use of non-rotating tests. The shaft was supported on rigid foundations at each end and was therefore analysed as a simply supported beam. (Fig. 3.5).

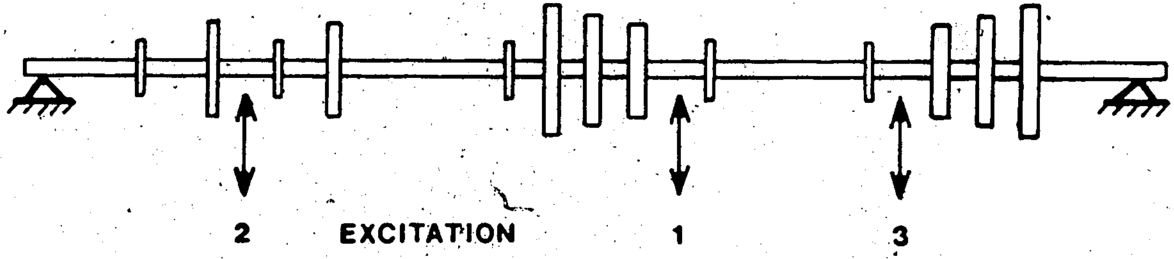

Fig. 3.5 In-House Rotor on Rigid Foundations

The numerical results were compared with experiment via the three excitation locations shown in Fig. 3.5. The shaft was excited with a shaker table with frequency sweeps from 0-500 HZ. An accelerometer was placed at various locations along the shaft and a spectrum analyser was used to measure the mode shapes at each of the natural frequencies.

Fig. 3.6 shows a typical frequency vs amplitude plot.

Table 3.1 : Natural Frequencies

NUMERICAL		EXPERIMENTAL		
MODEL 1	MODEL 2	EXCITATION LOCATION		
18 EL	24 EL	1	2	3
6.0HZ	7.0	10.0HZ	8.0	9.0
22.7	29.5	32.0	29.7	31.5
52.2	57.2	56.0	55.5	55.5
107.0	114.4	146.0	112.2	107.0
267.6	133.3	171.0	170.0	225.0

Two numerical models, which consisted of 18 and 24 elements, were compared with experimental data. The only difference in the models was the method used to incorporate the large discs into the system. The major effect of the discs on the system is the addition of mass. In the in-house rig the discs were shrunk onto the shaft and therefore will also add some stiffness to the system. The 18 element model has only the mass effect while the 24 element model incorporates both mass and stiffness (see Fig. 3.7).

From Table 3.1 the 24 element model matches the experimental data more accurately than does the 18 element model.

The 24 element model adds the stiffness of the discs by introducing them into the system as a small element. The length of the element is the same as the

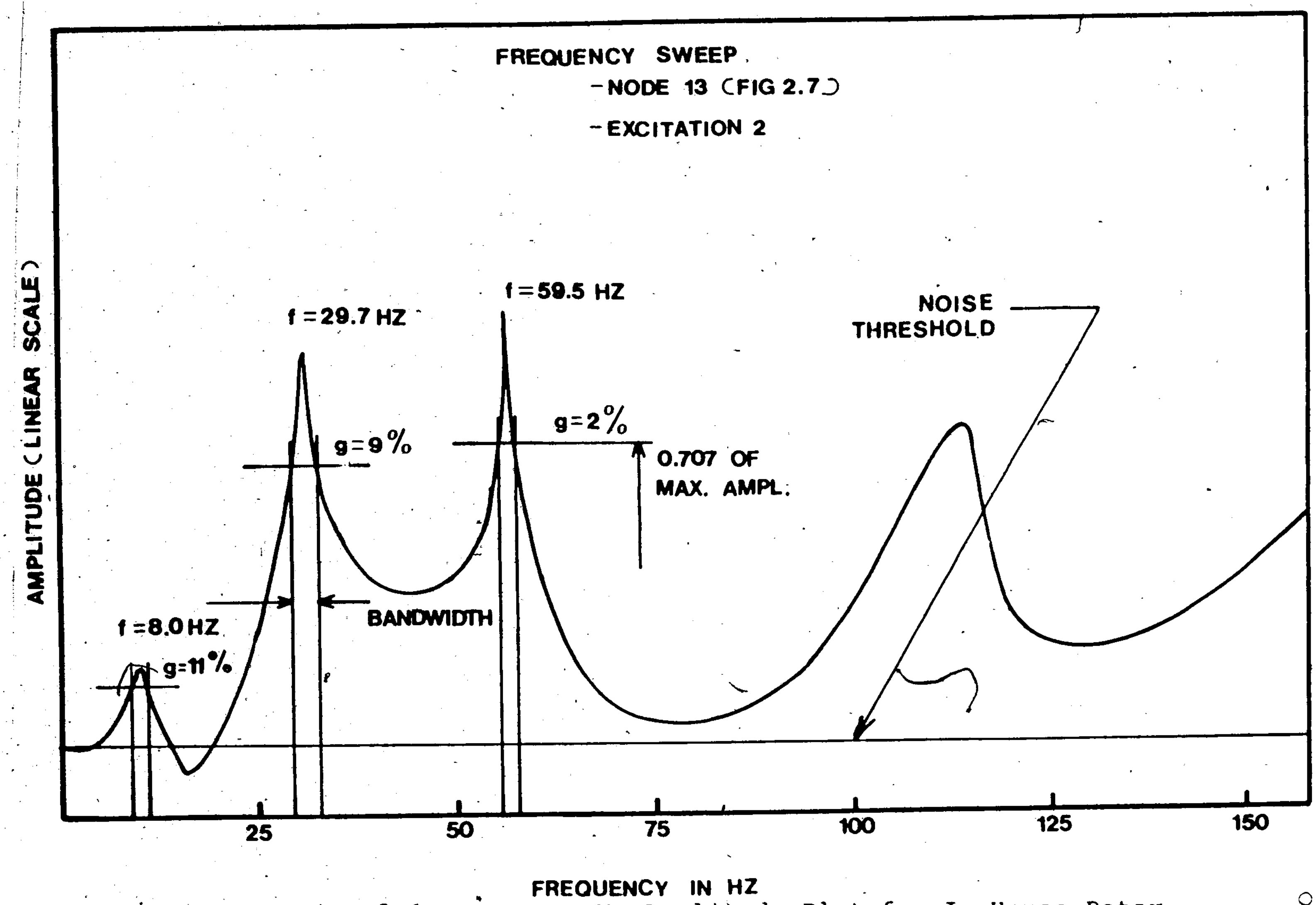

Fig. 3.6 Frequency Vs Amplitude Plot for In-House Rotor

thickness of the disc while the diameter was chosen to be 2.25 in which is 0.5 in larger than the shaft diameter. The diameter of the element was chosen to add sufficient stiffness to the system without causing numerical errors due to small $^r/d$ factors. The value of 2.25 in yielded the best correlation with experimental data.

The 24 element model compares best with excitation location No. 2 (Fig. 3.5). The natural frequencies, for the second and third modes, are 0.02% low and 0.1% high respectively. The first mode, however, is 12% low. From Table 3.1 it is seen that the location of the excitation force has a marked effect on the values of the natural frequencies, especially on the fundamental mode. The displacements were of the order of 3-4 in, at the centre span, due to the large shaft mass. This caused the excitation to be non-linear at this low frequency. Excitation at position No. 2 was chosen for the analysis due to the relatively low mass of the shaft at this location. The non-linear effect was therefore minimized.

Fig. 3.9 compares the measured mode shapes with the numerically predicted ones. The mode shapes are almost identical for modes 1 and 2. The computed amplitudes for the third mode are lower than the measured values in

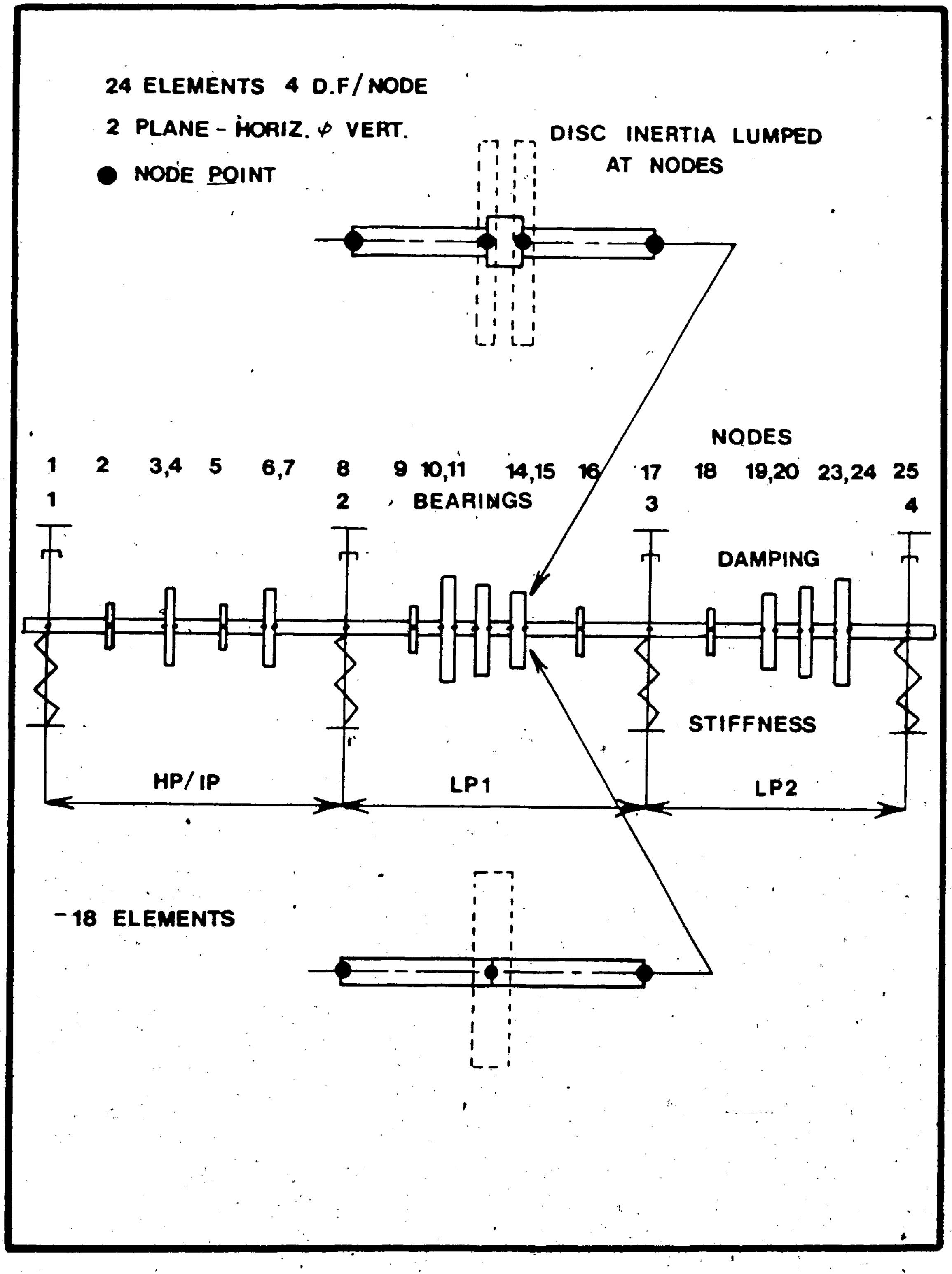
24 ELEMENTS 4 D.F/NODE
2 PLANE - HORIZ. & VERT.
● NODE POINT
DISC INERTIA LUMPED AT NODES
NODES
1 2 3,4 5 6,7 8 9 10,11 14,15 16 17 18 19,20 23,24 25
1 2 BEARINGS 3 4
DAMPING
STIFFNESS
HP/IP
LP1
LP2
-18 ELEMENTS

Fig. 3.7 Finite Element Model For In-House Rig

the LP1 and LP2 end of the shaft. The overall shape, however, compares reasonably well. The divergence from experiment in the high modes is indicative of any computer model. For this paper only the first three modes are analyzed and therefore, the stiffness and mass matrices are considered accurate enough.

Once the stiffness and mass matrices were established static tests were analyzed to estimate the internal or structural damping in the system. From Kennedy & Pancu(2) the damping factor g is different for each mode and is proportional to the stiffness of the system but 90° out of phase with it. For one mode the equation of motion with structural damping is

$$M\ddot{X}+K[1+ig]X = Fe^{i\omega t} \qquad (3.13)$$

From Craggs(3) this damping factor can be determined from the half power points. Fig. 3.8 shows the half power points.

The quantity g is then defined as

$$g = \frac{\omega_2 - \omega_1}{\omega_n} \qquad (3.14)$$

where ω_n is the natural frequency

ω_1, ω_2 are the natural frequencies corresponding to the ½ power points

3

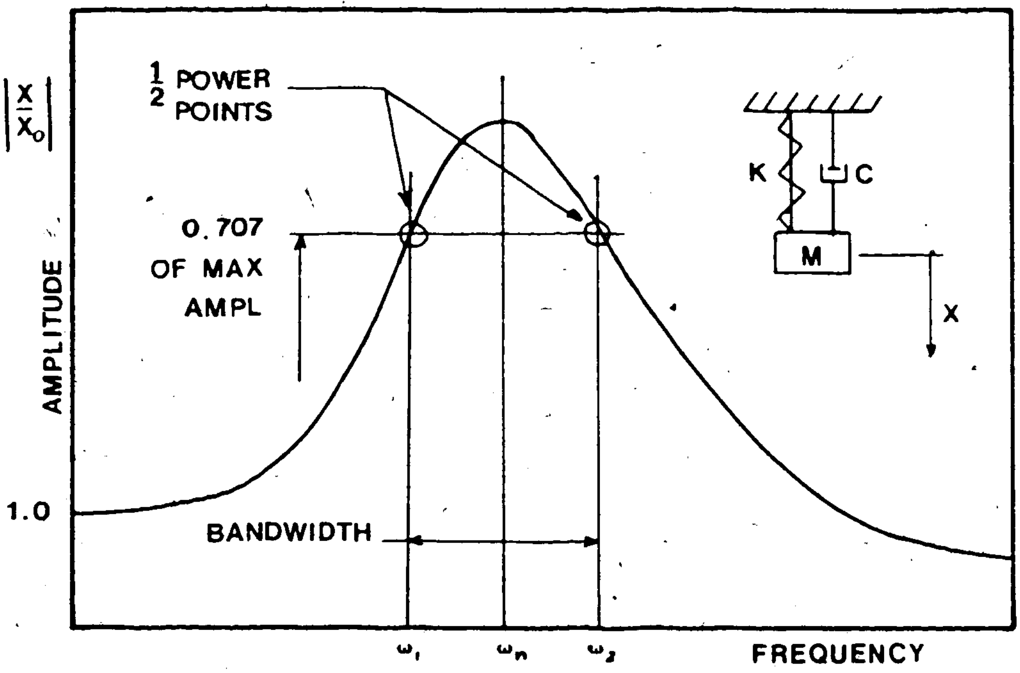

Fig. 3.8 Definition of ½ Power Points

From Fig. 3.6 it is obvious that for each mode there will be a different value of the structural damping factor g. For the generalization of the single degree of freedom system described above into the continuous nature of the 24 element model the values from the first three modes were averaged:

$g_1 = 0.11$
$g_2 = 0.09$
$g_3 = 0.02$ (See Fig. 3.6)

to yield an average value of ≈ 7%. This value will be

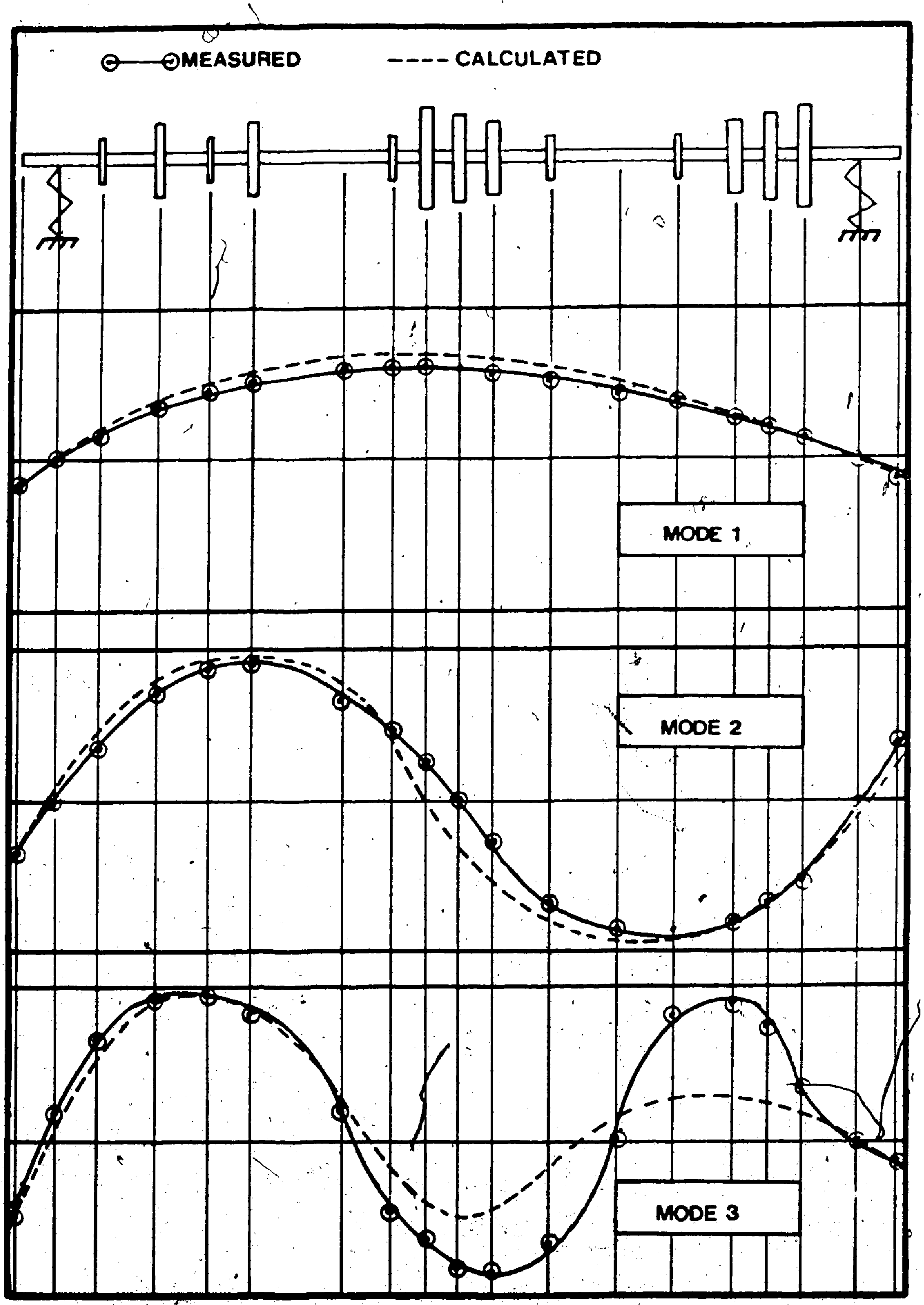

Fig. 3.9 Mode Shapes for Non-Rotating Test

termed the proportional damping factor and will be used for the rotating rotor analysis which will be described in Chap. 4. The bulk of the study is concerned with frequencies below 70 HZ and therefore damping factors above the third mode were not considered.

4. ROTATING ANALYSIS

Abstract

Two major factors are added to a rotating system as opposed to the non-rotating system of chapter 3. The whirling of the rotor adds a gyroscopic effect and the fluid film bearings add both stiffness and damping to the system. As well, the magnitude of the bearing terms are frequency dependent. These effects will be added to the system and the natural frequencies and mode shapes compared for experimental data with numerical results.

4.1 Gyroscopic Effects

As described in Chapter 3 the mass (and rotatory inertia) and stiffness of the discs have been taken into account for a single plane vibrating system. The gyroscopis effect, i.e., the moments of the inertia forces due to angular movements of the axis of the rotating masses, must also be accounted for (Timoshenko(11)). The shaft whirling speed is considered to be equal to the rotating speed. This is termed synchronous whirling. This component dominates the shaft vibration near critical speeds and is therefore, the one used to balance rotors. The higher order components, such as half frequency whirl, is a stability characteristic of journal bearings, and are not considered here.

Fig. 4.1 shows a single disc on a shaft which is a problem presented by Timoshenko(11). Once the equations of motion for this simple system have been developed the generalization to the finite element model can be made.

The position of the disc is completely described by the position of the center of gravity 0 and the angles β and γ.

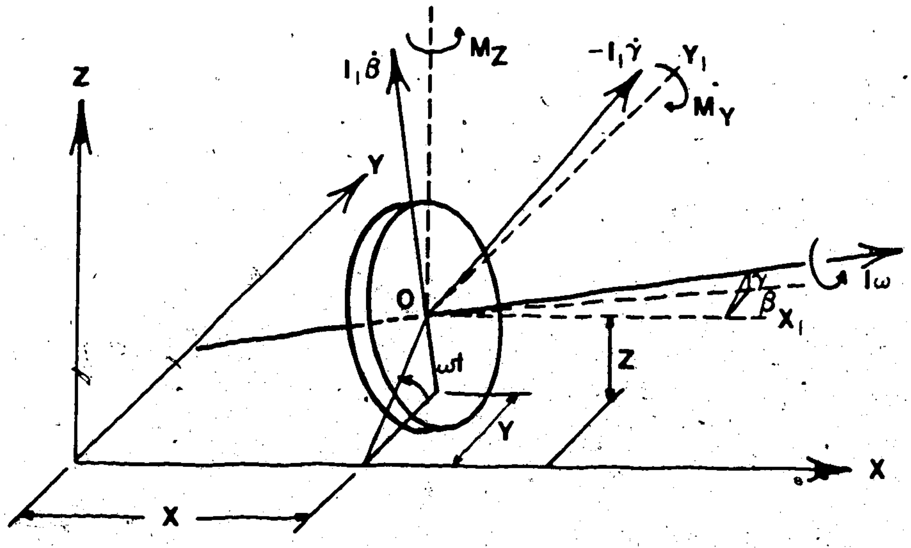

Fig. 4.1 Gyroscopic Terms for a Disc

Thus four variables are required to fully describe each node in the shaft disc system of Chapter 3. The simple Timoshenko beam element with ω and θ as the nodal degrees of freedom must be expanded to two planes with W_X, θ_X, W_y, θ_y, which correspond to y, β, z, γ respectively.

The static deflection of the shaft due to its own weight and the weight of the discs is not included in the analysis since for any vibrations problem, the reference position is at static equilibrium. The solution is based on the principle of angular momentun, i.e., the rate of increase of the total moment of momentum of any moving system about any fixed axis is equal to the total moment of the external forces about this axis. Letting I = moment of inertia of the disc about axis 00 and $I_1 = I/2$ = mo[illegible]t of inertia of the disc about a diameter.

From the principal of angular momentum:

$$-d/_{dt}[I\omega\beta - I_1\dot{\gamma}] = My$$

$$d/_{dt}[I\omega\gamma + I_1\dot{\beta}] = M_Z \qquad (4.1)$$

Summing the moments about the disc center of gravity gives:

$$My = -m^1 z + n^1 \gamma$$

$$Mz = m^1 y - n^1 \beta \qquad (4.2)$$

m^1, n^1 = constants

Similarly, summing the forces:

$$\frac{W}{g}\ddot{y} + my + n\beta = 0$$

$$\frac{W}{g}\ddot{z} + m\dot{z} + n\gamma = 0 \qquad (4.3)$$

$\frac{W}{g}$ = disc mass

M, n = constants

Equating 4.1 to 4.2 in conjunction with 4.3 yields four equations which are solved simultaneously to obtain the four variables y, z, β, γ. The assumed solutions are

$$y = A \sin \omega T$$
$$z = B \cos \omega T$$
$$\beta = C \sin \omega T$$
$$\gamma = D \cos \omega T \qquad (4.4)$$

These assumed solutions correspond to Eq. 3.8 and thus the gyroscopic terms can be incorporated into the system easily.

The general differential equation from Meirovitch(4) for a damped gyroscopic system is

$$[M]\ddot{X} + \{[G]+[C]\}\dot{X} + [K]X = F \qquad (4.5)$$

where M, C, K, G are real matrices. The stiffness and damping matrices are symmetric only for symmetric bearings. Journal bearings, however, are not symmetric. The gyroscopic matrix is skew symmetric and is incorporated into the damping matrix since the force it produces is proportional to the velocity of the shaft.

According to Homes(8), assuming asynchronous circular whirl, the gyroscopic terms, combined with the equations of motion for a Timoshenko beam element, can be incorporated into the mass matrix with a single factor H. This factor is the whirl ratio which is defined as the shaft speed divided by the whirl speed. This paper is concerned only with synchronous whirling and therefore, H has the value +1.0. The gyroscopic terms are placed in the mass matrix at the location of the discs. The discs, being much larger in diameter than the shaft will dominate the gyroscopic effect on the system.

At the location of the discs the rotary inertia term is $\frac{mr^2}{4}$ where m = disc mass and r = disc radius. To incorporate the gyroscopic force the term becomes $\frac{1}{4}mr^2(1-2H)$. This procedure simplifies the general equation of motion (4.5) by placing the gyroscopic terms in the mass matrix. When the shaft experiences forward whirl (H=+1) the shaft spin velocity and the whirl velocity are equal and in the same direction. This tends to stiffen the shaft and to raise the natural frequencies. For backwards (H=-1.0) whirl the effect is to lower the natural frequencies.

The mass matrix for a disc will be:

$$\rho \Pi r^2 \ell \begin{bmatrix} 1.0 & & & \\ & (1-2H)\frac{r^2}{4} & & \\ & & 1 & \\ & & & (1-2H)\frac{r^2}{4} \end{bmatrix} \begin{Bmatrix} W_X \\ \theta_X \\ W_Y \\ \theta_Y \end{Bmatrix} \tag{4.6}$$

These terms are added at the disc nodes.

4.2 Effect of Bearings

Journal bearings add stiffness and damping terms to the system. Four terms are added to the stiffness matrix at the bearing nodes, i.e.

$$\begin{bmatrix} K_{HH} & K_{HV} \\ K_{VH} & K_{VV} \end{bmatrix} \begin{Bmatrix} X_H \\ X_V \end{Bmatrix} \tag{4.7}$$

The terms K_{HV} and K_{VH} are not equal rendering the matrix non-symmetric. The sign convention adopted is from Smith(12) and is given in Chapter 5.

The equations of motion for a journal bearing from NRC(10) are:

$$\begin{bmatrix} K_{HH} & K_{HV} \\ -K_{VH} & K_{VV} \end{bmatrix} \begin{Bmatrix} H \\ V \end{Bmatrix} + \begin{bmatrix} C_{HH} & -C_{HV} \\ -C_{VH} & C_{VV} \end{bmatrix} \begin{Bmatrix} \dot{H} \\ \dot{V} \end{Bmatrix} = \begin{Bmatrix} F_H \\ F_V \end{Bmatrix} \tag{4.8}$$

where F_x and F_y are the forces on the shaft. Kim & Lowe(10) present a literature survey for these eight terms. Both experimental and analytical results are presented in a graphical manner with Sommerfeld number on the horizontal axis and $\frac{W}{C}$ and $\frac{W\omega}{C}$ on the vertical for stiffness and damping coefficients respectively. W is the load on the bearing and C is the bearing radial clearance.

For bearings with no cross coupling terms ($K_{HV}=0$, $K_{VH}=0$) and $K_{HH}=K_{VV}$ the motion of the center of the shaft due to a rotating load would be a circle (Fig. 4.2a). The maximum vertical displacement would equal the maximum horizontal displacement. This is typical of any rolling element bearing. Since the motion is symmetric with respect to either the horizontal or vertical axis a single plane analysis is adequate.

Fig. 4.2b shows a bearing with no cross-coupling terms but K_{HH} and K_{VV} are different. The result is an orbit with axis on the principle axis. Here the horizontal and vertical motions are independent and can therefore be analyzed separately. This system is typical of a rolling element bearing which is mounted on a foundation which is stiffer in one direction than the other.

The general case of a journal bearing with both cross coupling stiffness and damping terms is shown in Fig. 4.2d. The resulting orbit is still an ellipse

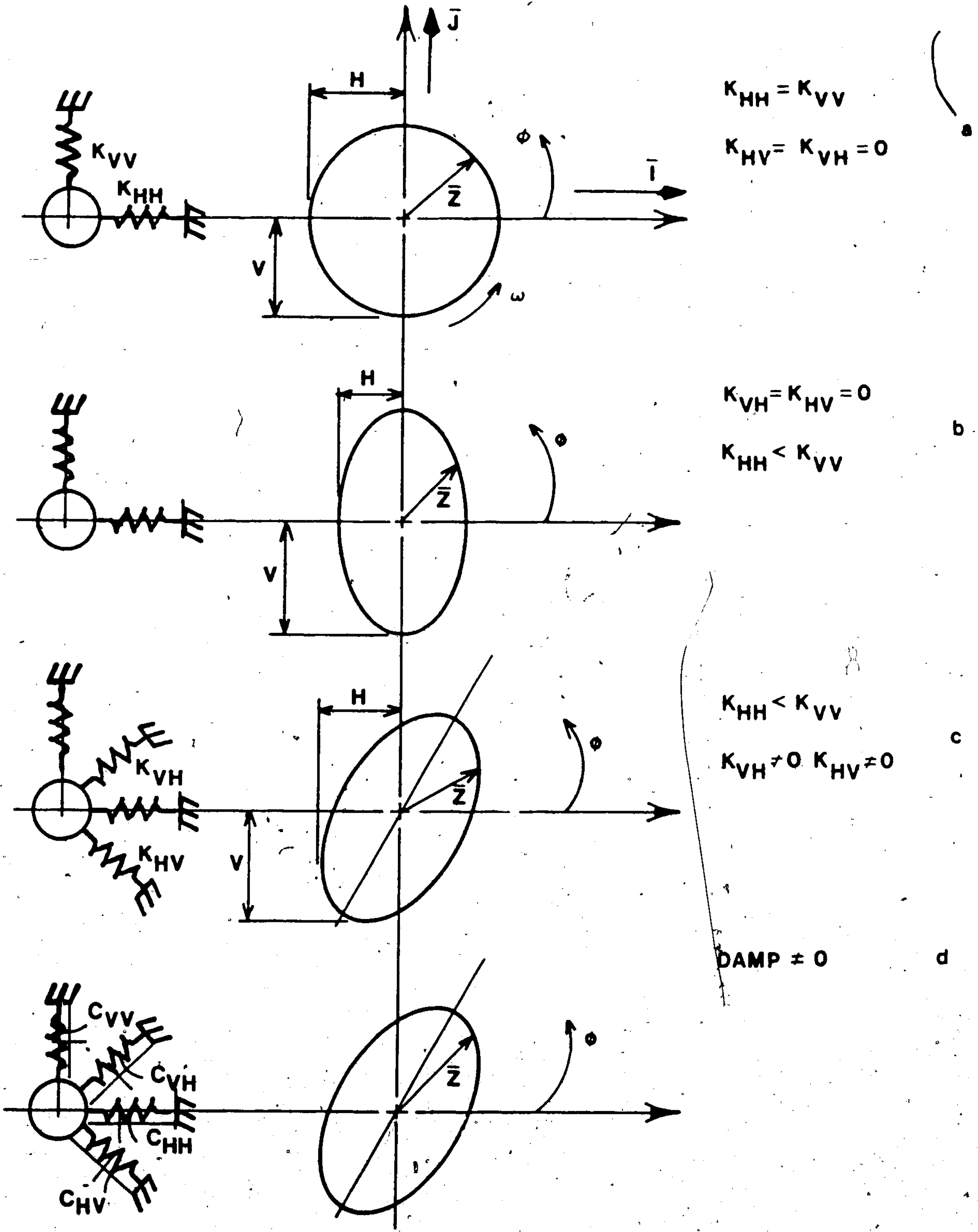
J̄
H
K_VV
K_HH
Ī
Z̄
φ
ω
V
K_HH = K_VV
K_HV = K_VH = 0
a
K_VH = K_HV = 0
K_HH < K_VV
b
K_VH
K_HV
K_HH < K_VV
K_VH ≠ 0 K_HV ≠ 0
c
C_VV
C_VH
C_HH
C_HV
DAMP ≠ 0
d

Fig. 4.2 Effect of Bearing Coefficient on the Orbit of a Rigid Rotor

but the axis is at some angle ϕ. This angle can take on any value and will depend on all eight of the values for damping and stiffness. The general equation for the ellipse is

$$\bar{z}(t) = H\cos(\omega t+\phi_H)\bar{i}+V\cos(\omega t+\phi_V)\bar{j} \tag{4.9}$$

It is obvious from this equation that four variables are required to describe the motion at each node and, therefore, a two plane finite element model is required.

Fig. 4.3 shows a typical bearing stiffness curve. The stiffness is speed dependent and is based on a small rotating load. The predominant load on the bearing must still be in the direction of load (Fig. 4.4). For large rotating loads the curves for stiffness and damping

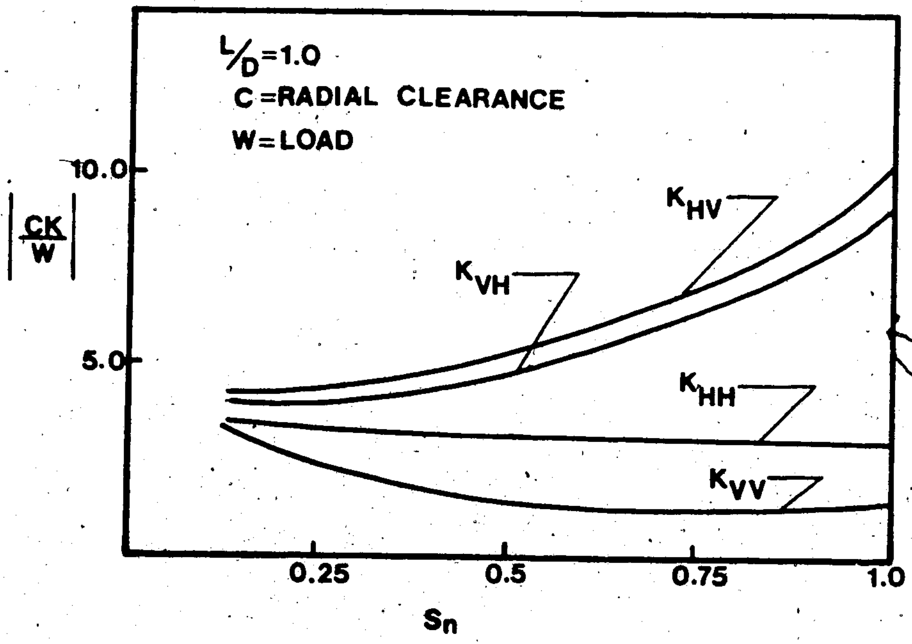

Fig. 4.3 Bearing Stiffness Terms

are due mainly to the squeeze film as in crank shaft bearings. This increased stiffness due to the squeeze film is not included in the determination of the bearing parameters.

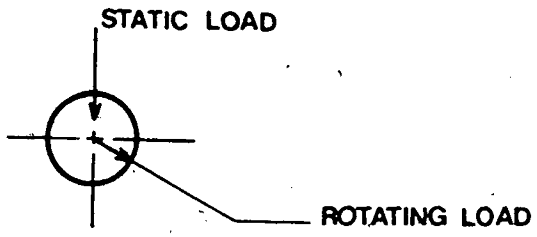

Fig. 4.4 Static Vs Rotating Loads

Since the bearing parameters are speed dependent the mathematical model to solve for the eigenvalues would require an iterative procedure. To eliminate this problem an average value for the Sommerfeld number is used. The Sommerfeld number used for each bearing is based on an average speed between the first and third critical speeds. This is the most useful speed range and the coefficients have a wide scatter (Fig. 5.1) and thus the average is justified. Table 4.1 gives the bearing data for the in-house rig.

The NRC Report(10) makes several assumptions regarding the bearing coefficients which should be noted here:

Table 4.1 Bearing Coefficients

BRG	LOAD LBS	Sn	STIFFNESS X10^{-4}				DAMPING X10^{-5}			
			k_{VV}	k_{VH}	k_{HV}	k_{HH}	C_{HH}	C_{HV}	C_{VH}	C_{VV}
1	28.4	.75	2.0	6.0	- 5.0	3.5	1.2	.24	.23	.87
2	106.2	.49	2.0	16.0	-10.0	3.0	2.5	.80	.77	2.1
3	116.8	.47	2.5	16.0	-10.0	3.5	2.8	.90	.44	2.0
4	62.5	.57	2.6	8.5	- 6.4	3.2	1.6	.41	.36	1.1

1. The oil flow is purely laminar and therefore the Reynolds equations can be used to describe the fluid motion.
2. Inertia effects of the oil around the bearing are neglected.

4.3 General Dynamic Model

The mathematical model which has been described thus far is a purely linear one. The stiffness and damping terms are assumed not to vary with radial shaft amplitude or velocity. The magnitude of the bearing terms change with shaft rotational speed but, as stated before, the terms have been taken at an average rotor speed between the first and third critical speed.

The motion of the model is further assumed to be at steady state, i.e., the complimentary solution to

Eq. 4.5 has dampened out. This physically requires the speed of the rotor to be increased or decreased at a slow rate in order to dampen the acceleration terms which also will have an effect of the shaft motion.

The system of equations, although linear, are complex. The complete equations of motion are written in the following form:

$$[M_{SHAFT} + M_{GYRO}]\ddot{\underline{X}} + [C_{BRG} + C_{PROP}]\dot{\underline{X}} + [K_{SHAFT} + K_{BRG}]\underline{X} = \underline{F}(t) \qquad (4.10)$$

where [M] = shaft mass matrix (Eq. 3.6)
+ disc inertia (Eq. 4.6)
+ disc gyroscopic effect (Eq. 4.6)
[C] = bearing damping (Eq. 4.8)
+ proportional damping (Eq. 3.14)
[K] = shaft stiffness matrix (Eq. 3.5)
+ bearing stiffness (Eq. 4.8)
$\underline{X}$, $\dot{\underline{X}}$, $\ddot{\underline{X}}$ are the radial displacement velocity and acceleration respectively
F(t) = forcing function

The mass matrix is symmetric and contains the mass of the shaft (Eq. 3.6), the disc inertia, and finally the gyroscopic effect of the discs. The damping matrix is not symmetric due to the non symmetry of the bearing cross coupling terms. The complete damping matrix consists of the bearing damping as well as proportional damping (see chapter 5). The stiffness matrix is not symmetric which is also due to the bearing terms. The shaft stiffness (Eq. 3.5) plus the bearings terms constitute the complete stiffness matrix.

The natural frequencies and mode shapes of this mathematical model, are arrived at by considering the complementary solution:

$$[M]\ddot{X} + [C]\dot{\underline{X}} + [K]\underline{X} = 0 \qquad (4.11)$$

with

$$X = Xe^{i\omega t} \qquad (4.12)$$

giving

ω = eigenvalue

X = eigenvector

$$[-M\omega^2 + i\omega C + K] = 0 \qquad (4.13)$$

For the purposes of calculating the eigenvalues the proportional damping terms in [C] are dropped. The bearing damping terms are arrived at from the equation $C = \frac{W}{C\omega} f$ (f = value from Kim & Lowe$^{(10)}$. The ω in this equation and in Eq. 4.13 will cancel leaving a relatively simple eigenvalue problem:

$$[K + iC]\underline{\phi} - [M]\omega^2\underline{\phi} = 0 \qquad (4.14a)$$

$$[M]^{-1}[[K] + i[C]]\underline{\phi} = \omega^2\underline{\phi} \qquad (4.14b)$$

This was the equation used to determine the natural frequencies and mode shapes for Sec. 4.4.

4.4 Natural Frequencies and Mode Shapes

The natural frequencies and mode shapes of a multi degree of freedom system are not always easy to determine from experimental data. The method used in this paper was suggested by Kennedy and Pancu(2). It is assumed that the response of any multi degree of freedom system is the vector sum of its response in its characteristic modes of vibration at that location. This type of analysis is termed "normal modes".

The properties of normal modes from Kennedy and Pancu are as follows:

1. Each normal mode responds to an applied force as a single degree of freedom system, i.e., there is no coupling between normal modes.
2. In a normal mode, each point of the system oscillates about its equilibrium position along a certain line in space, fixed relative to the equilibrium position and straight when the oscillations are small enough so that all angles are equal to their sines.
3. All points are exactly in or out of phase with each other. That is, all points reach maximum departures from their equilibrium position at the same instant.

4. The shape of each normal mode is fixed for a given system and is independent of the magnitude, frequency, or location and direction in space of the applied external forces or of the deflections in other normal modes present. That is, in any given normal mode, the ratios of the deflections at all the points of a structure to the deflection at an arbitrary reference point are constant.

The properties of normal modes hold rigorously only for proportional damping. The rotating system in question has low structural damping and high damping only at the bearings and therefore the method presented by Kennedy and Pancu will be utilized. The method requires plotting polar frequency responses as in Fig. 4.8.

The procedure provides a method of extracting the characteristic or normal modes from polar frequency sweeps measured at different locations along the shaft. Fig. 4.5 gives a typical polar plot for a single degree of freedom system.

The phase angle changes through 180° and the amplitude at resonance is determined by the amount of damping present and the size of the reference load. For zero damping the response is infinite at resonance but all real systems have some damping. From Fig. 4.5 the damping in the system is defined by

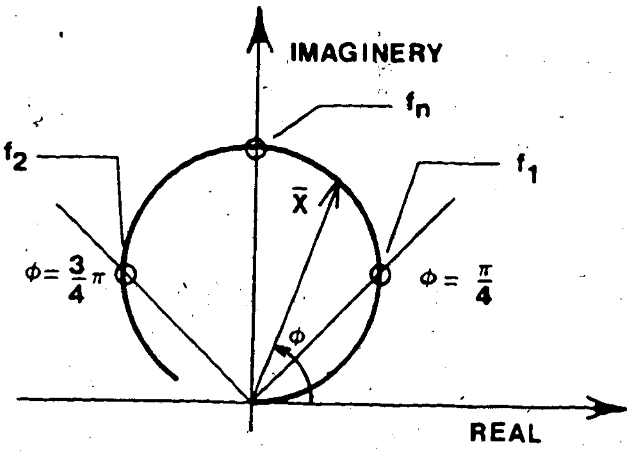

Fig. 4.5 Polar Response For a Single Degree of Freedom System

$$g = \frac{f_1 - f_2}{f_n} \tag{4.15}$$

where f_1 and f_2 are the frequencies at $\phi = \frac{\Pi}{4}, \frac{3\Pi}{4}$ respectively.

For a multi degree of freedom system with natural frequencies which are close together the response is more complicated. The response at any location is a vectorial addition of the response of each mode. During a frequency sweep the response due to one mode has not subsided before the response due to the next mode has begun. Fig. 4.6 shows this vector addition in both polar and Bode plots.

In order to plot the mode shape of the shaft one must examine the polar plots corresponding to each of the locations on the shaft, individually. Two items of information are essential in plotting the mode shapes:

1 - relative magnitude of each mode

2 - relative phase of each mode.

This information can be extracted from the polar plots at each location along the shaft and therefore, the modes are described completely.

To extract the relative magnitudes a circle is drawn following the contour of each mode as in Fig. 4.6b and 4.6c. The relative diameters of the modes correspond to the relative magnitudes. As long as the same scale is used for each of the plots the magnitudes can be taken directly from the diameters.

The relative phase angles are slightly more complicated to extract. Unless the natural frequencies are extremely close together $\frac{f_1}{f_2} < 0.96$ a loop is always present when the modes are in phase. If the loop is not present the modes are out of phase. This relative phase (in or out) is determined in both the vertical and horizontal directions at each point. Now one has a magnitude and a relative sign (+ or -) in both directions and thus the three dimensional mode shapes are described completely.

The natural frequencies are also determined from the polar plots. Fig. 4.5 indicates the natural frequency of a single degree of freedom system at the

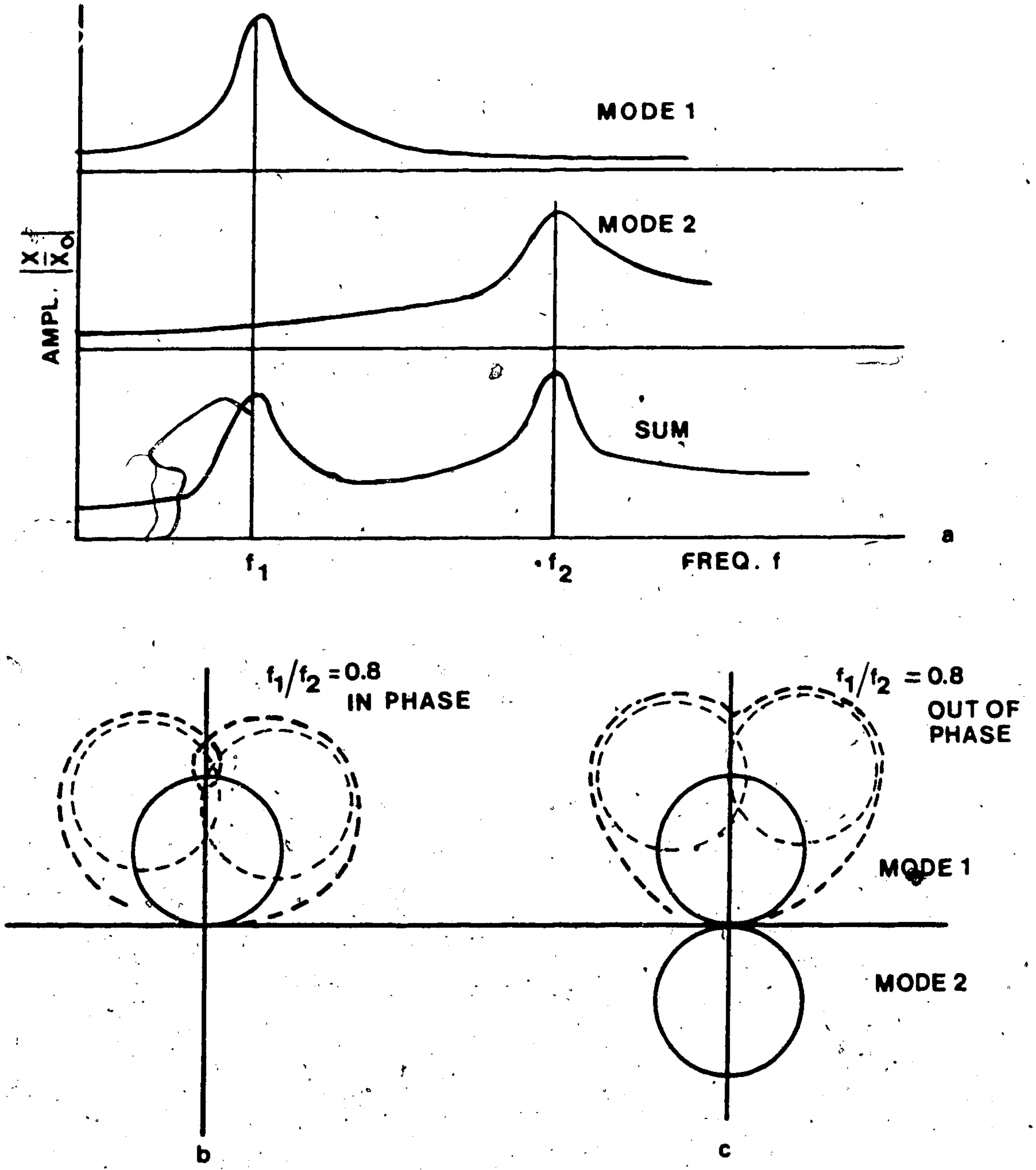

Fig. 4.6 Vector Addition of Two Normal Modes

maximum amplitude which corresponds to a phase angle of 90°. For a multi degree of freedom system, such as the one in question, the maximum amplitude is not always indicative of a natural frequency. Also, the phase angle does not always sweep through 180° for each mode. The natural frequencies are indicated by the maximum rate of change of the phase angles. Kennedy and Pancu(2) suggest plotting $\partial\phi/\partial s$ (s = speed) vs speed to predict the values of critical speeds more accurately. (Fig.4.7)

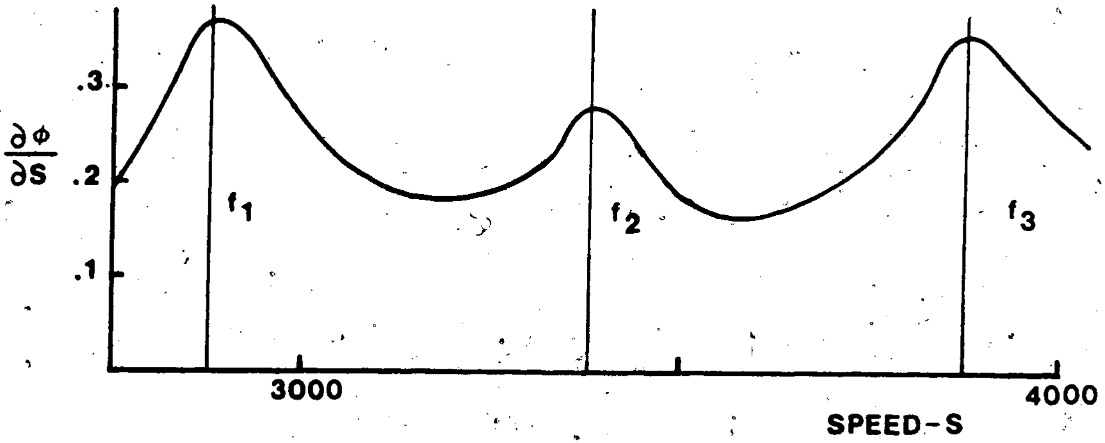

Fig. 4.7 Rate of Change of Phase Angle Vs Speed

Fig. 4.7 shows the three natural frequencies to be 2900, 3400, 3900 RPM. Fig. 4.8 corresponds to Fig.

4.7, which is a polar plot showing the three natural frequencies. From Fig. 4.8 one can clearly see mode 1 and 3 but mode 2 can only be seen from 4.7. The rig was accelerated from 2600 RPM to 4100 RPM in steps of 100 RPM. At each data point the rig was held at the speed for 30 seconds in order to let any acceleration terms dampen out. The bearings, as indicated before, are not symmetric, and therefore for a two plane model the horizontal and vertical natural frequencies will not be exactly the same for the same mode. Rather, due to the slight difference in the cross coupling terms the natural frequencies will occur in pairs. Each pair, of course, corresponds to two mode shapes but these mode shapes are very similar in shape (Fig. 4.10) and when measurements were made to verify the computer model only one natural frequency for each mode was detected.

For clarity, for the rest of the paper, there will be three mode shapes and not six as indicated by the computer model (Table 4.2). The six natural frequencies will be referred to as three pairs. Indeed, if the bearings were symmetric the pairs of shapes would be identical.

Equation 3.14a is a complex equation which indicates that the eigenvalues and eigenvectors will also be complex.

Consider first a simple two degree of freedom system with a diagonal mass matrix and no damping.

$$\begin{bmatrix} k_{11} & k_{12} \\ k_{21} & k_{22} \end{bmatrix} \begin{Bmatrix} X_1 \\ X_2 \end{Bmatrix} + \begin{bmatrix} m & o \\ o & m \end{bmatrix} \begin{Bmatrix} \ddot{X}_1 \\ \ddot{X}_2 \end{Bmatrix} = \begin{matrix} 0 \\ 0 \end{matrix} \qquad (4.16)$$

From Table 4.1 it is obvious that the off diagonal terms in the stiffness matrix are larger in magnitude than the diagonal terms. The determinant of the stiffness matrix is greater than zero which is a necessary condition for a positive definite matrix. For the matrix [K] to be positive definite there must exist some matrix [V] such that

$$[V]^T[K][V] = \left\{[V]^T[K][V]\right\}^T \qquad (4.17)$$

Any stiffness matrix involving journal bearings will not satisfy this condition and is therefore not positive definite.

Solving equation 4.16 for the eigenvalues yields

$$\omega^2 = \lambda = k/_M[A \pm i\sqrt{B}] \qquad (4.18a)$$

The assumed solution is

$$X = Ae^{i\omega t} \qquad (4.18b)$$

using polar coordinates and the euler identity

$$\omega_1 \ \omega_2 = \sqrt{A^2+B}\ \exp[i\mathrm{TAN}^{-1}\sqrt{B}/_{2A}]$$

$$= \alpha \pm i\beta \qquad (4.18c)$$

Substituting into 3.18a yields:

$$\omega_1 = C_1 e^{\alpha it} e^{-\beta t}$$

$$\omega_2 = C_2 e^{\alpha it} e^{\beta t} \qquad (4.18d)$$

It is obvious from these two relations (4.18d) that ω resembles the solution for an elementary underdamped single degree of freedom system with viscous damping. ω_2 is an unstable system due to the positive βt term which will diverge as time increases.

The eigensolutions are of the form in equation 4.18a and the natural frequencies are found from $\sqrt{A^2+B}$. If the B term is negative then the system is unstable. Equation 3.14a also has a non-symmetric damping matrix which changed the complex conjugate solution (4.18c) to the results shown in Table 4.2. The terms in the eigenvalues are all positive which indicates a stable system.

The corresponding eigenvectors are also complex. For each node in the system the eigenvectors are of the form:

$$V = a+ib$$
$$H = c+id \qquad (4.19)$$

The complex terms b and d come from the bearing damping. Complex eigenvectors are not present in systems which have only proportional damping and symmetric mass and stiffness matrices. These terms indicate that the modes are not "normal modes". This means that each point on the rotor does not reach its maximum position at the same time as an adjacent point. The measurements on the shaft will be the maximum values i.e.

$$V_{MAX} = \sqrt{a^2+b^2}$$
$$H_{MAX} = \sqrt{c^2+d^2} \qquad (4.20a)$$

The phase angles (in time) for each node are

$$\phi_V = TAN^{-1}({}^{b}/{}_{a})$$
$$\phi_H = TAN^{-1}({}^{c}/{}_{d}) \qquad (4.20b)$$

These time based phase angles can be determined from experimental data by subtracting the phase angle (measured from key phasor) at the critical speed from the phase angle at the next point on the rotor.

For practical comparison of numerical to experimental equations 4.20a were used to plot the mode shapes. The time based phase angles will have a large effect on balancing rotors and they are accounted for by the two plane complex analysis described above.

Polar frequency plots for the same load distribution, were conducted at several points along the shaft (Fig. 4.9) in order to plot the mode shapes in Fig. 4.10 - 4.12. The experimental mode shapes are compared with those predicted by the finite element model. The first and third modes are clearly defined on the polar plots (Fig. 4.9) but mode 2 is somewhat obscrued since the first and third modes appear to dominate the response.

Table 4.2 Natural Frequencies

Mode	Measured	Calculated
1	2900 RPM	V 2850 RPM H 3100 RPM
2	3400 RPM	V 3350 H 3600
3	3900 RPM	V 3800 H 4700

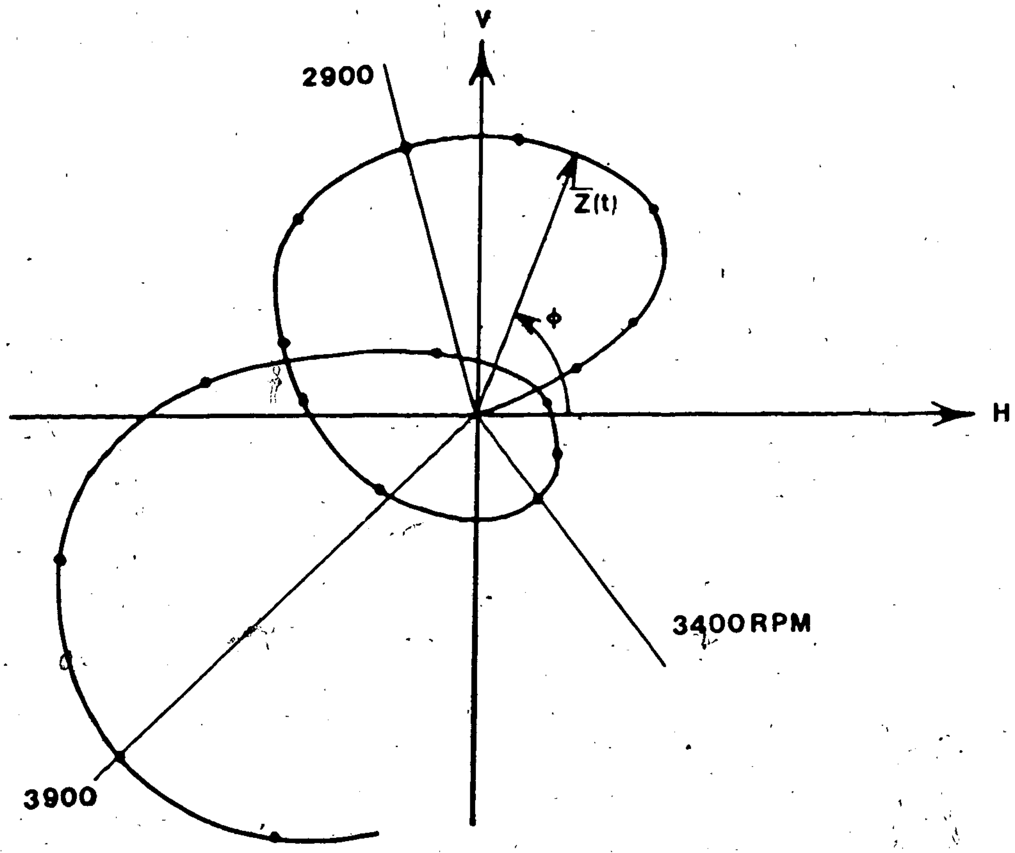

Fig. 4.8 Polar Response For Natural Frequencies

From Fig. 4.10 - 4.12 it is evident that the first mode is best verified by experiment. The mathematical and experimental plots are almost identical. The phase angles at each point along the shaft are either in or out of phase with each other. The change in phase across each of the bearings is almost exactly 180°. This is also true for the third mode. The second mode however, displays relative phase angles to range anywhere from 0° to 180°. Also, the phase change across each bearing is not 180°. This characteristic made the second mode extremely difficult to extract from Fig. 4.9.

It is interesting to note that the first mode has the highest response in the first span, the second mode in the second span, and finally the third mode in the third span. As the shaft speeds up the response resembles a wave propagating from the heavy end to the lightest. Each of the three critical speeds is the fundamental mode for each span. The next critical speed would be the second mode for span 1 and so on. This is characteristic of all flexible rotors such as the turbine of chapter 1 which runs above the second generator mode.

In all computer modelling, the correlation with experiment diverges at higher modes. For this model the first and second modes are fairly close to experiment but mode 3 shows a 180° discrepancy in the second span, i.e., the experimental mode is almost 180° out of phase with the numerical. The predominant response is in the third span however, and the prediction of the forced response (chapter 5) is not greatly affected by this discrepancy.

The divergence from experiment for the natural frequencies are as follows:

Mode 1	6% Low
Mode 2	7% Low

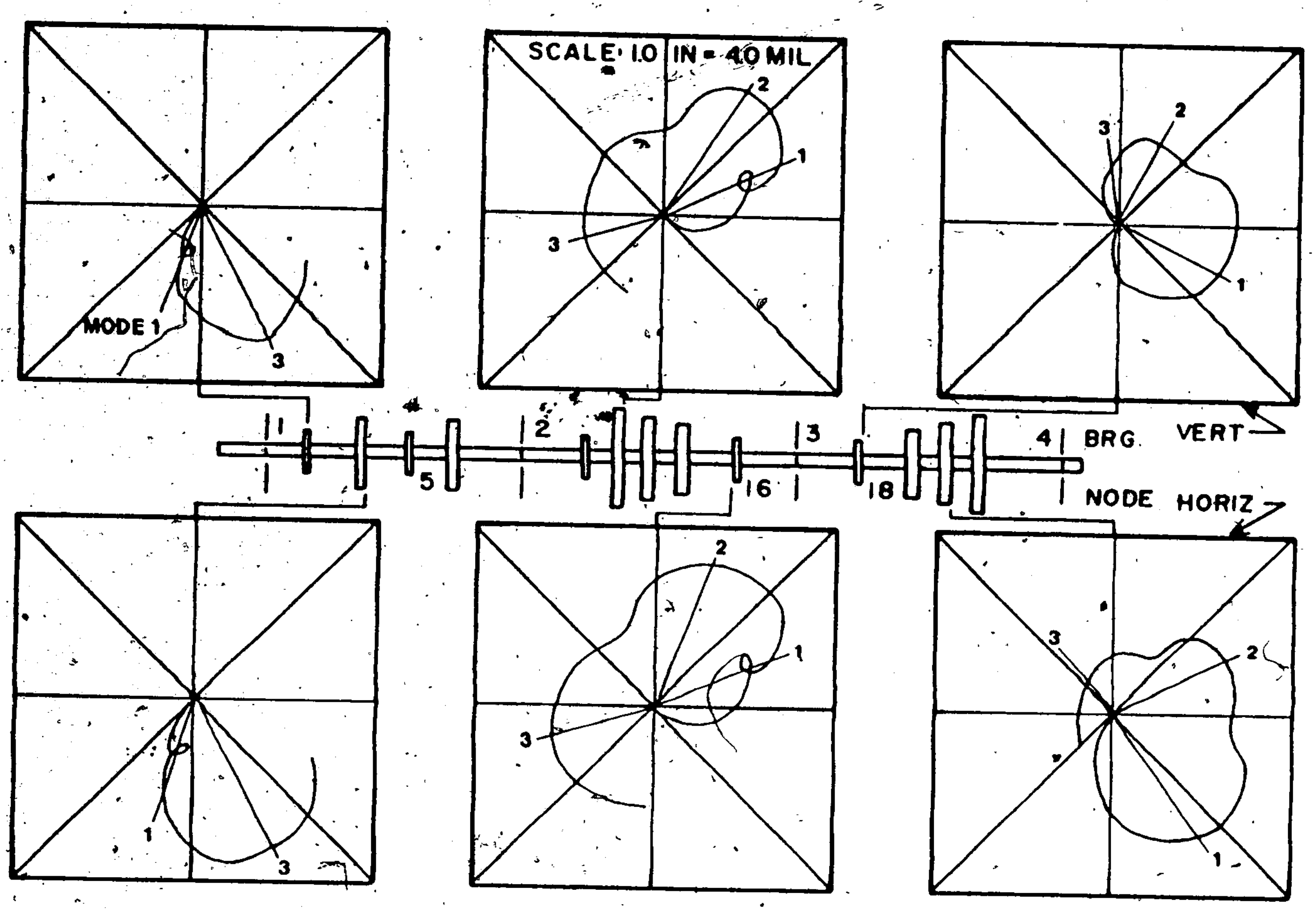

Fig. 4.9 – Polar Plots for Mode Shapes

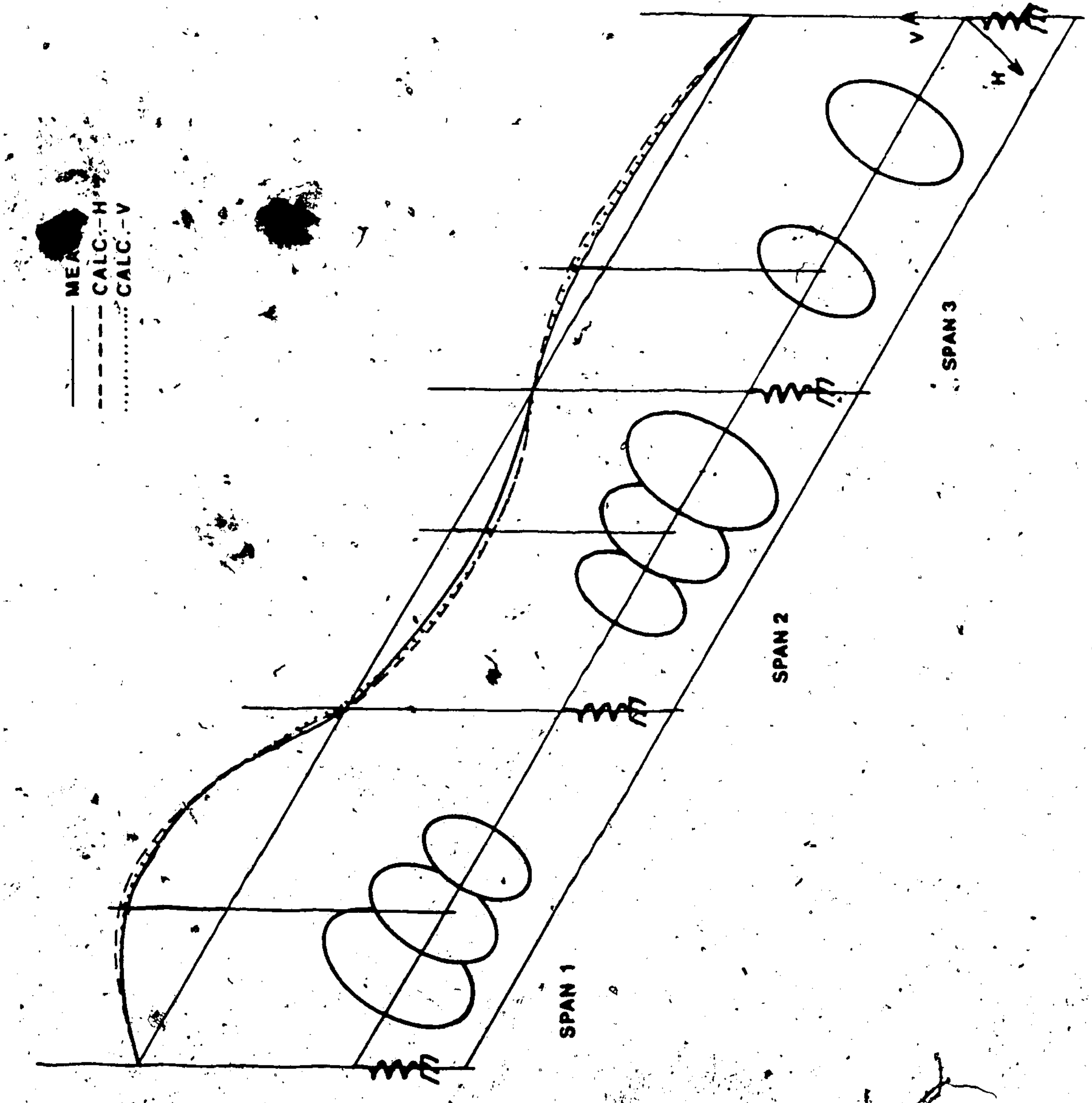
MEA
CALC.-H
CALC.-V
V
H
SPAN 1
SPAN 2
SPAN 3

FIG.4.10 - MODE 1

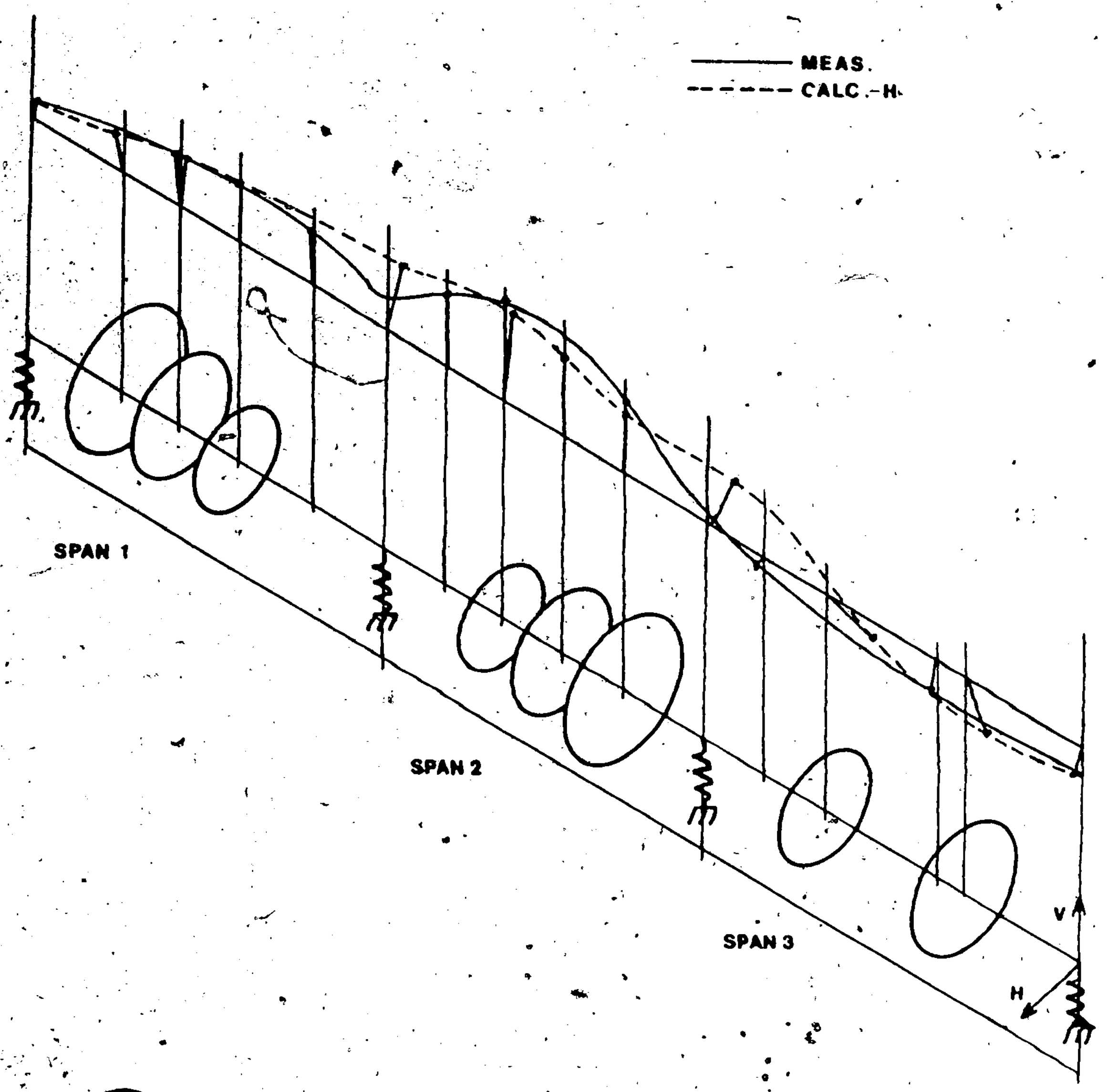
MEAS.
CALC.-H.
SPAN 1
SPAN 2
SPAN 3
V
H

FIG 4.11 – MODE 2

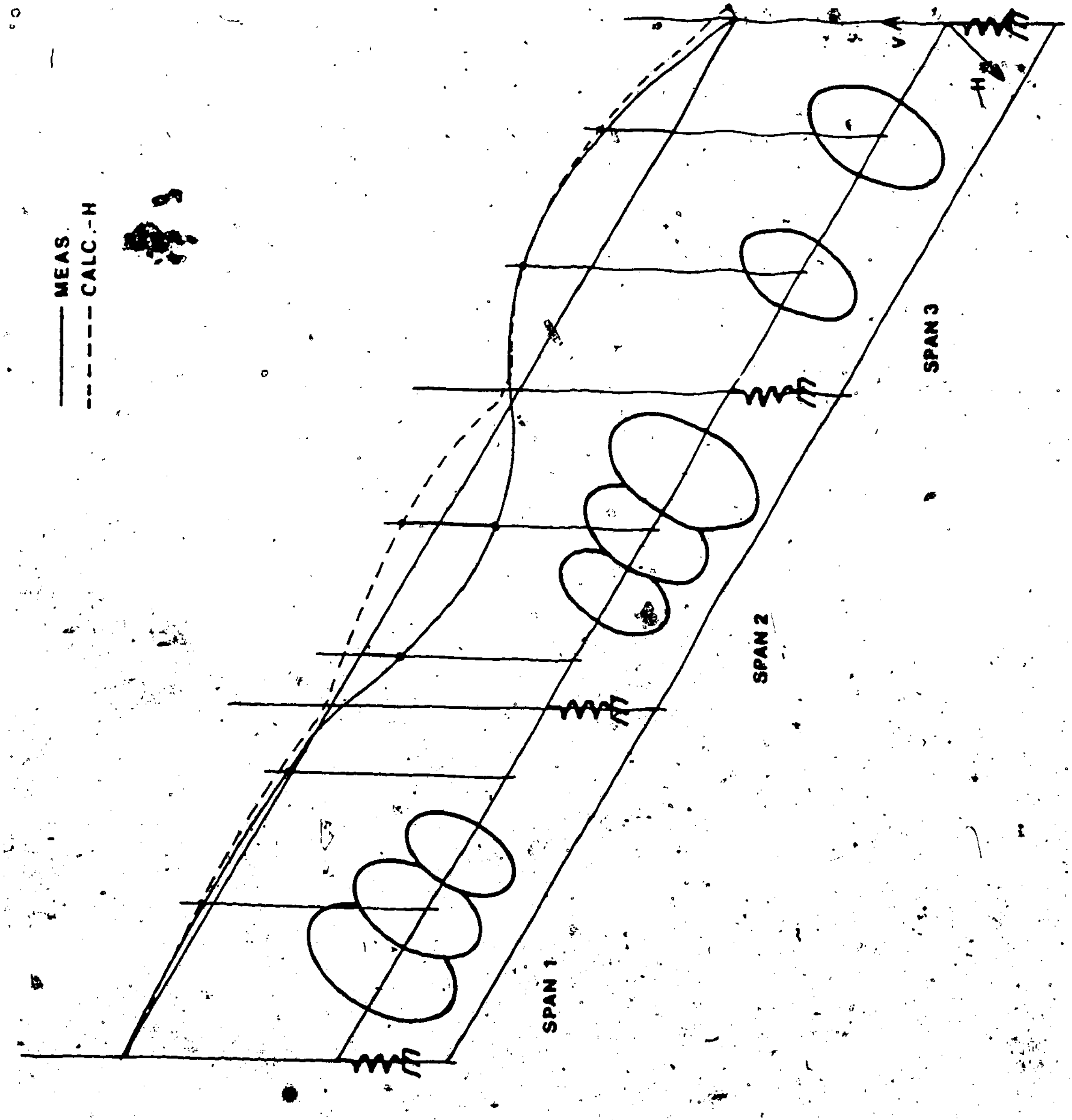
MEAS.
CALC.-H
SPAN 1
SPAN 2
SPAN 3
V
H

FIG 4.12 – MODE 3

Mode 3 8% Low

The damping in each mode was extracted through the use of Eq. 3.14 and Fig. 4.9.

$$\text{Mode 1} \quad g = \frac{3060-2790}{2900} = 0.093$$

$$\text{Mode 2} \quad g = \frac{3050-3280}{3400} = 0.065$$

$$\text{Mode 3} \quad g = \frac{4120-3710}{3900} = 0.105$$

These damping ratios could be used in Eq. 3.11 to reduce the system to a simple three degree of freedom system. Each span would be represented by a point mass, a spring and a viscous damper.

The above damping ratios represent the total damping in each mode, i.e., bearing damping and proportional damping combined.

5. RESPONSE DUE TO A ROTATING LOAD

Abstract

The final test for the numerical analysis is to predict the system response for various load distributions. Comparison to experimental data for the same load distributions will be shown. Discussion of the prediction of the load from measured data, i.e. balancing the shaft, will also be given. As well, the system's linear range is also explored.

5.1 Linearity Tests

Chapter 3 indicated that a linear mathematical model was used for the non-rotating mode shape predictions. The same model was used in the forced response and therefore tests were conducted to measure the linear range of the rig.

The first linearity tests were conducted at the same phase angle. Figs. 5.1 and 5.2 are plots of speed vs response at two locations on the shaft. Loads of 10, 15 and 25g were used for a speed range from 2500 to 4000 RPM.

Examining Fig. 5.1 one can see that the three load curves have identical shapes and only differ by magnitude of response. This is indicative of a linear model. The location of load and measurement is on the first span and, therefore, the first critical speed (2900 RPM) is clearly indicated. It is interesting to note the similarity between Fig. 5.1 and the response to a single degree of freedom system (Fig.4.5 This is explained by examining the mode shapes (Fig.4.10 - 4.12). Span 1 has a large response in the first mode but very little response from the second or third modes.

Figure 5.2 is also a load vs response curve. As in Fig. 5.1 the three load curves have the same basic shape and the response increases linearly with load. Again, the first critical speed is indicated. Table 4.2 shows the first critical speed is actually split into two criticals (in the horizontal and vertical directions). This graph confirms the computed results of 2850 and 3100 RPM for the vertical and horizontal directions, respectively.

Figure 5.3 is a graph of load vs response at the critical speed for both cases discussed above. Note the straight line indicating a linear system.

Figures 5.4 and 5.5 are corresponding polar plots taken from the same shaft position as the first two linearity tests. The purpose of these plots is to change the phase angle of the load and to hold the size constant. The shape of the plots should be identical but displaced by a phase angle equal to that of the load change. Both Figs. 5.4 and 5.5 indicate this to be the case.

The in-house rig can now be considered linear and, therefore, a linear computer model (chapter 3) is used through this chapter.

5.2 Forced Resp

Before a comparison of the measured vs computed forced response can be made a consistent coordinate system must be established. The adopted coordinated system (Fig. 5.7) is a right hand one given by Smith(12).

The corresponding bearing stiffness and damping terms are:

$$\underset{\text{Stiffness}}{\begin{bmatrix} K_{HH} & K_{HV} \\ -K_{VH} & K_{VV} \end{bmatrix}} \qquad \underset{\text{Damping}}{\begin{bmatrix} C_{HH} & -C_{HV} \\ -C_{VH} & C_{VV} \end{bmatrix}} \qquad (5.1)$$

The force and displacement vectors must also be consistent with Smith's system:

Force

$$F_H = F[\cos(\omega t+\phi) + i \sin(\omega t+\phi)]$$
$$F_V = F[\sin(\omega t+\phi) - i \cos(\omega t+\phi)] \qquad (5.2)$$

Displ.

$$U_H = U_H[\cos(\omega t+\phi_H) + i \sin(\omega t+\phi_H)]$$
$$U_V = U_V[\cos(\omega t+\phi_V) + i \sin(\omega t+\phi_V)] \qquad (5.3)$$

Where F = magnitude of force

ϕ = angle of force relative to key phasor

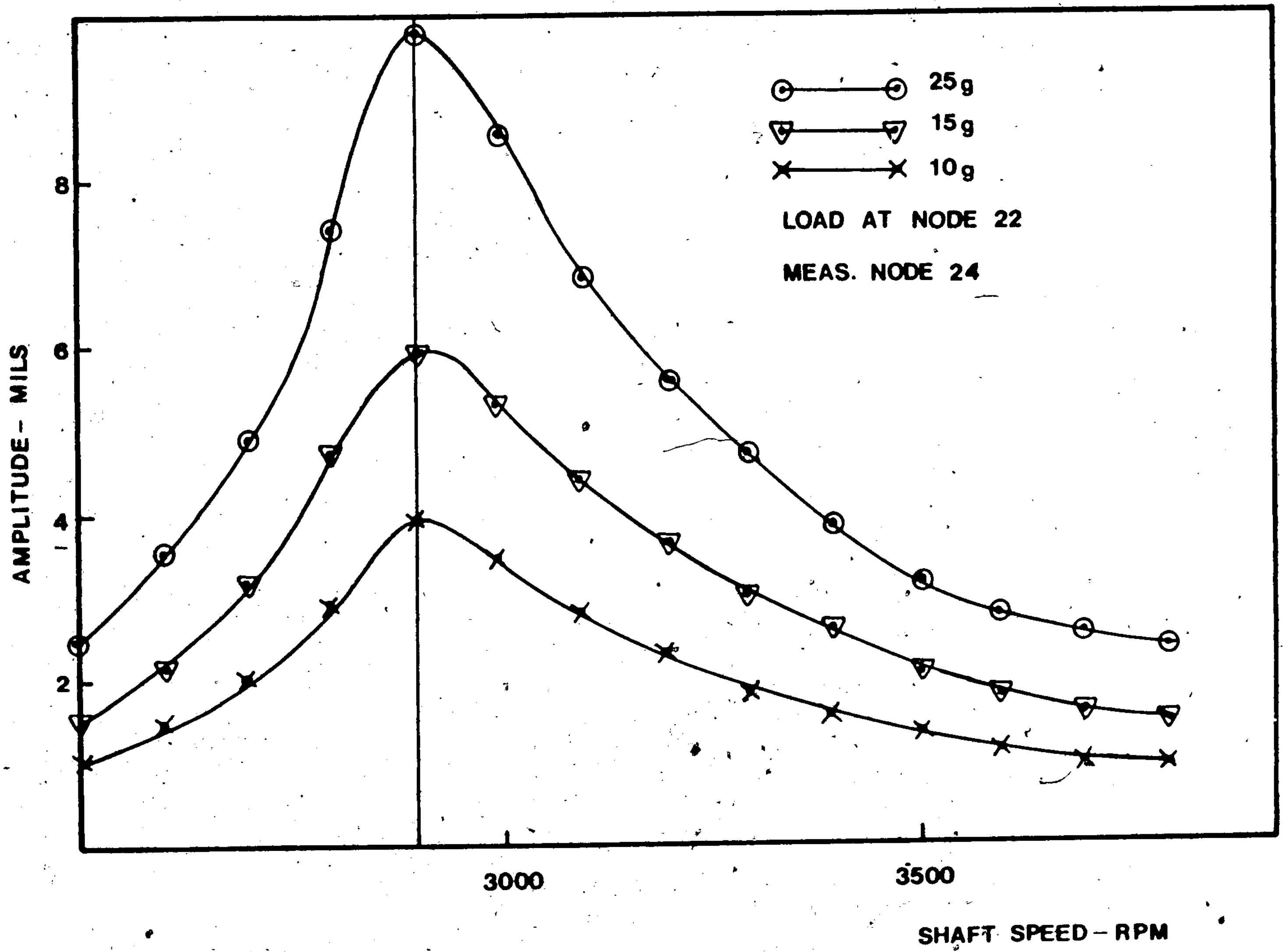

Fig. 5.1 Linearity Test #1

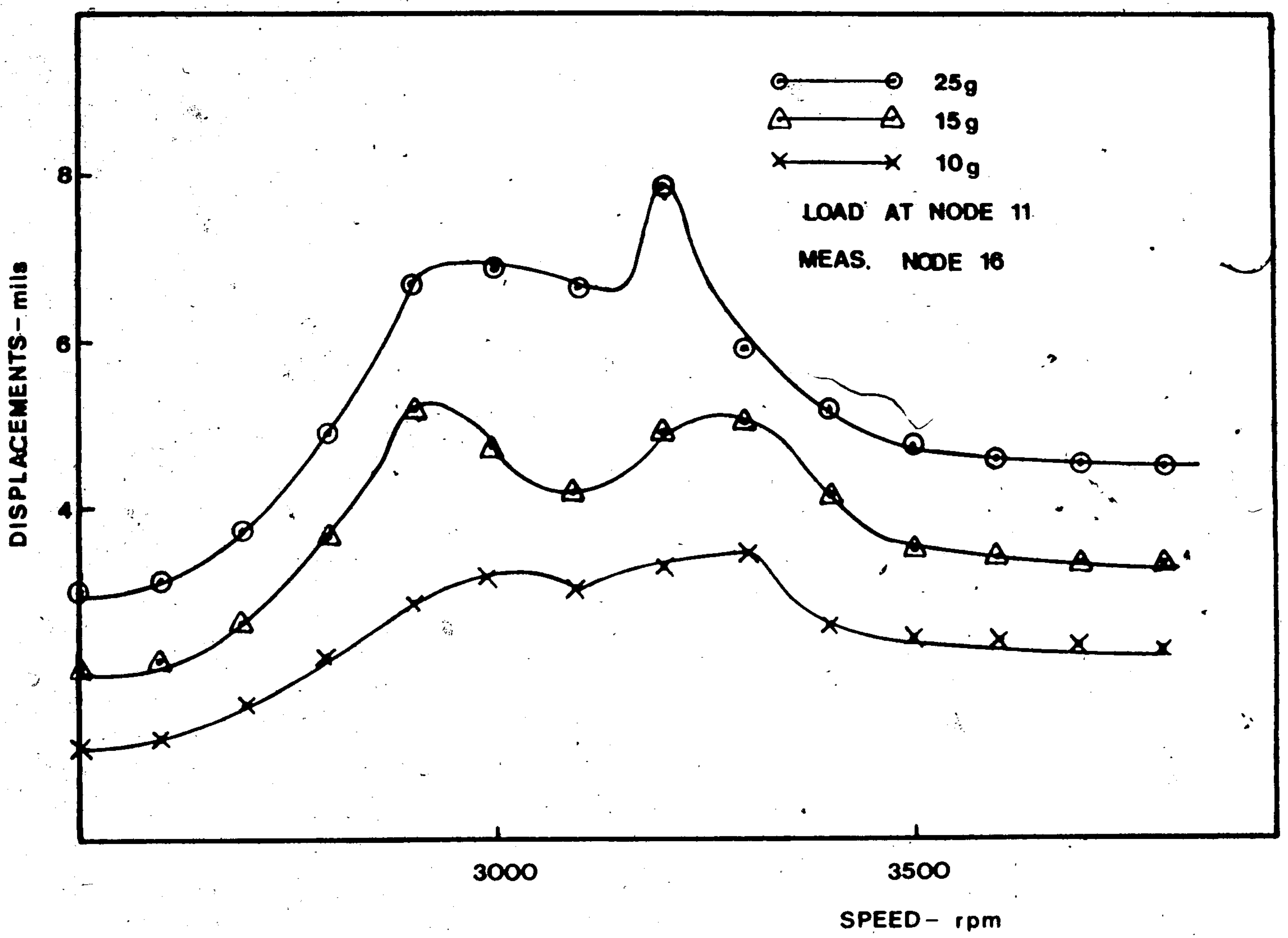

Fig. 5.2 Linearity Test #2

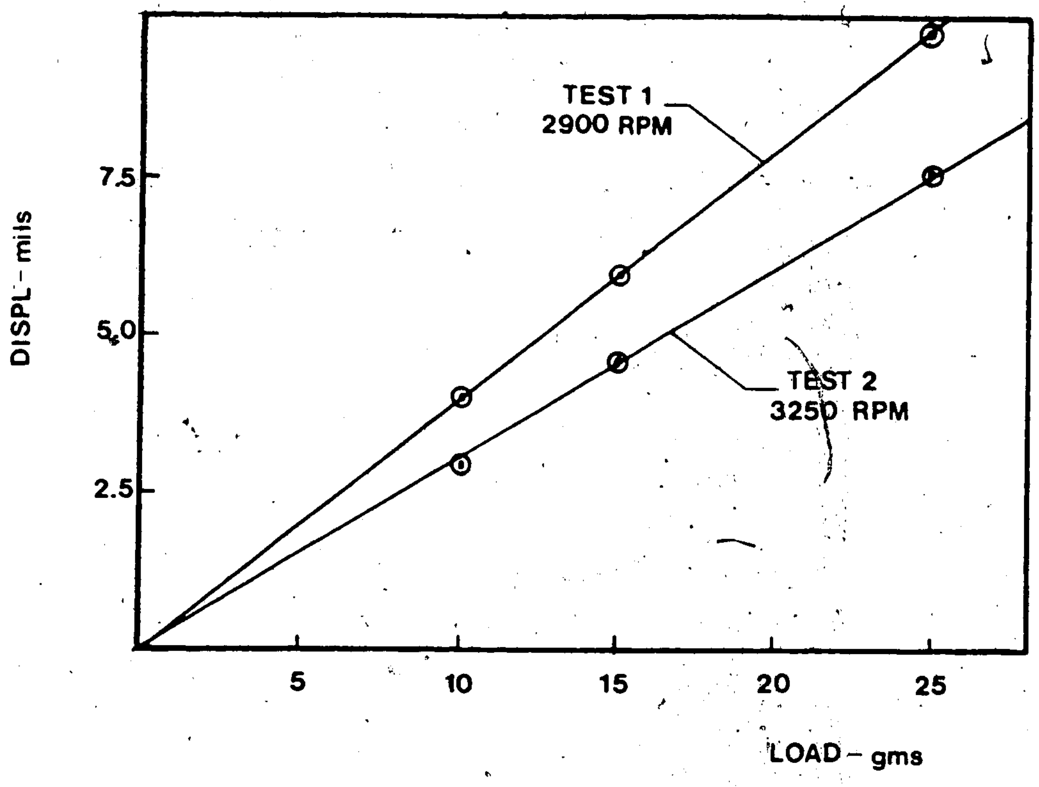

Fig. 5.3 Load Vs Displacement For Linearity Tests #1 & 2

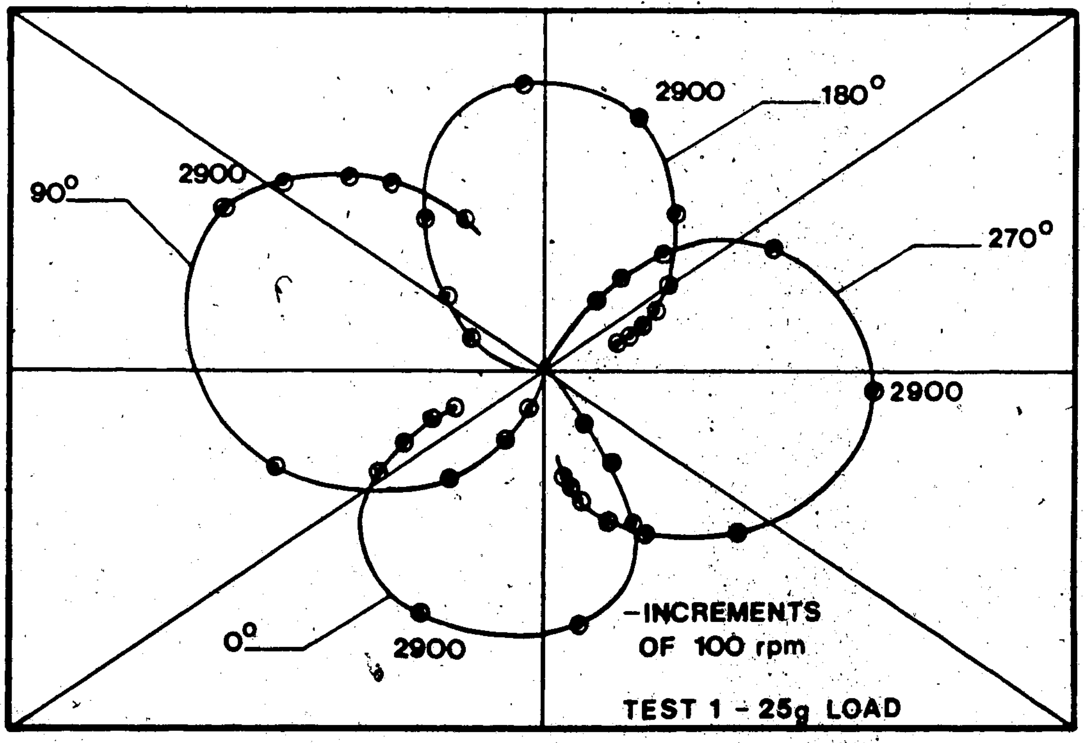

Fig. 5.4 Linearity Test #3

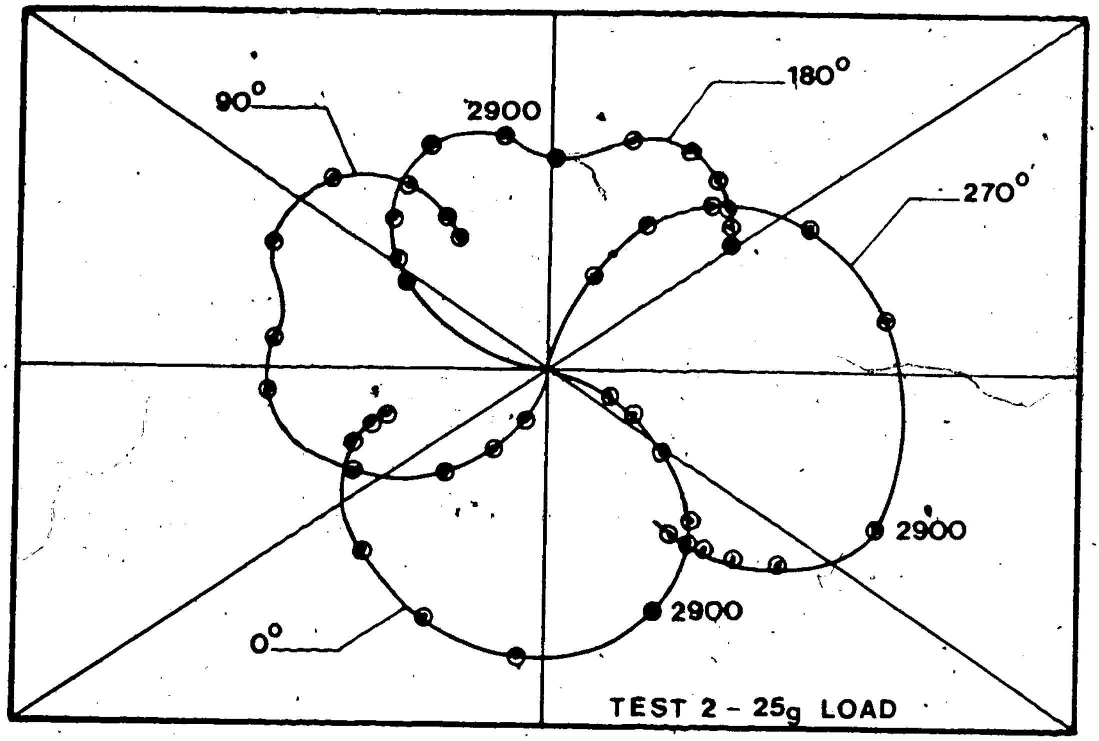

FIG 3.16

Fig. 5.5 Linearity Test #4

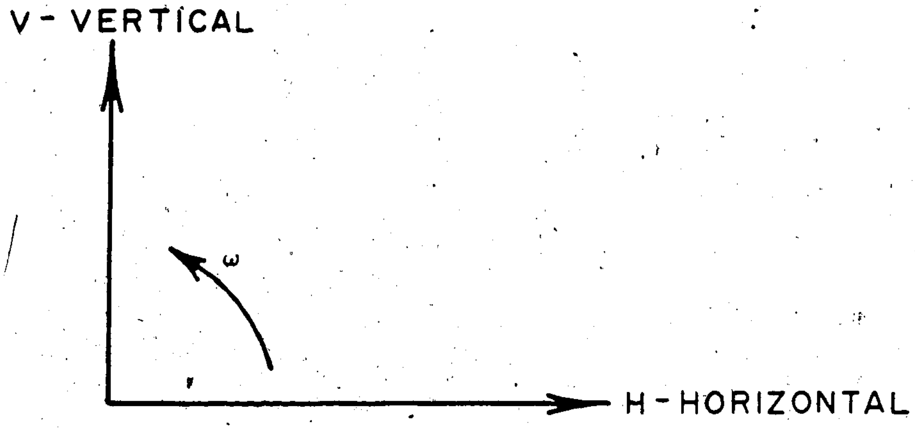
V - VERTICAL
ω
H - HORIZONTAL

Fig. 5.6 Definition of Coordinate System

U_H = magnitude of displacement in horizontal direction
U_V = magnitude of displacement in vertical direction
ϕ_H = angle of displacement in horizontal direction
ϕ_V = angle of displacement in vertical direction

Fig. 5.7 shows all the parameters listed above.

Data for three different load distributions were compared with computed results. Table 5.1 gives the load distributions which correspond to the finite element model used in this chapter (Fig. 3.7).

Table 5.1 Load Distributions for Forced Response

Trial	Load Vector		
	me [Lb-sec^2]	Angle* [DEG]	Node [Fig. 3.7]
1	0.0020	0°	16
2	0.000177 0.000183	0° 180°	18 16
3	0.000172	0°	5

*Angle measured from key phasor notch in the opposite to shaft rotation

5.2.1 Orbits

Trial #2 was chosen to compare measured orbits with those predicted by the computer model. An orbit is defined as the synchronous motion of the center of the shaft at a point. The balancing of any shaft is based on the synchronous vibration since at resonance

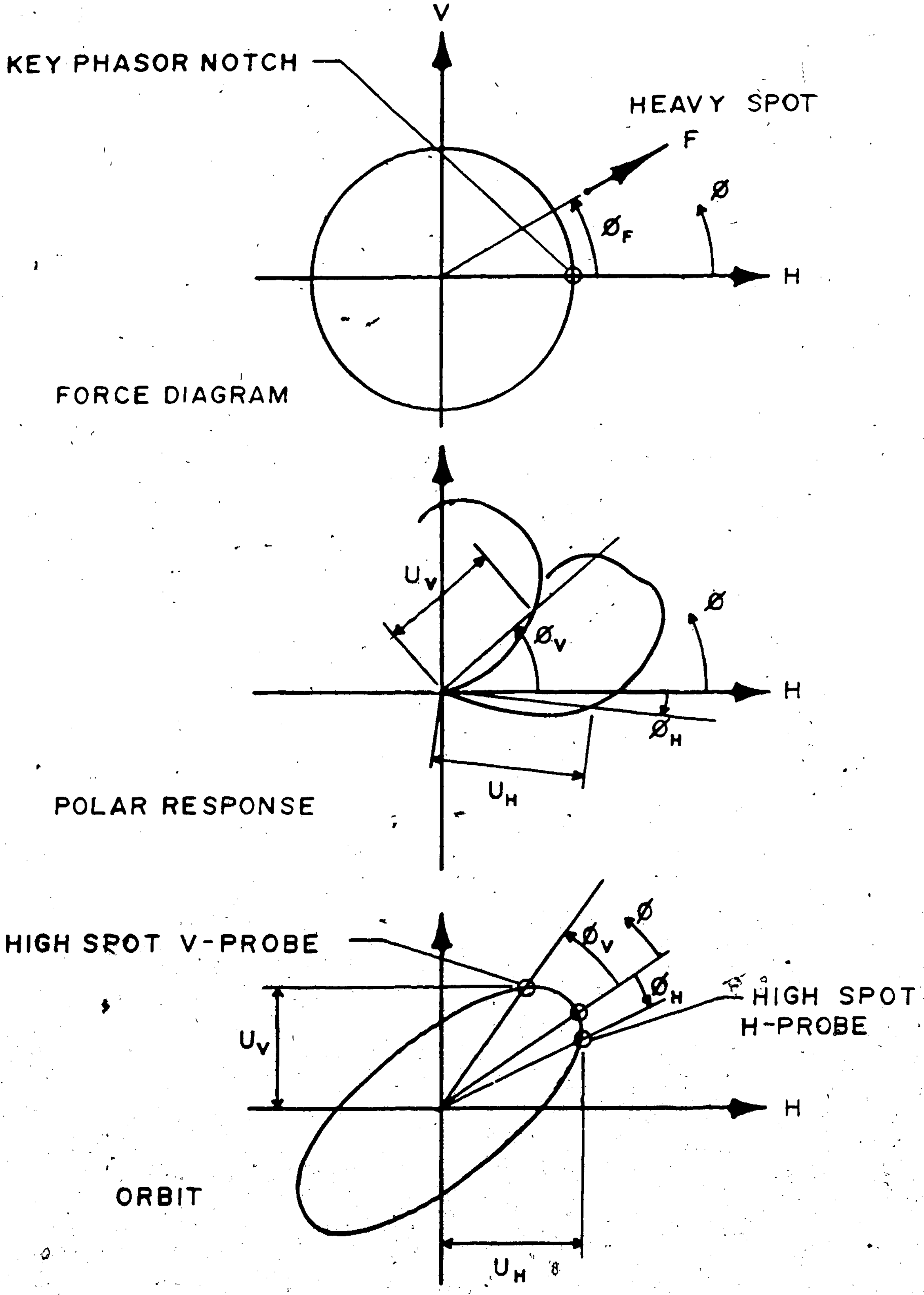
V
KEY PHASOR NOTCH
HEAVY SPOT
F
Ø
Ø_F
H
FORCE DIAGRAM
U_V
Ø_V
Ø
H
Ø_H
U_H
POLAR RESPONSE
Ø
Ø_V
HIGH SPOT V-PROBE
Ø_H
HIGH SPOT
H-PROBE
U_V
H
ORBIT
U_H

Fig. 5.7 Response Coordinate System

this component dominates the motion. Fig. 5.8 compares the complete vibration signal with the synchronous signal. This entire chapter is concerned with only the synchronous vibration.

The orbit will naturally change size and shape as the shaft speed is varied. Figs. 5.9a to 5.9c are the measured and computed orbits at node 13 for Trial 3. To plot an orbit from experimental data one needs five items of information:

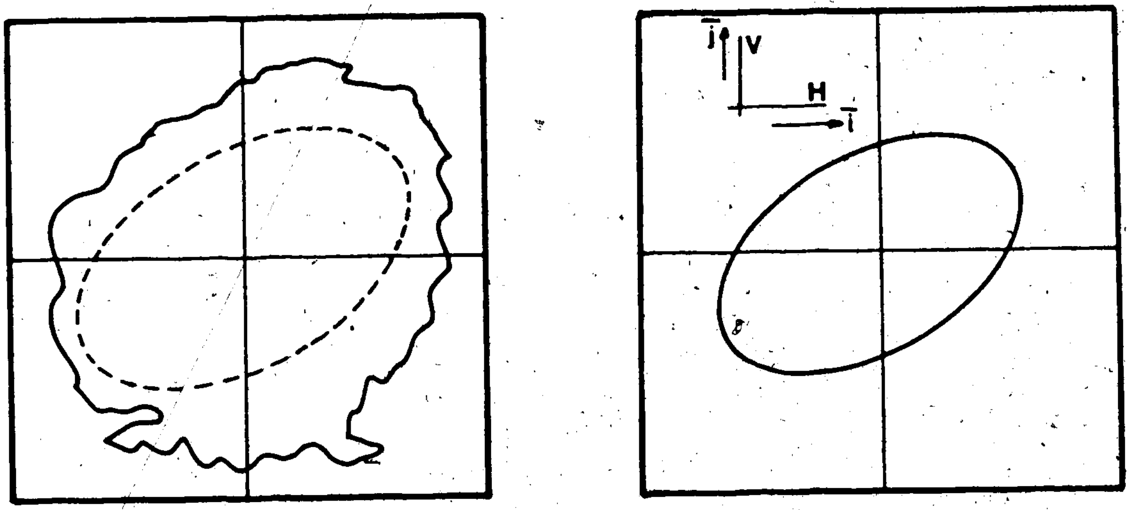

DIRECT SIGNAL **SYNCHRONOUS SIGNAL**

Fig. 5.8 Direct Vs Synchronous Signal

1. H - magnitude
2. H - phase
3. V - magnitude
4. V - phase
5. ω - speed of shaft.

The H and V phase angles refer to the angle between the high spot on the shaft and the key phasor notch in the shaft. The equation of the orbit is

$$\bar{Z} = H_{mag} \cos(\omega t+\phi_H)\,\bar{I} + V_{mag} \cos(\omega t+\phi_V)\,\bar{J} \qquad (5.4)$$

knowing the V and H components of magnitude and phase, as well as the shaft speed, enables one to plot the orbit. As mentioned this is the synchronous vibration and, therefore, the values of V_{mag}, V_{ph}, H_{mag}, H_{ph} must be filtered to the shaft speed. In other words all the higher (2x, 3x...) and lower (½x, 1/3x...) harmonics must be filtered out.

Since the key phasor notch in the shaft is at some arbitrary angle the ϕ_V and ϕ_H angles are not measured from 0° on the graph paper but from the point where t = 0 on the orbit (Fig. 5.9a). The V and H magnitudes are also shown in Fig. 5.7. Knowing only the V and H magnitudes one knows the limits of vibration but the exact orbit cannot be plotted without the phase angles.

From elementary vibration theory it is known that in a single degree of freedom system the phase angle changes by 180°, i.e., the response changes from in phase to out of phase with respect to the forcing function. This phenomenon is shown in orbit plots as a sudden shift in the orientation of the axis of the ellipse. This is much the same as a large phase angle change on orbit plots. Figs. 5.9a

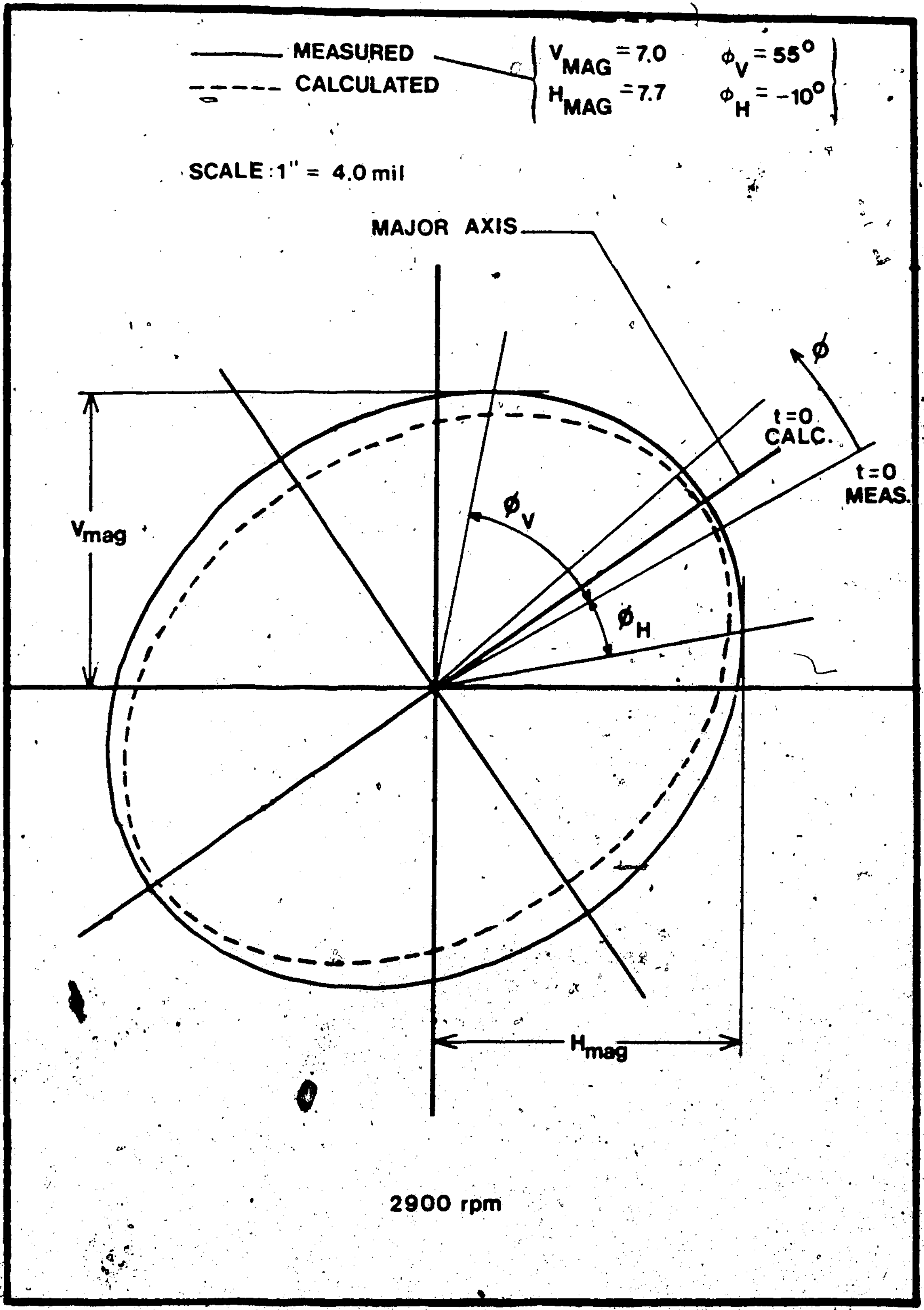

Fig. 5.9a Orbit For 2900 RPM

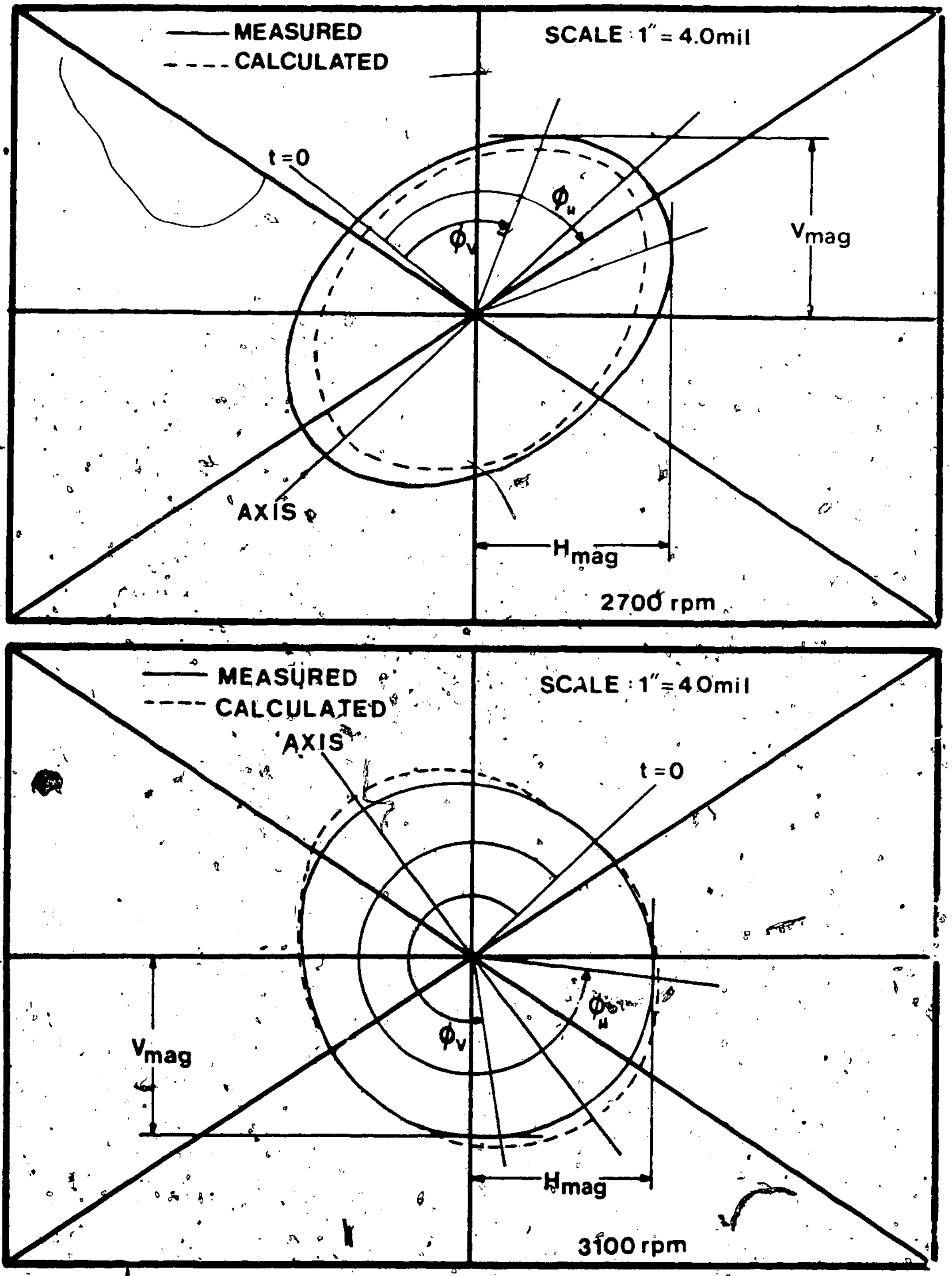

Fig. 5.9c Orbit For 3100 RPM

to 5.9c show the first critical speed to be between 2900 RPM and 3000 RPM. The orbits also show the critical speed to be closer to 2900 RPM than 3100 RPM due to the larger amplitudes at 2900 RPM.

The most important parameter to model at resonance is damping since stiffness no longer constrains the system. Unfortunately bearing damping is also the most difficult to predict. These two factors cause the predicted orbits to differ from experiment more at critical speeds. Fig. 5.9b and 5.9c are more accurately predicted than 5.9a which is near the first critical speed of 2900 RPM.

5.2.2 Polar Plots

The in-house rig, in its simplest form, has three degrees of freedom: span 1, span 2, span 3 (Fig. 4.9). In view of this, experimental data was plotted as three polar plots taken at the center of each span in both the vertical and horizontal directions (Figs. 5.10 to 5.12).

The computed results are plotted on the same graphs for comparison. The most obvious point to be noted is the very accurate prediction of phase and magnitude below the first critical speed. This is true for all three load distributions. Near the critical speeds (noted by a *) the predicted results differ in both phase and magnitude. As stated before, near critical speeds the damping matrix is the most important one to model accurately.

For each of the load distributions the basic shape of the polar plots are matched fairly well. For balancing purposes, speeds below the first critical would yield the best results. One could also balance between two critical speeds where the predicted response is more accurate. Indeed, most machines cannot be balanced at a critical speed due to excessive vibration amplitudes which are harmful to the journal bearings.

Fig. 5.10 is the response for a single point load located in span 2. The in-house rig is a continuous shaft with no couplings between the bearings. Most turbo machinery bearings are mounted on a catenary in order to ensure zero bending moment and shear force at the couplings. This has the effect of lowering the response at one stage due to a load in another. This is not the case with the rig and therefore, large responses at the two end spans are produced by a single load at the center (Fig. 5.10). This type of response is much more difficult to predict than in the case of couplings between bearings. The in-house rig cannot be balanced in stages (one span at a time) as sometimes can be done with large machines.

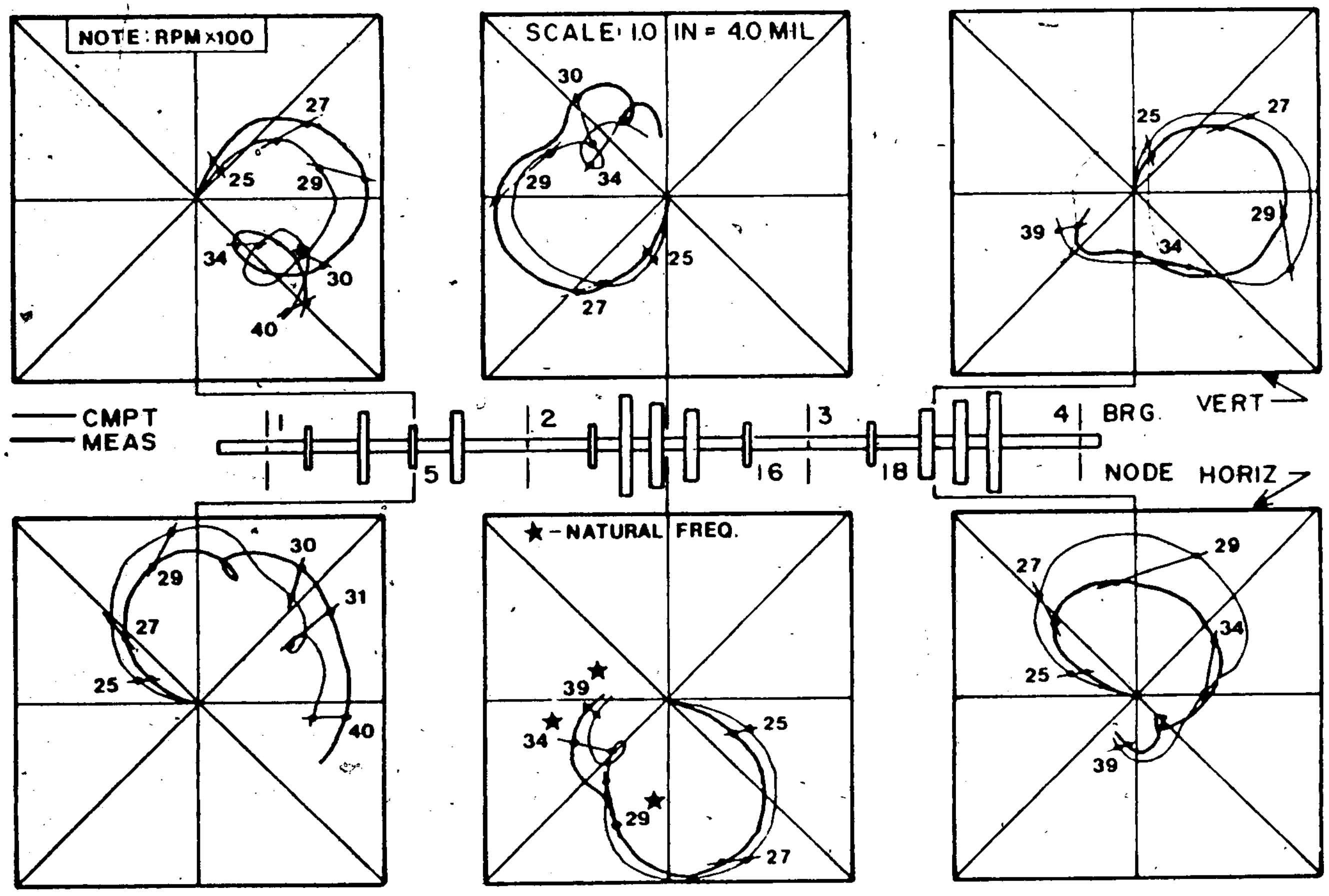

Fig. 5.10 Load Distribution 1

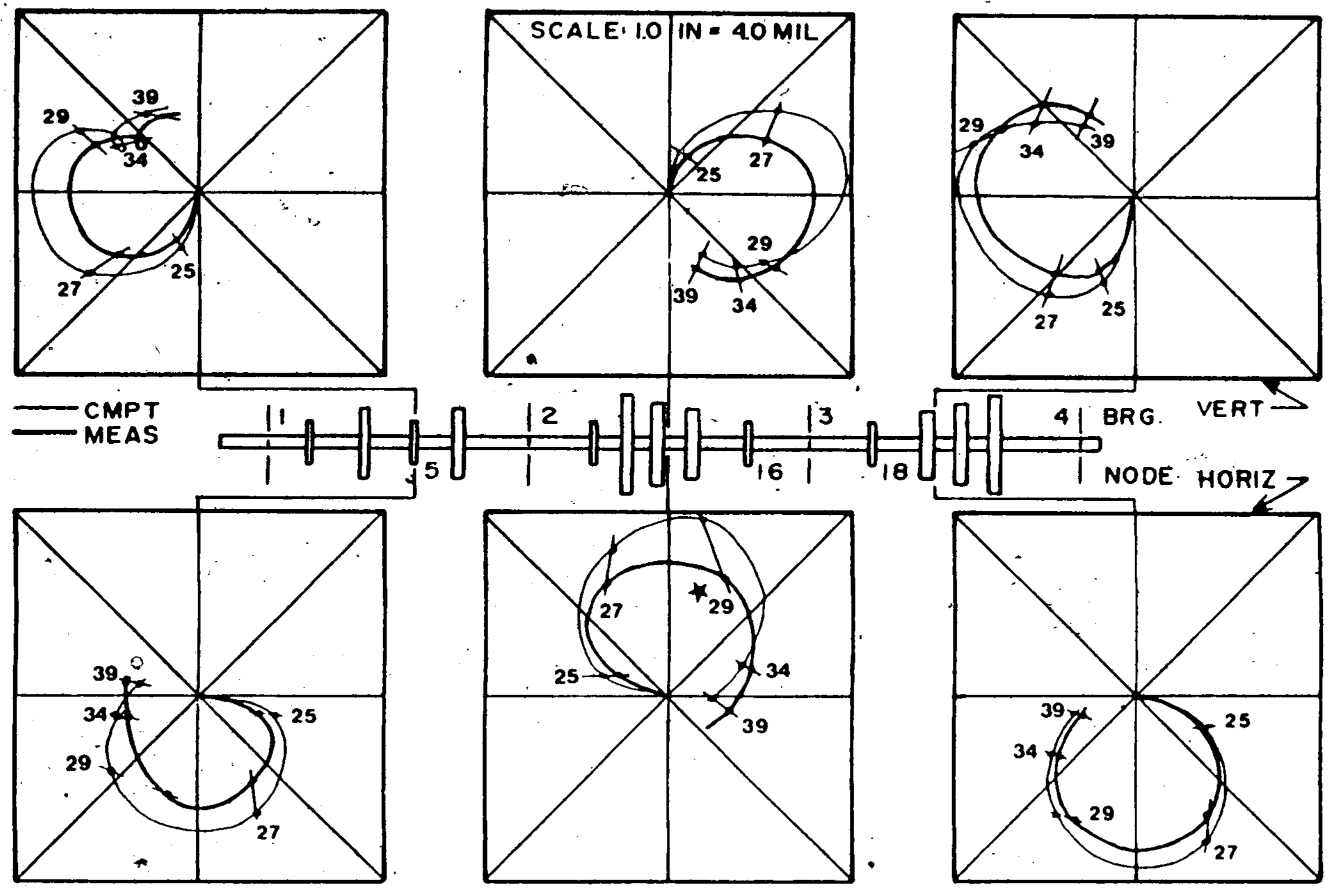

Fig. 5.11 Load Distribution 2

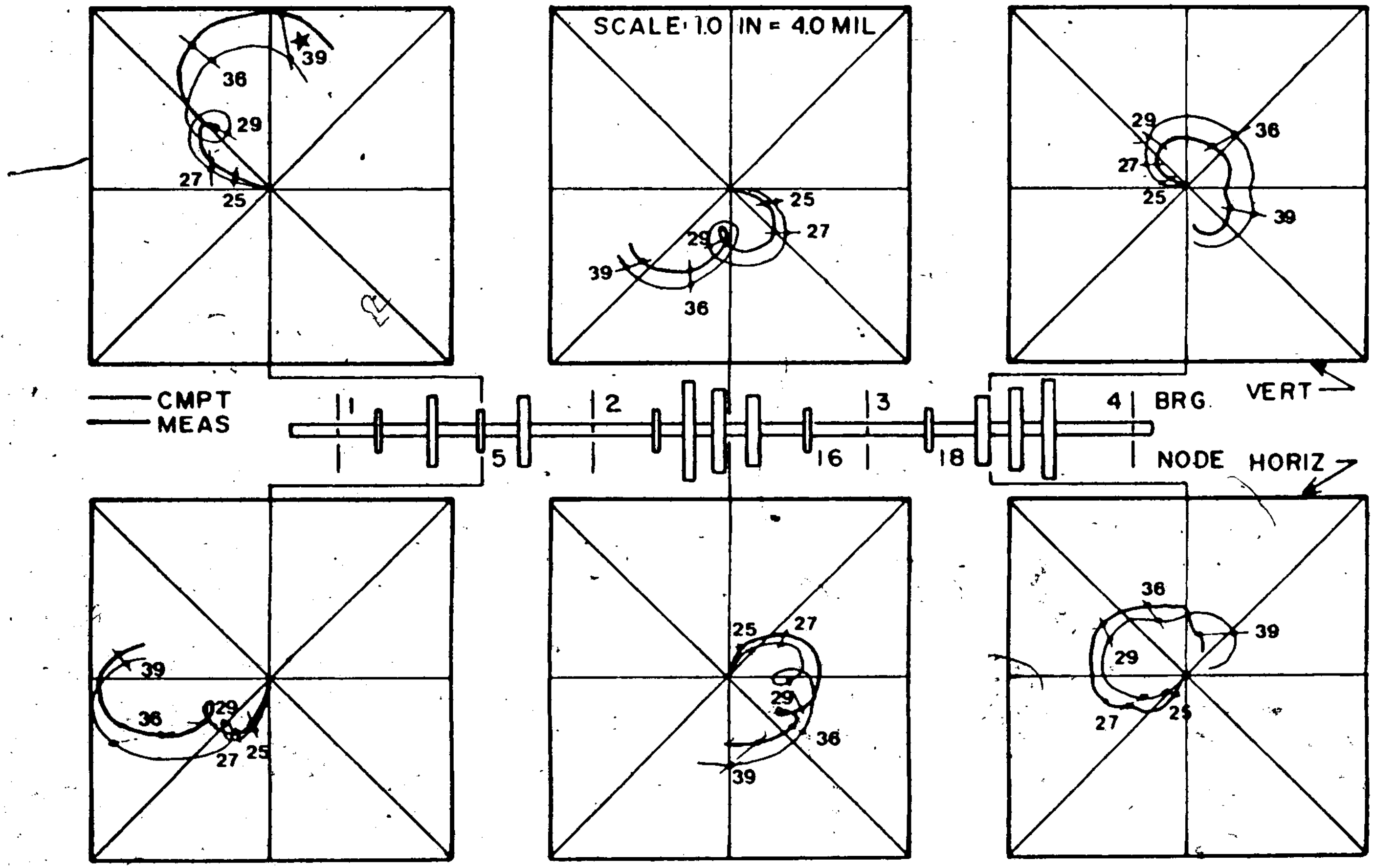

Fig. 5.12 Load Distribution 3

It is obvious that balancing one span at a time, with this method, would be far easier than balancing the entire shaft as one system.

5.3 Comparison of Experimental Results with Theoretical

The mode shapes (Figs. 4.10 - 4.12) and polar plots (Figs. 5.10 - 5.12) were first measured on the in-house rig. From this data the damping ratios present in the three modes were calculated. Accurate mathematical prediction of these modes and responses required adjustment of the bearing stiffness and damping coefficients as well as the proportional damping factor.

These adjustments were a trial and error procedure. The NRC bearing coefficient charts presented a wide range of coefficients depending on the source (Fig. 5.13). The mode shapes and natural frequencies are not affected by the proportional damping factor. Using the measured mode shapes presented a method to adjust the bearing coefficients independent of the proportional damping. The polar plots are affected by both and therefore, once the bearing coefficients had been determined the proportional damping was determined from the measured polar plots.

Adjustment of both these factors gave rise to a much improved mathematical model. This adjustment would be required for any rotating shaft system intended to be balanced with this method.

The 32 bearing coefficients were first determined from the measured mode shapes. For each bearing the Sommerfeld number is required for the coefficients. The speed chosen to calculate this number was 3400 RPM which was half way between the first and third critical speeds. There is some error in the load prediction at each bearing, radial clearance, and oil viscosity. These errors also widen the range of bearing coefficient values for each bearing. Fig. 5.13 shows an example of this range for K_{VH} on bearing #2.

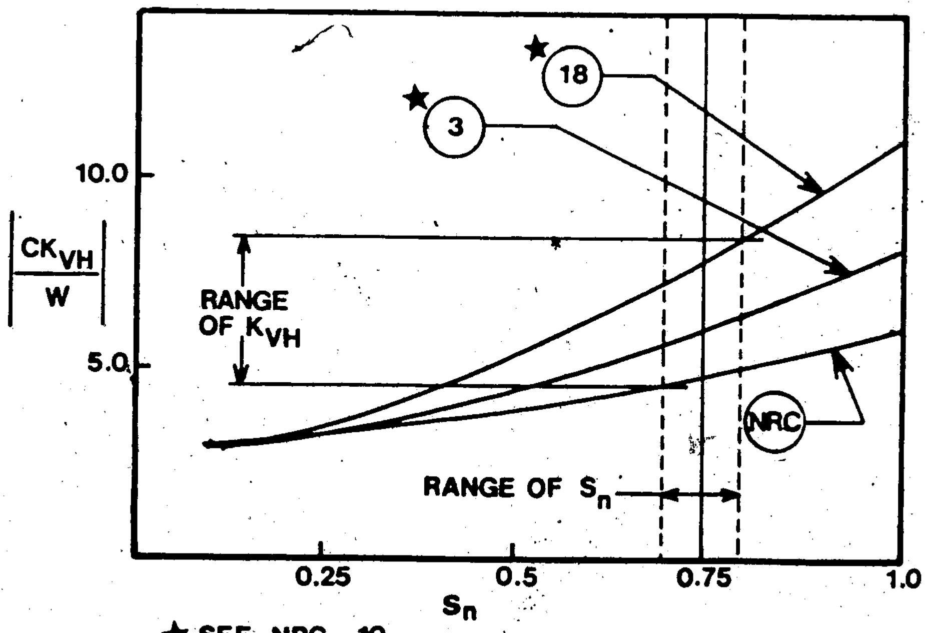

★ SEE NRC - 10

Fig. 5.13 Scatter In Bearing Coefficients

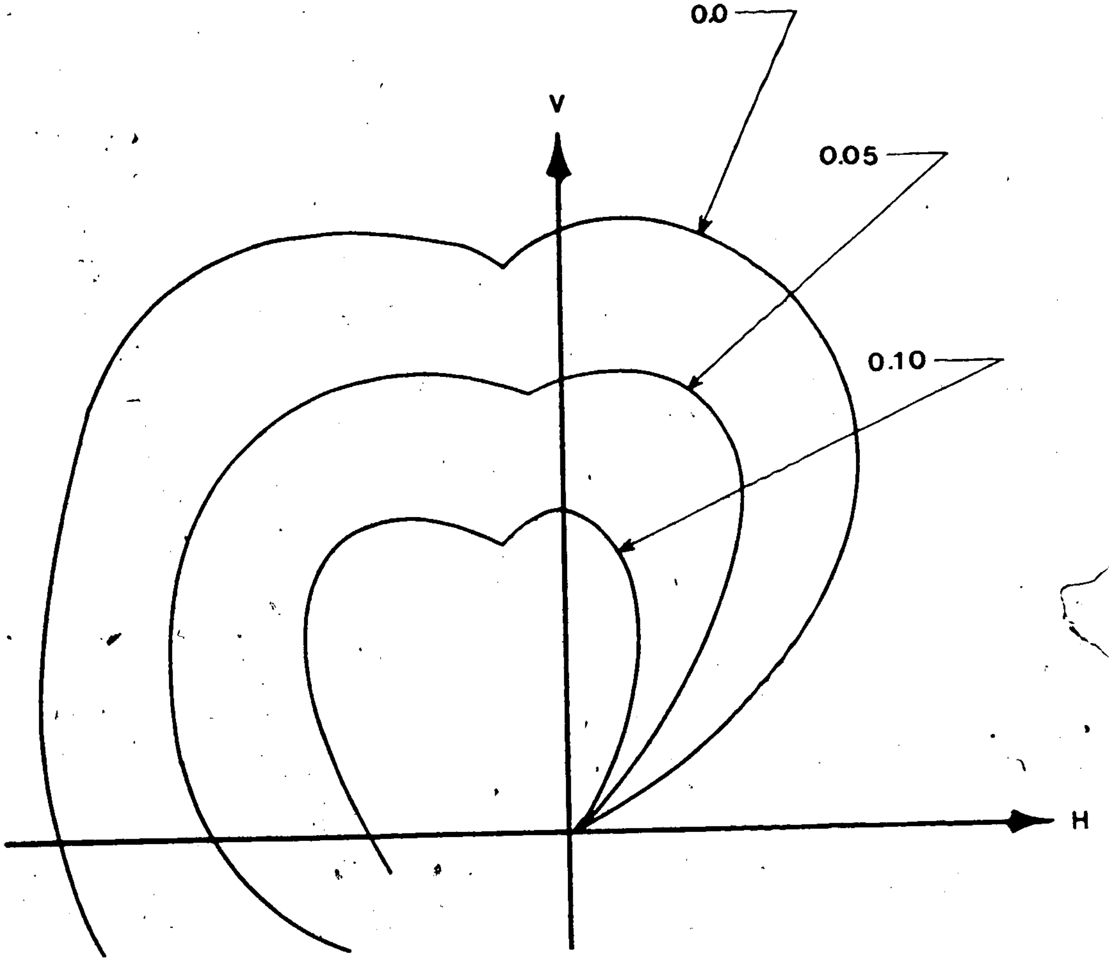

Fig. 5.14 Effect of Proportional Damping Factor

All of the bearing coefficient ranges were determined and then each was adjusted in order to predict the mode shapes shown in Figs. 4.10 - 4.12.

The damping factor was adjusted from 0 to 0.1X[K]. The value of 0.05X[D] produced the closest response at critical speeds on the polar plots. The basic shape of the polar plots remained unchanged regardless of which damping factor was used. The magnitude of the response near critical speeds, however, changed drastically. Fig. 5.14 gives an example of this.

5.4 Prediction of Load

Load distribution #2 was chosen for the prediction of the load vector. Chapter 4 indicated that speeds below the first critical show the best correlation between the experimental and theoretical forced responses and therefore a speed of 2700 RPM was chosen for the prediction. Prediction of the load vector from displacement measurements is essentially balancing the machine.

Predicting the load from the measured response requires simply multiplying the dynamic matrix [D] by the response vector {U}

i.e. $$\{F\} = [D]\{U\} \tag{5.5}$$

The predicted force, at any node, will be given as a complex pair. To be consistent with the coordinate system of Smith$^{(12)}$ given in Fig. 5.15 the predicted force vector must be given as follows:

$$F_V = F[\cos(\omega t+\phi) + i\ \sin(\omega t+\phi)]$$

$$F_H = F[\sin(\omega t+\phi) - i\ \cos(\omega t+\phi)] \qquad (5.6)$$

The force vector which was calculated from the finite element program differed slightly from Eq. 5.6 and was subsequently averaged. The slight errors in first measuring {U} added to the numerical errors (i.e. *Guyan Reduction*) resulted in the load vector not being exactly of form in 5.6.

The full system, i.e., V, H, ϕ_V, and ϕ_H was used to predict all of the mode shapes, natural frequencies, polar plots, and orbits presented thus far. For load prediction and balancing however, the full system cannot be used for two reasons. First, the nodal rotations (θ) are very impractical to measure and second in all machines there are relatively few locations in which measurements can be taken. Usually measurements are taken only at the bearings. For the in-house rig bearing displacements cannot be measured which leaves only measurements at each of the discs.

The full system has 24 elements and therefore 100 degrees of freedom. The slopes constitute 50 degrees of freedom and the bearing nodes further reduce the system by 8. Three measurements (vertical and horizontal displacements and phase angle) in each span were considered practical. The size of the system was therefore reduced from 100 to 18 degrees of freedom.

To carry out this reduction the well known "Guyan Reduction" technique was used. Meirovitch(14) explains the method in detail, which is also referred to as "mass condensation". One must first partition the stiffness matrix into the form:

$$\left[\begin{array}{c|c} K_{11} & K_{12} \\ \hline K_{21} & K_{22} \end{array}\right] \cdot \left\{\begin{array}{c} X_1 \\ \hline X_2 \end{array}\right\} = \left\{\begin{array}{c} F_1 \\ \hline F_2 \end{array}\right\} \qquad (5.7)$$

Assuming $F_2 = 0$, i.e., all the displacements are a result of only the F_1 loads:

$$\begin{aligned} K_{11}X_1 + K_{12}X_2 &= F_1 \\ K_{21}X_1 + K_{22}X_2 &= 0 \end{aligned} \qquad (5.8)$$

Therefore

$$X_2 = -K_{22}^{-1}\ K_{21}X_1 \qquad (5.9)$$

Substituting into 5 yields:

$$K_{11}X_1 + K_{12}[-K_{22}^{-1}\ K_{21}X_1] = F_1 \qquad (5.10)$$

The stiffness matrix for the reduced system is then

$$K_r = K_{11} - K_{12}K_{22}^{-1}K_{21} \qquad (5.11)$$

This is the basis for "static condensation" where for frames and trusses, etc. there are no approximations and the results are exact. The method can also be applied to dynamic systems where the mass matrix is diagonal with zero rotatary inertia terms. Here again, exact results are obtained. For the system in question, however, the mass matrix is not diagonal and therefore some approximations are involved in using the *"Guyan Reduction"* technique.

The kinetic and potential energies for the system are:

$$V = \tfrac{1}{2}\underline{X}^T[K]\underline{X}$$

$$T = \tfrac{1}{2}\underline{\dot{X}}[M]\underline{\dot{X}} \qquad (5.12)$$

From equation 5

$$\underline{X} = \begin{matrix} X_1 \\ X_2 \end{matrix} = [T]\underline{X}_1 = \frac{I}{-K_{22}^{-1}K_{21}} \quad \underline{X}_1 \qquad (5.13)$$

Substituting 5 into 5 gives the reduced stiffness and mass matrices to be

$$[K_r] = [T]^T[D][T] = K_{11}-K_{12}K_{22}^{-1}K_{21}$$

$$[M_r] = [T]^T[M][T] = M_{11}-K_{21}^TK_{22}^{-1}M_{21}-M_{12}K_{22}^{-1}K_{21}$$

$$+ K_{21}^TK_{22}^{-1}M_{33}K_{22}K_{22}^{-1}K_{21} \qquad (5.14)$$

The approximation in the technique is reduced by retaining nodal displacements in areas of low stiffness and high mass. In *"Guyan Reduction"* the retained nodes are referred to as "master" variables and the others are "slave" variables. For the in-house rig the master variables are at the disc nodes which are areas of very high mass and, therefore this technique was reasonable.

The basic assumption in this reduction is Eq. 5.8 where the slave forces (F_2) are zero. With regards to balancing this physically means that all displacements are a result of only the master forces (F_1). In other words the correction masses from Eq. 5.5 will force all the displacements to be zero and will yield a balanced rotor. Obviously then, the more balance planes the better the prediction of the load vector.

Fig. 5.15 shows the predicted load vector given the above 18 displacement measurements. A point load was placed at node 5 and measurements taken at 2700 RPM. Since only one load was placed into the shaft, at 0^{o} phase angle, the horizontal plane should show only a point load of 0.0002 Lb-in at node 5 and zero load in the vertical. This balancing attempt is quite unsuccessful but does not prove that the "dynamic matrix" technique is inadequate.

Several factors contribute to the poor load prediction in Fig. 5.15. The in-house rig rides on bearings with spherical seats designed to eliminate any rotational stiffness. For any real system there will be friction in the bearing housings which will add some rotational stiffness. These rotational stiffnesses will affect the displacements by adding

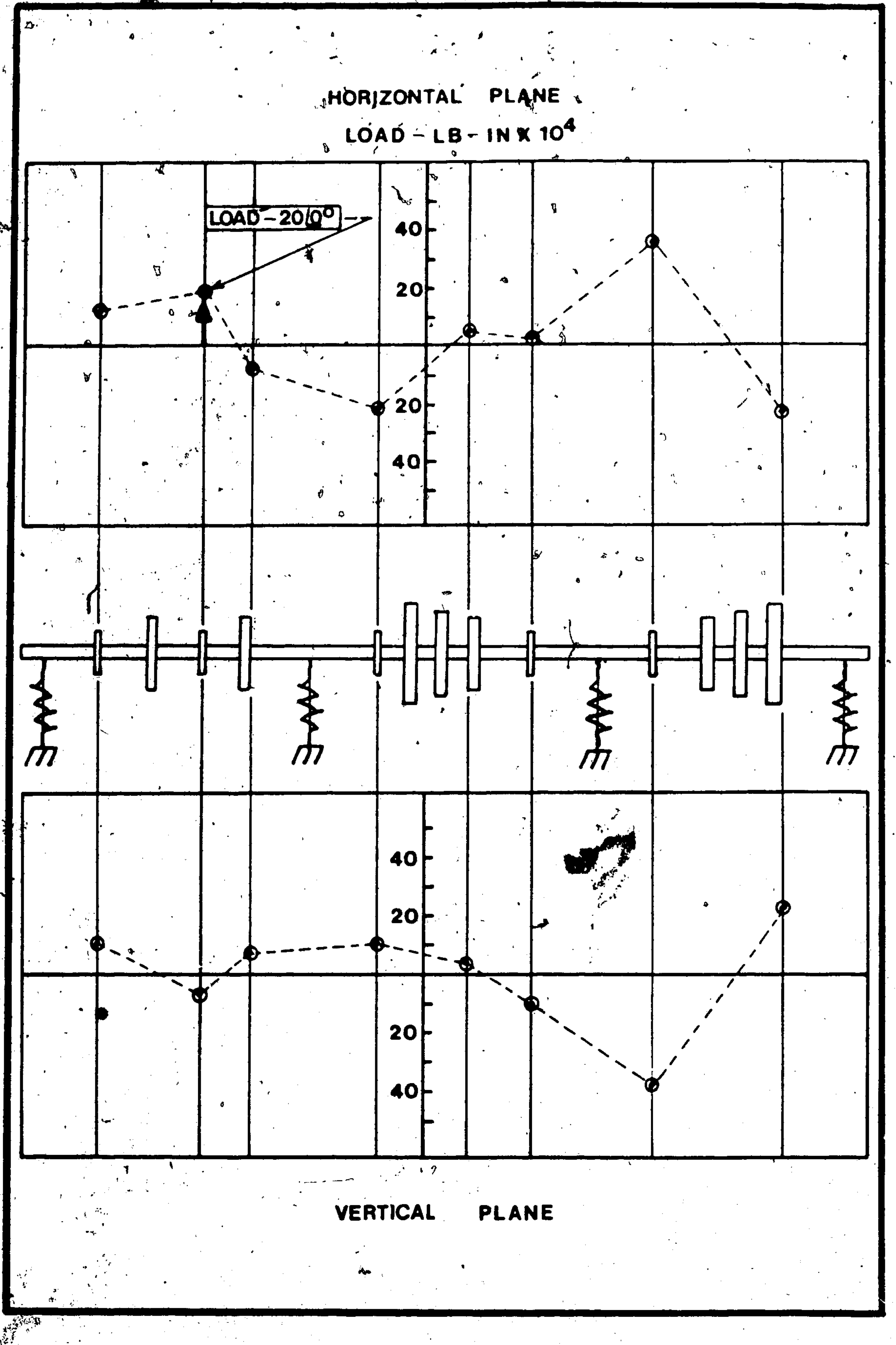

Fig. 5.15 Prediction of Load

another constraint. The computer model does not have these rotational stiffnesses and therefore the measurements taken from the physical system will introduce some error in the load vector. Placing this rotational stiffness into the finite element program will eliminate this problem.

Another source of error lies in the *"Guyan Reduction"* technique. As stated before this method is only exact for static systems or simple dynamic systems. The author feels that a more sophisticated reduction technique would yield a load vector which is closer to the initial imbalance. Such a method would be to use the accurate mode shape predictions and use a modal reduction in which a few of the lower modes are used along with a least squares fit. Thus the measured deflection vector is adjusted to take on a shape governed by the modes.

A closer examination of Fig. 5.15 indicates that the load prediction in the region of the load is fairly accurate. Most large machines are balanced in stages, i.e., HP then IP, etc. and perhaps if the rig were also balanced in stages the balance would be more successful.

6. CONCLUSIONS

6.1 Dynamic Model

The in-house rig was designed through the aid of the scaling parameters described in chapter 2. A single plane analysis of the 286 MW turbine defined the parameters. For the same single plane analysis for the rig the mode shapes (Fig. 2.10) matched very closely. The natural frequency ratios were within +6% for $^{\omega}1/\omega_3$ and 1% for $^{\omega}1/\omega_2$. The Sommerfeld numbers and stiffness ratios were within ±15%. The mode shapes and natural frequencies were considered to be the most important design considerations.

Comparing the mode shapes and natural frequencies for the rig as a two plane system (Table 4.2 and Figs. 4.10 - 4.12) with the single plane system (Fig. 2.10) reveals a large discrepancy in the values for the natural frequencies. The mode shapes have the same general shape however. The reason for this lies in the long journal bearings on the rig. The cross coupling terms (Table 4.1) are very large which increase the stiffness of the system considerably which, of course, raises the natural frequencies. The single plane analysis was merely a method of design but the two plane analysis reveals the danger in treating any rotating system with journal bearings as an axi-symmetric problem.

6.2 Numerical Model

Comparison of the static (or non-rotating) mode shapes (Fig. 3.9 and Table 3.1) for measured Vs calculated results shows very good correlation. The symmetric part of the stiffness and mass matrices, i.e., the Timoshenko beam element were considered quite accurate. Addition of bearing terms in the stiffness and damping matrices rendered the system to be somewhat less accurate judging from the two plane mode shapes. The correlation is still quite good but the non-rotating results were better.

Damping was also introduced into the system as both bearing damping and proportional damping. One would assume the bearing damping to be as accurate as the bearing stiffness. Examining the relatively good correlation for the polar plots (Figs. 5.10 - 5.12) the combined damping matrix is fairly accurate. The average proportional damping factor from the non-rotating tests was 7% and a value of 5% was used for the polar plots.

For synchronous whirling there is no reverse bending but the higher order frequencies (½X, 2X, etc.) will produce structural damping and from Fig. (5.8) these higher order vibrations are present. Damping due to the air between the discs is also present.

the value of 5% was arrived at from the polar plots when the magnitude of the response at resonance showed good correlation for all three load distributions. The proportional damping factor, then, includes all the damping that cannot be measured.

6.3 Balancing

The purpose of this paper was to produce and test a purely numerical balancing technique. The evidence of accurate mode shapes and polar plots indicate that the method has potential. The actual balance run (Fig. 5.15) was not successful but this does not label the method a failure. The reduction technique is the major factor which has to be improved upon. Using a modal approach will produce better results. As well, the addition of rotational bearing stiffness will improve the balancing.

It is the opinion of the author that a slightly improved reduction technique as well as fine adjustments of the bearing terms will yield a balancing method which will be more accurate than the techniques presently employed.

REFERENCES

1. Thomas, D.L., Wilson, J.M. and Wilson, R. R., 'Timoshenko Beam Finite Elements', J. Sound Vib., Vol. 31, No. 3, 1973, pp. 315-330.

2. Kennedy, C. C. & Pancu, C. D. P., "Use of Vectors in Vibration Measurement and Analysis', J. Aero. Sci., Vol. 14, No. 11, Nov., 1947, pp. 603-625.

3. Craggs, A., 'The Low Frequency Response of Car Bodies', Mira Peport, Aug. 1965.

4. Meirovitch, L. 'Analytical Methods of Vibration', MacMillan, 1967.

5. Tse, F. S., Morse, I. E. & Hinkle, R. T., 'Mechanical Vibrations - Theory & Applications', 2nd Edition, Allyn & Bacon Inc., 1978.

6. Thompson, W. T., 'Theory of Vibration with Application', 2nd Edition, Prentice-Hall Inc., 1981.

7. Kim, P. Y., 'Review of Flexible Shaft Balancing Techniques', Sixth Machinery Dynamics Seminar - National Research Council of Canada, Oct., 1980.

8. Den Hartog, J. P., 'Mechanical Vibrations', McGraw-Hill Book Co., New York, 1956.

9. Shigley, J. E., 'Mechanical Engineering Design', McGraw-Hill Inc., Third Edition, 1977.

10. Kim, P. Y., Lowe, I. R. G., 'A Comparative Study of Fluid Film Bearing Coefficients', NRC Paper No. LRT-ENG-109, Aug. 1981.

11. Timoshenko, S., 'Vibration Problems in Engineering', D. Van Nostrand Co., New York, 1955.

12. Smith, D. M., 'Journal Bearings in Turbomachinery', Chapman and Hall, London, 1969.

13. Archer, J. S., 'Consistent Mass Matrix for Distributed Mass Systems', J. Struc. Div., ASCE, Aug. 1963, pp. 161-178.

14. Meirovitch, L., 'Computational Methods in Structural Dynamics', Sijthoff & Noordhaaf, 1980.

REFERENCES

15. Gasch, R., 'Vibration of Large Turbo-Rotors in Fluid Film bearings on an Elastic Foundation', J. Sound Vib., Vol. 47, 1976.

16. Adams, M.L. & Padovin, J., "Insights into Linearized Rotor Dynamics', J. sound Vib., Vol. 71, No.1, 1981. pp.129-142.